

THE THERMODYNAMIC ANALYSIS OF APTAMER –
LIGAND BINDING BY ISOTHERMAL TITRATION
CALORIMETRY

SLADJANA SLAVKOVIC

A DISSERTATION SUBMITTED TO
THE FACULTY OF GRADUATE STUDIES
IN FULFILLMENT OF THE REQUIREMENTS
FOR THE DEGREE OF
DOCTOR OF PHILOSOPHY

GRADUATE PROGRAM IN CHEMISTRY
YORK UNIVERSITY
TORONTO, ONTARIO

April 2020

© Sladjana Slavkovic 2020

Abstract

Aptamers are short, single stranded nucleic acid molecules typically 15 to 60 nucleotides in length with the capacity of binding diverse molecular targets, ranging from small molecules to whole cells primarily due to their specific three-dimensional structure. The cocaine binding aptamer is a DNA aptamer that contains 3 stems built around a 3-way junction. This aptamer was selected by Stojanovic in 2000 using classic SELEX to bind cocaine, but not for its common metabolites, benzoylecgonine and ecgonine methyl ester. It is widely used as a model system in the development of a variety of biosensor applications.

The aim of this research was to gain an insight into understanding how aptamers interact with their ligands by measuring thermodynamics. Since very little work has been done in this field using isothermal titration calorimetry (ITC) studies, the thermodynamics of small molecule binding to the cocaine-binding aptamer was investigated in detail. The study included both quinine-based and non-quinine based antimalarial compounds. Some of the results that this study yielded are the importance of a quinoline ring in the ligand, the second binding site on the aptamer, the new tightest binding ligand for the cocaine binding aptamer – amodiaquine, and a ligand (artemisinin) that does not contain quinoline ring but binds tightly to the cocaine-binding aptamer.

In order to determine the selectivity of the antimalarial compounds (amodiaquine, mefloquine, chloroquine and quinine) for the cocaine-binding aptamer, the investigation was further expanded to other DNA structures such as three-way junctions and duplex

DNA of varying length. Results showed that quinine and chloroquine are specific for the cocaine binding aptamer, while amodiaquine binds DNA in general. Artemisinin, a non-quinine based antimalarial compound is a generic DNA binder, a previously unknown property of this antimalarial agent.

Similarly to the cocaine-binding aptamer, the ATP-binding aptamer binds two copies of its ligand. But unlike the cocaine-binding aptamer, the ATP aptamer binds its ligand in a cooperative two-site binding manner. In addition, this aptamer must have both sites functional; otherwise, the ligand will bind very weakly. Studies also showed, that if two binding sites are separated, the aptamer becomes more structured and stable, and binding model switches from cooperative to independent for adenosine but not ATP.

Acknowledgments

I would like to thank my husband Sandro and my sons Filip and Marko to whom this thesis is dedicated for their unconditional love, support and patience. Thank you for being there for me and helping me maintain perspective. Without you I would never be able to reach this stage of my life. You made all my achievements possible.

I would like to extend my deepest gratitude to my supervisor and mentor Professor Philip E. Johnson for providing me with this incredible opportunity. From the first day I met him, Professor Johnson has always been encouraging and enthusiastic. He gave me the freedom and confidence to approach problems independently yet was always available for advice. Thank you for your patience, guidance and most importantly support at every step of this journey.

To my parents, Verica and Dusko Cavic and my parents-in-law Vera and Vlada Todosijevic who were always there for me. The support you have given me is more than I could have asked for. Thank you being there when I needed you and when I did not know I need you.

To my sister Sanja thank you for being you and listening without comments. I am very fortunate to have such a wonderful sister as you.

I would like to thank my committee members Jennifer Chen and Logan Donaldson for your time, expertise, support and guidance you have provided throughout this project.

My sincere thanks to Zach Churcher and Aron Shoara for stimulating discussions. Thank you for your support and your friendship and doing extra experiments to make sure my results make sense. Your expertise guided me through many hurdles. I would also like to thank many friends and colleagues I have met throughout this journey whose advice and friendship is greatly appreciated. Thank you for some truly memorable moments.

Table of Contents

Abstract	ii
Acknowledgments.....	iv
Table of Contents.....	vi
List of Tables	x
List of Figures	xii
List of Abbreviations	xvi
<i>Chapter 1 Aptamers.....</i>	<i>1</i>
1.1. Background	1
1.2 Systematic Evolution of Ligands by Exponential Enrichment (SELEX)	3
1.3 Aptamer Targets.....	6
1.4 Applications of Aptamers	8
1.4.1 Aptamers as Therapeutic Agents	8
1.4.2 Aptamers as biosensors	11
1.4.3 Riboswitches.....	12
1.5 The Cocaine-Binding Aptamer	13
1.6 Bioanalytical techniques used to characterize aptamer–target interactions	17
1.7 Isothermal Titration Calorimetry.....	19
1.7.1. General Sample Preparation.....	21
1.7.2 General ITC Experimental Setup.....	23
1.7.3. Cell Cleaning.....	27
1.7.4. Data Analysis.....	28
1.7.5. Troubleshooting.....	31
1.8 Thesis project	36
<i>Chapter 2 Methods and Materials</i>	<i>37</i>
2.1 Preface	37
2.2. Aptamer preparation.....	37
2.3. Ligand preparation.....	37
2.3.1. Cocaine, cocaine Analogues, quinine and quinine analogues	38
2.3.2 Antimalarial compounds	38
2.3.3 ATP, ADP, AMP, adenosine and adenine	38
2.4. Isothermal titration calorimetry experimental setup.....	39
2.4.1 General ITC setup.....	39
2.4.2. Quinine analogues experiments.....	39
2.4.3. Cocaine and quinine two-site binding experiments	40
2.4.4. The ATP-binding aptamer experiments	40
2.4.5. Dangling nucleotide experiments.....	41
2.4.6. Antimalarial compounds binding to the cocaine-binding aptamer experiments.....	42
2.4.7. Various DNA structures binding to antimalarial compounds experiments.....	42
2.4.8. Artemisinin and 2-deoxyartemisinin binding experiments.....	43

2.5 Data fitting.....	43
Chapter 3 Structure affinity relationship of the cocaine-binding aptamer with quinine derivatives	44
3.1 Preface	44
3.2 Introduction.....	44
3.3 Results.....	47
3.3.1. Binding affinity and thermodynamics of quinine and cocaine.	47
3.3.2. Cocaine metabolites.....	50
3.3.3. The importance of fused ring.	50
3.3.4. Methoxy variants.	51
3.3.5. Isomerism.	52
3.3.6. Effect of saturating the vinyl group.	53
3.4 Discussion.....	53
3.5 Concluding remarks	57
Chapter 4 Salt-Mediated Two-Site Ligand Binding by the Cocaine-Binding Aptamer.....	58
4.1 Preface	58
4.2 Introduction.....	58
4.3 Results and Discussion.....	62
4.3.1. Salt-controlled two-site binding of cocaine.....	62
4.3.2. Salt-mediated two-site binding of quinine.	64
4.4.3. Salt mediated binding of quinine to MN19 aptamer.	65
4.4.4. Effect of NaCl concentration in buffer on binding.	67
4.4 Concluding Remarks	68
Chapter 5 Analysis of cooperative ligand binding by the ATP aptamer.....	69
5.1. Preface	69
5.2 Introduction.....	69
5.3 Results.....	72
5.3.1. Ligand binding to ATP3 aptamer.....	72
5.3.2. Binding Mechanism of Adenosine to ATP3 Aptamer.	74
5.3.3. Relationship between two binding sites.....	77
5.3.4. ATP aptamer variants with one binding site.	78
5.3.5. Adenosine binding to ATP6 aptamer.	80
5.3.6. ATP and adenosine binding to ATP7 aptamer.	81
5.3.7. Adenosine binding to ATP17 aptamer.	84
5.3.8. Hill coefficient analysis.....	85
5.4 Discussion.....	85
5.5 Concluding remarks	90
Chapter 6 Designed Alteration of Binding Affinity in Structure-Switching Aptamers Through the Use of Dangling Nucleotides.....	91
6.1 Preface	91

6.2 Introduction	91
6.3 Results	94
6.3.1. Cocaine-binding aptamer dangling nucleotide constructs.....	94
6.3.2. ATP-binding aptamer dangling nucleotide constructs.....	97
6.4 Discussion	100
6.5 Concluding remarks	105
<i>Chapter 7 Nanomolar Binding Affinity of Quinine-Based Antimalarial Compounds by the Cocaine-Binding Aptamer</i>	106
7.1 Preface	106
7.2 Introduction	106
7.3 Results and Discussion	109
7.3.1. Binding affinity and thermodynamics of antimalarial compounds.....	109
7.3.2. Competition binding experiments.....	113
7.3.3. Binding at different NaCl concentrations.....	115
7.3.4. Binding of short stem 1 constructs.....	119
7.4 Concluding remarks	121
<i>Chapter 8 Antimalarial Compounds: Cocaine-binding aptamer specific or Generic DNA binders?</i>	122
8.1 Introduction	122
8.2 Results	126
8.2.1. Binding of chloroquine and quinine.....	126
8.2.2. Binding of amodiaquine.....	126
8.2.3. Binding of mefloquine.....	127
8.3 Discussion	128
8.4 Concluding remarks	132
<i>Chapter 9 Analysis of Artemisinin Binding to the Cocaine-binding Aptamer and other DNA structures</i>	133
9.1 Introduction	133
9.2 Results	135
9.2.1. Effect of stem length on binding of artemisinin.....	135
9.2.2. Binding of artemisinin to three-way junctions.....	136
9.2.3. Binding of artemisinin to duplex DNA.....	137
9.2.4. The cocaine-binding aptamer stem deletion.....	139
9.2.5. Binding at 0 mM NaCl concentration.....	141
9.2.6. Effect of endoperoxide bridge.....	143
9.3 Discussion	144
9.4 Concluding remarks	148
<i>Concluding Remarks</i>	149
10.1 Summary	149
10.2. Future work	150

Appendix A	152
A1. Two-site independent binding model.....	153
A2. Two-site cooperative binding model.....	154
Appendix B	156
B1. Hill coefficient determination.....	156
Bibliography	158

List of Tables

Table 1-1: List of aptamers approved for clinical trials (adapted from Reference 58)	10
Table 3-1: Binding affinities and thermodynamic parameters of ligands used in this study.....	49
Table 4-1: Individual two-site independent fits of cocaine bound to MN4 aptamer..	63
Table 4-2: Individual two-site independent fits of quinine bound to MN4 aptamer.	64
Table 4-3: Average individual fits and global fits comparison.....	65
Table 5-1: Binding affinities and thermodynamic parameters of adenine-based ligands to the ATP-binding aptamer and comparison of fits	72
Table 5-2: Individual independent and cooperative fits comparison of adenosine binding to ATP3 aptamer	74
Table 5-3: Average of the individual fits comparison	74
Table 5-4: Global fits for cooperative and independent binding model comparison	75
Table 5-5: ATP9 and ATP10 aptamers binding to adenosine.....	77
Table 5-6: ATP6 binding to adenosine fit comparison	80
Table 5-7: ATP7 binding to adenosine fit comparison	82
Table 5-8: ATP7 binding to ATP fit comparison.....	82
Table 5-9: ATP17 binding to adenosine comparison fits.....	84
Table 5-10: Hill coefficient results for ATP and adenosine binding to ATP-binding aptamer constructs.	85
Table 6-1: Binding affinities and free energy of quinine binding by aptamers used in this study.....	95
Table 6-2: Thermodynamic parameters of aptamers used in this study upon binding to quinine	96
Table 6-3: Binding affinities and free energy of adenosine binding by the ATP-binding aptamers used in this study	99

Table 6-4: Thermodynamic parameters of adenosine binding by the ATP-binding aptamers used in this study	99
Table 7-1: Binding affinities and thermodynamic values for the binding between the MN4 cocaine-binding aptamer and ligands in high salt buffer	111
Table 7-2: Binding affinities and thermodynamic values for the binding between the MN4 cocaine-binding aptamer and ligands in low salt buffer.....	116
Table 7-3: Binding affinities and thermodynamic values for the interaction between the MN4 cocaine-binding aptamer and amodiaquine at different NaCl concentrations.....	118
Table 7-4: Binding affinities and thermodynamic values for the interaction of amodiaquine and chloroquine with the short stem 1 aptamers OR7 and OR8.	119
Table 8-1: Comparison of binding affinities and thermodynamic properties of amodiaquine by aptamers used in this study.....	127
Table 8-2: Comparison of binding affinities and thermodynamic properties of mefloquine by aptamers used in this study.....	127
Table 9-1: Comparison of binding affinities and thermodynamic properties of artemisinin by three-way junctions used in this study	135
Table 9-2: Comparison of binding affinities and thermodynamic properties of artemisinin by three-way junctions used in this study.....	137
Table 9-3: Comparison of binding affinities and thermodynamic properties of artemisinin by DNA duplexes	137
Table 9-4: Comparison of competitive binding of quinine and artemisinin by the MN4 aptamer.	138
Table 9-5: Comparison of binding affinities and thermodynamic properties of artemisinin by aptamers used in this study	141
Table 9-6: Comparison of binding affinities and thermodynamic properties of artemisinin in different buffer conditions.....	142

List of Figures

Figure 1-1: Schematic representation of the classic SELEX protocol.....	4
Figure 1-2: Pie chart representation of various types of aptamer targets that have been selected between 1990 and 2019.....	7
Figure 1-3: Structure of the original cocaine-binding aptamer	13
Figure 1-4: Structures of (a) MN4, long stem 1 variant and (b) MN19, short stem 1 variant of the cocaine-binding aptamer proposed by Neves <i>et al.</i>	15
Figure 1-5: Diagram of a typical ITC instrument.....	20
Figure 1-6: Illustration of the effect of the c-value.....	22
Figure 1-7: Adjustment of the time between injections.....	25
Figure 1-8: Examples of different possible heats of dilution.....	26
Figure 1-9: Titration of water into water is a good check of ITC cleanliness.....	28
Figure 1-10: Examples of potential problems with ITC experiments.....	32
Figure 1-11: Baseline unable to equilibrate during the final baseline equilibration.....	33
Figure 1-12: Example of a mismatch in DMSO concentration.....	34
Figure 1-13: Examples of different solvent effect.....	34
Figure 3-1: Structure of the MN4 cocaine-binding aptamer	45
Figure 3-2: Structures of quinine, cocaine and their analogues used in this study. ..	46
Figure 3-3: Sample ITC data showing the interaction of MN4 with (a) quinine and (b) atropine.....	48
Figure 3-4: ITC data showing the interaction of MN4 with (a) quinoline and (b) benzo(h)quinoline.	51
Figure 3-5: Plot for binding enthalpy versus entropy for the ligands used in this study	54
Figure 4-1: Secondary structure of the MN4 and MN19 cocaine-binding aptamer and chemical structures of the cocaine and quinine ligands.	60

Figure 4-2: Titrations of cocaine into MN4 aptamer with buffer conditions of (a) 140 mM NaCl and (b) 0 mM NaCl.....	62
Figure 4-3: ITC data for MN4 binding quinine acquired at various aptamer concentrations at 0 mM NaCl.....	65
Figure 4-4: Two-site binding of the short stem 1, MN19 cocaine-binding aptamer using ITC.....	66
Figure 4-5: Ligand binding at the second site is controlled by the concentration of NaCl.....	67
Figure 5-1: Secondary structures of the ATP-binding aptamer constructs.....	71
Figure 5-2: Binding of ATP, ADP, AMP, adenosine and adenine by the ATP3 aptamer.....	73
Figure 5-3. Global cooperative fit showing binding of adenosine to ATP3 aptamer acquired at various aptamer concentrations.....	76
Figure 5-4: Global independent fit showing binding of adenosine to ATP3 aptamer acquired at various aptamer concentrations.....	76
Figure 5-5: ITC thermograms showing binding of adenosine to (left) ATP9 and (right) ATP10.....	77
Figure 5-6: Thermogram showing binding of adenosine to ATP11 aptamer.....	78
Figure 5-7: Structures of one-site ATP aptamer variants.....	79
Figure 5-8: Thermograms showing interaction of one-site aptamers binding to adenosine.....	79
Figure 5-9: Binding of adenosine to the ATP6 aptamer.....	81
Figure 5-10: Binding of adenosine to the ATP7 aptamer.....	83
Figure 5-11: Binding of ATP to the ATP7 aptamer.....	83
Figure 6-1: Secondary structures of the cocaine-binding aptamers containing dangling nucleotides as well as the OR8 and MN19 aptamers.....	93
Figure 6-2: ITC data showing the interaction of the different cocaine-binding aptamers binding quinine.....	97
Figure 6-3: Secondary structures of the ATP-binding aptamers containing dangling nucleotides as well as the ATP1d and ATP1e aptamers.....	98

Figure 6-4: ITC data showing the interaction of the different ATP-binding aptamers interacting with adenosine.	100
Figure 6-5: Free energy diagram of ligand binding by selected dangling nucleotide cocaine-binding aptamer constructs.	101
Figure 6-6: Plot of the predicted ΔG°_{37} values of adding a dangling nucleotide versus the observed change in ΔG of binding ($\Delta\Delta G$).	104
Figure 7-1: Secondary structure of the different cocaine-binding aptamer constructs used in this study.	108
Figure 7-2: ITC analysis of ligand binding by the MN4 cocaine-binding aptamer... ..	110
Figure 7-3: ITC analysis of the binding of structural pieces of amodiaquine by the MN4 cocaine-binding aptamer.....	113
Figure 7-4: ITC-based competition binding experiments..	115
Figure 7-5: ITC analysis of the binding of primaquine by the MN4 cocaine-binding aptamer in (a) the presence and (b) the absence of 140 mM NaCl.....	117
Figure 7-6: ITC analysis of the binding of amodiaquine by the MN4 cocaine-binding aptamer in different concentrations of NaCl.....	118
Figure 7-7: ITC data showing the interaction of two different stem 1 length aptamers with chloroquine and amodiaquine.....	120
Figure 8-1: Secondary structures of (a) MN4, the cocaine-binding aptamer; (b) SS1 aptamer, a version of the cocaine-binding aptamer where two AG base pairs are switched to GA base pairs; (c) TWJ, a generic three-way junction; (d) DDD, a Dickerson – Drew dodecamer; and (e) hexamer.	124
Figure 8-2: Structures of quinine-based antimalarial compounds used in this study.	125
Figure 8-3: ITC thermograms showing binding of antimalarial compounds to a version of the cocaine-binding aptamer (SS1).....	129
Figure 8-4: ITC thermograms showing binding of antimalarial compounds to the generic three-way junction (TWJ).	130
Figure 8-5: ITC thermograms showing binding of antimalarial compounds to Dickerson-Drew dodecamer (DDD).	131
Figure 8-6: ITC thermograms showing binding of antimalarial compounds to the hexamer.	132

Figure 9-1: Secondary structures of (a) cocaine-binding aptamer constructs; (b) different three-way junctions; and (c) different DNA duplexes. 134

Figure 9-2: Thermogram showing the interaction of artemisinin with the cocaine-binding aptamer, MN4 136

Figure 9-3: ITC thermograms showing competition titration..... 139

Figure 9-4: Secondary structures of (a) MN4 aptamer; (b) SS2 aptamer, the cocaine-binding aptamer with stem 1 deleted; (c) SS3 aptamer, the cocaine-binding aptamer with stem 2 deleted; and (d) SS4 aptamer, the cocaine-binding aptamer with stem 3 deleted. 140

Figure 9-5: Thermograms showing binding of artemisinin to variants of the cocaine-binding aptamer where (a) stem 1 was deleted (SS2), (b) stem 2 was deleted (SS3), and (c) stem 3 was deleted (SS4)..... 141

Figure 9-6: ITC thermograms showing interaction of artemisinin with MN4 aptamer 143

Figure 9-7: ITC thermogram showing (a) interaction of artemisinin with the MN4 aptamer; (b) interaction of 2-deoxyartemisinin with the MN4 aptamer. 144

Figure B1: Hill plot for adenosine binding to ATP3 aptamer with two sites exhibiting positive cooperativity.158

List of Abbreviations

ATP#	ATP-binding aptamer variants
ADP	Adenosine diphosphate
AMP	Adenosine monophosphate
ATP	Adenosine triphosphate
AuNP	Gold nanoparticles
ΔG	Change in free energy
$\Delta\Delta G$	Change in free energy of binding
ΔH	Change in enthalpy
ΔS	Change in entropy
DCA	Deoxycholic acid
DMSO	Dimethyl sulfoxide
DNA	Deoxyribonucleic acid
DTT	Dithiothreitol
ddH ₂ O	Double distilled water
HEPES	4-(2-hydroxyethyl)-1-piperazineethanesulfonic acid
ITC	Isothermal titration calorimetry
K _a	Association constant
K _d	Dissociation constant
MN#	Cocaine-binding aptamer variants
nb	no binding

nt	Nucleotide
OR#	Cocaine-binding aptamer variants
PCR	Polymerase chain reaction
RNA	Ribonucleic acid
SELEX	Systematic evolution of ligands by exponential enrichment
ssDNA	Single stranded deoxyribonucleic acid
ssRNA	Single stranded ribonucleic acid
TCEP	Tris(2-carboxyethyl)phosphine
TRIS	Tris(hydroxymethyl)aminomethane
UV-Vis	Ultraviolet-visible
vwb	Very weak binding
WC	Watson-Crick

Chapter 1 Aptamers

1.1. Background

In 1908 German scientist Paul Ehrlich shared the Nobel Prize for Physiology or Medicine with Élie Metchnikoff for chemical theory to explain the formation of antitoxins to fight toxins released by the bacteria¹. He named them “magic bullets” as they would target only toxins with high specificity and affinity and leave healthy tissue undamaged². His work on “magic bullets” led to development of monoclonal antibodies and eventually aptamers.

Aptamers are synthetic, short, single stranded nucleic acid molecules typically 15 to 60 base nucleotides in length with the capacity of binding diverse molecular targets, ranging from small molecules to whole cells primarily due to their specific three-dimensional structure³. They were developed in 1990 by Tuerk and Gold from a random ssRNA library containing over 65000 possible combinations from which they selected two hairpins that bind to T4 DNA polymerase gp43 with similar affinity⁴. They named this process Systematic Evolution of Ligands by Exponential Enrichment (SELEX). At about the same time, starting from random ssRNA library, Ellington and Szostak selected aptamers capable of forming a binding pocket for small organic dyes⁵. They derived the term aptamer from Latin “aptus” meaning to fit and Greek “meros” meaning part. Two years later, the two also selected the first DNA-based aptamer⁶. Robertson and Joyce also published a paper in 1990 where they isolated a mutant form of RNA-splicing *Tetrahymena* ribozyme that is capable

of cleaving DNA efficiently using similar technique⁷.

Aptamers can be divided into three groups: DNA, RNA and peptide aptamers, which have similar properties but are distinctly unique. Specifically, RNA and DNA aptamers differ in sequence and folding pattern, even though they bind to the same target, such as ATP-binding RNA aptamer and ATP-binding DNA aptamer⁸. In early SELEX protocols, RNA libraries were used to generate RNA aptamers. Soon, it was discovered that DNA aptamer could also be selected to bind specific targets⁶. DNA aptamers became favoured over RNA aptamers as they are chemically and biologically more stable making them cheaper and easier to produce. Although RNA aptamers are able to adopt a wider array of 3D structures⁹, they require extra reverse transcription step during RNA SELEX. Peptide aptamers are polypeptide chains that are selected to bind their target using SELEX process¹⁰. Their targets are also wide ranging from proteins to nucleic acids and cells. Peptide aptamers are more chemically diverse compared to DNA and RNA aptamers since they have 20 monomeric base units compared to four for DNA or RNA. Because of this, their starting library must be larger than the one used for the oligonucleotide aptamer selection⁹.

One of the advantages of aptamers is their high stability as they retain their structure and can bind to target even after many cycles of denaturation and renaturation. Aptamers are easily modified; can be synthesized in desired quantity; they are reproducible; and it is possible to introduce fluorophores and quenchers. They bind to a variety of targets with high affinity and specificity for some ligands

that cannot be recognized by antibodies such as toxins, ions, etc¹¹⁻¹³. Aptamers have low immunogenicity since nucleic acids are not recognized by the human immune system as foreign agents, for example, the VEGF aptamer is used in the treatment of ocular vascular disease¹⁴. One of the major disadvantages is their small size, which results in renal filtration and degradation in biological media. Aptamer half-life in blood media is two minutes¹⁵. To overcome this, aptamers can be modified to include substitution of sulfurs for non-bridging oxygens in the phosphate backbone (i.e. thioaptamers) or modification of deoxyribose at the 2' position with amine, fluoro, methoxy, and thiol groups, which hinders degradation in serum and enhances binding affinities^{16,17}.

1.2 Systematic Evolution of Ligands by Exponential Enrichment (SELEX)

The process of selecting aptamers is called **Systematic Evolution of Ligands by Exponential Enrichment (SELEX)** and it involves screening desired aptamers from a large library of oligonucleotides through an *in vitro* process^{4,5}. A SELEX method (Figure 1-1) consists of three steps: selection, separation and amplification. The selection begins with random pool of 10^{13} - 10^{15} sequences. This mixture includes regions of fixed sequences (the same sequences at the same location) and a region of randomized sequences. The fixed sequence is chosen to assist in the amplification step to mimic sequence known to bind target, or to enhance concentration of a given structural arrangement of the nucleic acids¹⁸. Randomized sequences can be completely or partially randomized¹⁹. When building a library, several steps should be considered: backbone modifications, length of random region, primer binding

sites, libraries containing additional constant sequences, predefined structures, doping strategy or uniformly randomized libraries²⁰.

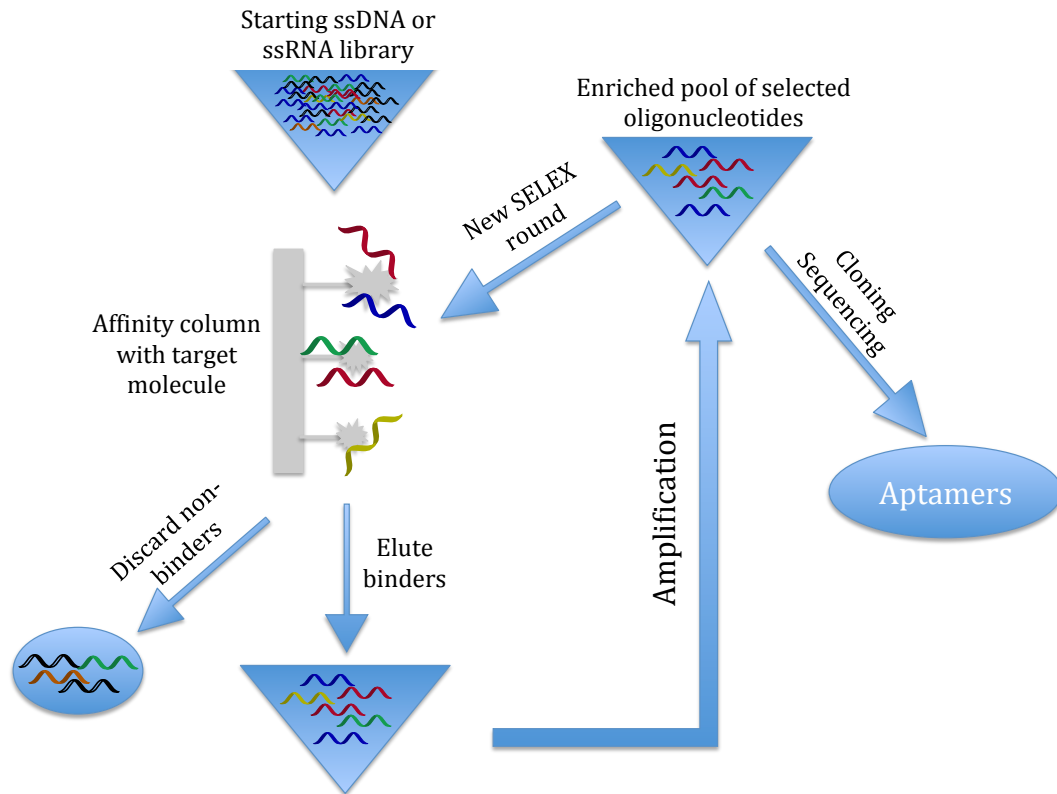


Figure 1-1: Schematic representation of the classic SELEX protocol

During the selection process, the DNA library pool is incubated with the target of interest under conditions favorable for binding. Purified target is usually immobilized onto a solid support matrix such as agarose to permit partitioning. Impure samples can easily yield aptamers for unintended targets and a major goal of SELEX includes elimination of non-specific binding. After this, DNA-target complex is separated from the unbound sequences. Non-binding sequences elute

out while sequences with high affinity for the target molecule are removed in a wash off step using chromatography²¹, attraction to a magnetic field²², or centrifugation²³. Under optimal conditions, non-specific and non-binding sequences can be removed from the nucleotide pool quite early. The high binding sequences are then amplified by polymerase chain reaction (PCR) to create a new candidate mixture. This process is then repeated about 4 – 20 times. Each repetition contains a DNA pool with fewer unique sequences, which have a relatively high affinity for the target. This is called positive selection. Over the past three decades, various SELEX methods have been developed to shorten selection time and increase success rate. In 1992, Ellington and Szostak⁶ selected oligonucleotides for solid support agarose matrix. The non-specific binding sequences that bind to agarose were removed during the wash. As a result, aptamers obtained through the negative selection had affinity about 10-times higher than that of aptamers without negative selection. Counter SELEX method was introduced in 1994 by Jenison *et al.* which has an additional step where structurally similar targets are incubated with aptamers to discriminate non-specific sequences²⁴.

As targets for SELEX advanced from small molecules to whole cells, new SELEX techniques (i.e. cell-SELEX) have emerged. In cell-SELEX, cancer cell line is often used as the target to generate aptamers that can distinguish between cancer and healthy cells^{25,26,27}. Various analytical techniques have been merged with SELEX process to reduce time needed for selection, such as CE-SELEX^{28,29,30,31}, non SELEX^{32,33}, Flu-Mag SELEX²², *in silico* SELEX³⁴. Modifications have been made to

generate aptamers with different functions (μ FFE-SELEX³⁵, Capture SELEX³⁶) and to increase process throughput (Sweep-CE-SELEX³⁷). These changes yielded different aptamers such as spiegelmers^{38,39}, SOMAmers⁴⁰⁻⁴², thioaptamers⁴³ and X-aptamers⁴⁴.

1.3 Aptamer Targets

Aptamers bind with high specificity and affinity, meaning that aptamers discriminate for their target and bind to it. Unlike antibodies, which require antigens, epitopes and immune response for their targets, aptamers structurally conform to wide variety of shapes such as hairpins, bulges, pseudoknots and G-quadruplexes⁴⁵. Aptamers are capable of binding any target as well as distinguishing between closely related molecules, such as conformational isomers⁴⁶, targets containing different functional groups⁴⁷, or even an amino acid mutations⁴⁸. Figure 1-2 shows the number of aptamers for various targets selected between 1990 and 2019. The list was generated using aptagen.com/aptamer-index and accessed on June 9, 2019.

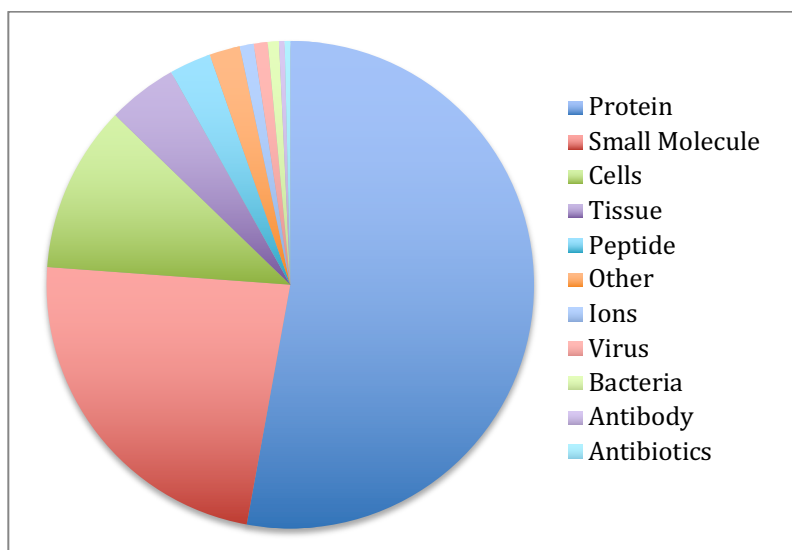


Figure 1-2: Pie chart representation of various types of aptamer targets that have been selected between 1990 and 2019.

The most common binding force between aptamers and target molecules is hydrogen bonding, which is important for stability of the aptamer. This is shown by Nagatoishi *et al.* in an example of thrombin binding to the thrombin aptamer^{49,50}. Electrostatic interaction is another force involved in the binding of a target to an aptamer. Commonly, the salt concentration of buffer can influence intensity of the electrostatic interactions as binding affinity decreases when more salt is added to the solution⁵¹. Other binding forces such as van der Waals forces, $\pi - \pi$ stacking and hydrophobic effect may also affect binding of the aptamers to their target. These binding forces are affected by many factors such as metal ion strength, pH value, temperature, and different forces may occur simultaneously in aptamer-target binding complex.

1.4 Applications of Aptamers

1.4.1 Aptamers as Therapeutic Agents

Aptamers are ideal as therapeutic agents, pharmaceuticals and biosensors since they are easier and cheaper to make than antibodies and are neither immunogenic nor toxic⁵². However, use of aptamers stretches beyond analytical applications. Aptamers as drugs, target delivery systems and imaging agents are constantly being investigated.

The first aptamer used as a diagnostic tool was developed by Bruno *et al.* in 1999 to detect anthrax spores⁵³. Wan *et al.* used aptamers to identify cancer cells with high sensitivity and specificity using epidermal growth factor receptor that is overexpressed in many cancer types⁵⁴. Aptamers can also be used as targeted drug delivery system. One example of this is the doxorubicin aptamer. Using 2'-fluoropyrimidine-modified RNA aptamer that targets prostate specific membrane antigen (PSMA) Bagalkot *et al.* showed that doxorubicin aptamer could specifically target PSMA with high affinity and specificity⁵⁵. Huang *et al.* linked doxorubicin to the sgc8c DNA aptamer targeting T-cell acute lymphoblastic leukemia cells, which resulted in reduced cellular toxicity to the non-target cells⁵⁶.

Another manner in which aptamers can be used is as drug delivery tools by linking them to the gold nanoparticles (AuNPs). Gold nanoparticles are stable, biocompatible, have low toxicity and are easily modified. For example, Dam *et al.*

attached AS1411 anti-nucleolin aptamer to the gold nanostar core in order to deliver a drug to the cancer cell nucleus and cause cancer cell death⁵⁷.

A prominent landmark in application of aptamers in therapeutics is drug Macugen®, a vascular endothelial growth factor (VEGF)-specific aptamer for the treatment of neovascular age-related macular degeneration (AMD). This drug was approved by the Food and Drug Administration in 2004. So far only 10 more aptamers have been approved in clinical trials for treatment of various conditions including cancer, coagulation, inflammation and macular degeneration (Table 1)⁵⁸.

Aptamers can also be isolated based on their kinetic parameters (SOMAmers). Their slow off-rate has helped in isolation of many biological targets with high affinity⁴¹. The major modifications that allow this are substitutions of hydrophobic components within the base. For example, the C-5 position in uracil is modified to include groups such as benzylaminocarbonyl, naphthylmethylaminocarbonyl, tryptaminocarbonyl and isobutylaminocarbonyl⁵⁹. SOMAmers interact with their target through hydrophobic effect and are less polar than standard aptamers^{40,41}.

Table 1-1: List of aptamers approved for clinical trials (adapted from Reference 58)

Name	Form	Target	Condition	Phase
Macugen	RNA	Vascular Endothelial Growth factor	Age - related macular degeneration	Approved in US and EU
E10030	DNA	Platalet derived growth factor	Age - related macular degeneration	Phase II/III
REG1	RNA	Coagulation factor IXa	Acute coronary syndrome	Phase III terminated, on hold due to serious anaphylactic reactions
ARC1905	RNA	Complement component 5	Age - related macular degeneration	Phase III
AS1411	G rich DNA	Nucleolin	Acute myeloid leukemia	Phase II
ARC1779	DNA	A1 domain of von Willebrand factor	Von Willebrand disease	Phase II
NOX-E36	L-RNA (Spiegelmer®)	CCL2	Chronic inflammatory diseases	Phase II
NOX-A12	L-RNA (Spiegelmer®)	CXCL12 or SDF-1	Multiple myeloma and non-Hodgkin's lymphoma	Phase II
NU172	Unmodified DNA	Thrombin	Heart disease	Phase II
NOX-H94	L-RNA (Spiegelmer®)	Hepcidin peptide hormone	Anemia	Phase II
ARC19499	RNA	TFPI	Hemophilia	Phase I

1.4.2 Aptamers as biosensors

One of the most common uses for aptamers is as sensors to detect and quantify analytes in solution. Fluorescence, colorimetry and electrochemical detection are often used as biosensing methods^{3,60,61}. Due to their high affinity and specificity to targets, antibodies are often used as biosensors, but they are unable to detect small molecules. Similarly to antibodies, aptamers are used as biosensors to detect proteins and cells but they are also able to detect small molecules and ions such as ATP, Na⁺, cocaine, theophylline⁶²⁻⁶⁴. But unlike antibodies, aptamers can undergo conformational changes upon binding to their target. The structural change that occurs upon binding of the aptamer to the target results in signal generation, which is needed for detection. For example, in fluorescence, an aptamer can have a fluorophore and/or quencher and binding of the target would result in increased fluorescence or quenching depending on where the target binds. A change in aptamer conformation can then be detected using electrochemical detection. For example, electroactive reporters, such as methylene blue, can be attached covalently to the aptamer in order to detect binding using signal on/off strategies^{65,66}.

Gold nanoparticles (AuNP) are often employed as colorimetric indicators due to their excellent extinction coefficients and strongly distance-dependent optical properties. Aptamers are often immobilized on the AuNP through the use of a thiol group⁶⁷. The target interacts with AuNP–aptamer complex where aptamer is utilized for binding and AuNP as colorimetric indicator. Upon target binding color change from red to blue occurs^{3,68,69}.

1.4.3 Riboswitches

Research conducted in early 2000 revealed that aptamers are also present in nature^{70,71}. Riboswitches are regulatory segment of mRNA that binds to a small molecule. They are directly involved in regulating its activity in response to small molecule concentrations. Most known riboswitches occur in bacteria but have been discovered in archaea, plants and certain fungi. These sequences fold into different complex structures, interact with small molecules and control downstream regions⁷². They have transcriptional and translational control in the presence of a small molecule metabolite and undergo conformational changes upon target binding. Riboswitches contain two parts: aptamer portion and expression platform, which is located downstream of the aptamer where it assesses the ligand binding status of the RNA and regulates gene expression accordingly⁷³. The aptamer portion can be structurally preorganized in the absence of ligand, but ligand binding induces some structural change that influences folding and function of the expression platform. Such case was observed for most common riboswitch class, coenzyme thiamin pyrophosphate (TPP), which controls splicing^{70,71,74}.

1.5 The Cocaine-Binding Aptamer

The cocaine-binding aptamer is a DNA aptamer that contains 3 stems built around a 3-way junction. This aptamer was selected by Stojanovic *et al.* in 2000 using classic SELEX to select for cocaine but not its common metabolites benzoylecgonine and ecgonine methyl ester⁷⁵. Their MNS 4.1 sequence contains 38 nucleotides and binds to cocaine with the affinity of 5 μM ⁷⁶. It was proposed to be only partially structured in free state and to fold in the presence of cocaine (Figure 1-3). Stem 2 has only Watson–Crick base pairs while stems one and three contain non-canonical base pairs.

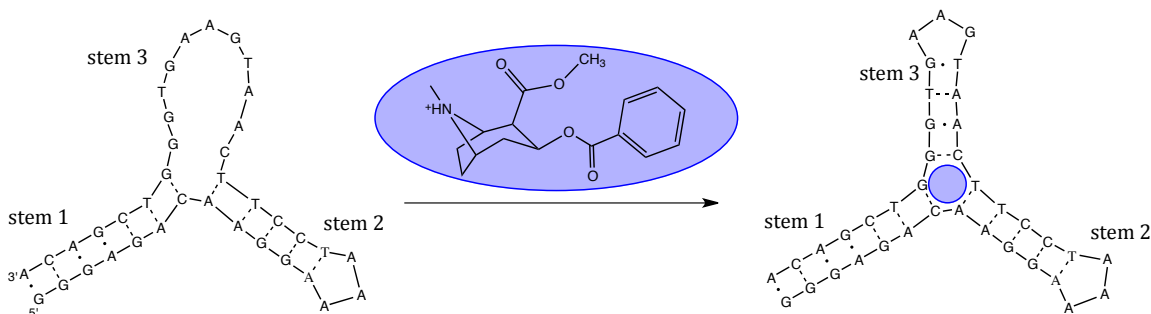


Figure 1-3: Structure of the original cocaine-binding aptamer proposed by Stojanovic *et al.* The blue circle represents the binding site of cocaine. Dashed lines represent Watson-Crick base pairs. Dots represent non-canonical base pairs. (Adapted from Reference 73)

In 2010, Neves *et al.* used NMR and ITC to study the structure of the cocaine-binding aptamer⁷⁷. Their NMR experiments indicated that the aptamer contains two non-canonical AG base pairs and T20 was not base paired in the absence of the ligand. They proposed a new secondary structure that contains three stems built around a

three-way junction, which contains the binding site of cocaine. Several ITC studies by the same group have demonstrated that conversion of the non-canonical base pairs (except those located at the binding site) in the original MNS4.1 to Watson-Crick base pairs increases the binding affinity and aptamer stability⁷⁸. Using NMR, fluorescence and ITC studies it has been shown that the binding mechanism is controlled by stem 1^{77,79}. If stem one contains 4 or more base pairs, the aptamer retains its secondary structure both in presence and absence of the ligand (Figure 1-4a). When stem one is shorted to three base pairs or less, the aptamer is partially folded in free state and ligand binding induces folding (Figure 1-4b). The variant of the cocaine-binding aptamer, MN4 has six base pairs in stem 1 and binds cocaine with affinity of 5 μ M.

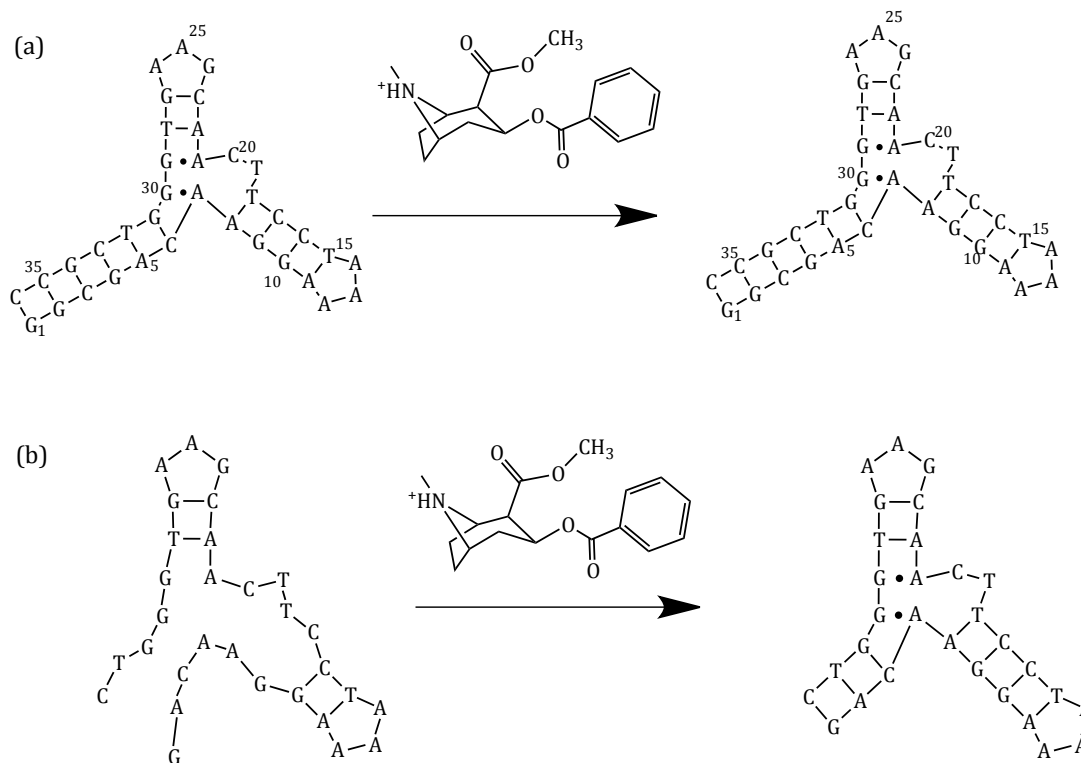


Figure 1-4: Structures of (a) MN4, long stem 1 variant and (b) MN19, short stem 1 variant of the cocaine binding aptamer proposed by Neves *et al.* (Adapted from Reference 77)

Two research groups determined that the cocaine-binding aptamer binds ligands other than cocaine. Stojanovic *et al.* used the original MNS4.1 cocaine-binding aptamer to build a sensor for hydrophobic ligands including deoxycholic acid⁸⁰. In 2011, Reinstein *et al.* have shown that four base pairs in stem 1 long variant of the cocaine-binding aptamer containing single non-canonical AG base pair binds steroid deoxycholic acid but not cocaine⁸¹. Although Stojanovic *et al.* showed that the cocaine-binding aptamer also binds quinine, Reinstein *et al.* determined that the binding affinity of quinine for the cocaine-binding aptamer is about 50-fold tighter than cocaine^{82,83}. Competitive binding studies demonstrated that the two ligands compete for the same binding site.

Since its selection, the cocaine-binding aptamer has been used in numerous studies where fluorescence, colorimetric and electrical signaling were used to detect the presence of cocaine. In 2001, Stojanovic *et al.* designed a variant of the cocaine binding aptamer by attaching a fluorophore on the 5' end and a quencher on the 3' end⁷⁶. In the absence of cocaine, fluorescence was observed, while upon binding of the ligand, quenching occurred indicating that the folding of the aptamer occurs. A year later, the same group showed that cyanine dye weakly bound to the original MNS4.1 aptamer could be displaced by cocaine, showing change in the intensity in visible spectrum⁸⁴. Stojanovic *et al.* also demonstrated that even though aptamer is split at the stem loops, it would assemble in the presence of cocaine and bind with affinity of 5 μM ⁷⁵. The ability to split and assemble the aptamer was also shown by Sharma and Heemstra who split the cocaine-binding aptamer into two fragments and using azide-alkyne cycloaddition promoted ligation⁸⁵. Baker *et al.* created reagentless biosensor for the detection of cocaine in blood serum, saliva and in the presence of other contaminants⁸⁶. In 2018, Gülbakan *et al.* analyzed interaction of short stem 1 variant of the cocaine-binding aptamer with quinine by native electrospray ionization mass spectrometry (ESI – MS) and obtained binding affinity of 8.5 μM ⁸⁷. Recently, Qui *et al.* reported using the original cocaine-binding aptamer MNS4.1 – invertase biosensor coupled with personal glucose meter to quantify quinine in reclaimed wastewater⁸⁸.

1.6 Bioanalytical techniques used to characterize aptamer–target interactions

There are several methods used to analyze interactions between an aptamer and a target. The affinity between aptamer and target is usually measured and expressed as a dissociation constant, K_d , shown in equation (1):

$$K_d = \frac{[A][L]}{[AL]} = \frac{1}{K_a} \quad (\text{Eq.1})$$

where [A] represents aptamer concentration, [L] is ligand concentration and [AL] is aptamer – ligand concentration. There are several methods that can be used to determine the binding affinity of an aptamer for a selected target through the measurement of affinity constant, kinetics or conformational changes during the formation of complexes. The most widely used technique used to probe interactions between aptamers and their targets is surface plasmon resonance (SPR). Here, an aptamer is immobilized on a thin gold film. By flowing various concentrations of a ligand, the change in refractive index is measured as the complex forms. These experiments provide K_a , K_d , k_{on} , k_{off} , analyte concentration and stoichiometry. Two of the most important structure analyzing methods are nuclear magnetic resonance (NMR) and X-ray crystallography. Both have been used to determine structural characteristics of aptamers in their free state as well as bound to ligand. For example, Lin and Patel used NMR to study structure of ATP-binding DNA aptamer bound to AMP⁸. Long *et al.* solved the crystal structure of the thrombin binding aptamer bound to thrombin at 1.9Å resolution⁸⁹. High performance liquid

chromatography (HPLC) can also be used to analyze aptamer-target complex. The binding between the aptamer and a target is shown with different peaks. Deng *et al.* have used HPLC to analyze adenosine binding to a DNA aptamer with varying parameters such as pH, ionic strength and Mg^{+2} concentration⁹⁰. Other analytical methods to study aptamer-target complexes include, but are not limited to, capillary electrophoresis⁹¹, mass spectrometry⁸⁷, quartz crystal microbalance⁹², fluorescence spectroscopy⁹³, small-angle X-ray scattering^{82,94}, etc. Each of these methods has its own advantages and disadvantages but this thesis shall focus on the use of isothermal titration calorimetry (ITC) to study aptamer – ligand interactions.

1.7 Isothermal Titration Calorimetry

All work presented in this section has been published in the article listed below⁹⁵

- **Slavkovic, S.** and Johnson, P.E. “Isothermal titration calorimetry studies of aptamer-ligand interactions: practicalities and pitfalls.” *Aptamers* **2**, 45-51 (2018)

Isothermal titration calorimetry (ITC) is a versatile technique for performing binding studies, as it is easy to perform a series of experiments under many different solution conditions. It is also a non-destructive label-free technique that provides the stoichiometry of interaction and a complete set of the thermodynamic binding parameters: the equilibrium binding constant (K_a or K_d) and the change in enthalpy (ΔH) and entropy (ΔS) of binding. These benefits do come with the disadvantages that ITC uses a lot of sample compared with many spectroscopic methods and it has a low throughput of 2 – 4 runs performed per day.

In a typical ITC instrument (Figure 1-5a) two cells are placed in an adiabatic jacket. One of these cells is a reference cell while another is loaded with sample. These cells are maintained at a constant temperature (Figure 5a; $\Delta T_1=0$). During an experiment, ligand is titrated into the sample cell in known aliquots (Figure 1-5b). In an exothermic binding event, the temperature in the sample cell increases upon addition of ligand causing a decrease of power to the heater around the sample cell that maintains the reference and sample cells at an identical temperature. As a result, the raw experimental data is comprised of a series of negative spikes, where

every spike corresponds to one ligand injection (Figure 1-5c, top). For an endothermic reaction, the opposite occurs and a positive peak results. These ligand injections are performed repeatedly and upon the ligand binding sites in the aptamer becoming saturated, the heat signal decreases until only the heat of dilution of the ligand is observed. Integration of the power supplied per unit time yields the heat per mole of injectant with respect to the molar ratio (Figure 1-5c, bottom). Data fitting is performed on the integrated heats to quantify the binding parameters.

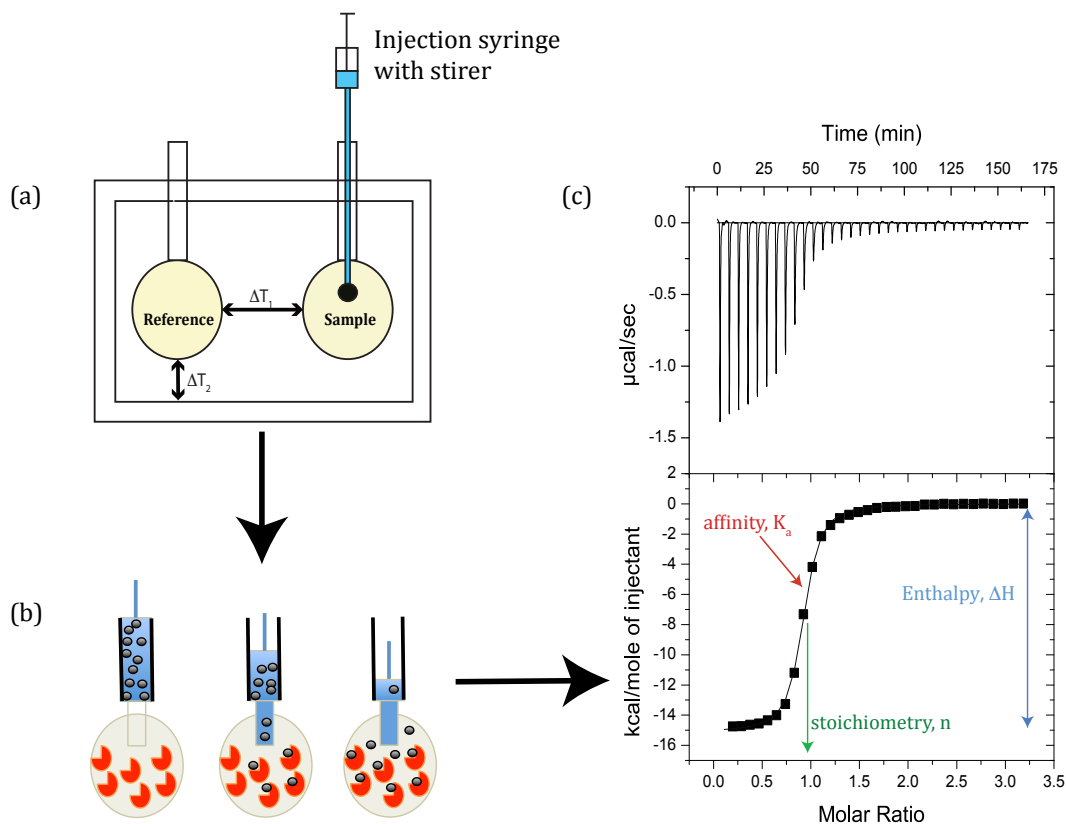


Figure 1-5: (a) Diagram of a typical ITC instrument. ΔT_1 corresponds to the temperature between the two cells. ΔT_2 corresponds to the difference between cell and adiabatic jacket. Both ΔT_1 and ΔT_2 are zero during an experiment. (b) Depiction of binding during the gradual injection of ligand into the ITC cell containing aptamer. (c) Thermogram showing interaction of a cocaine-binding DNA aptamer with its ligand⁹⁶. On the top is the heat from each injection with respect to time with the heat of dilution subtracted. On the bottom are the integrated heats for each injection (filled squares) fitted to a 1:1 binding model (solid line).

1.7.1. General Sample Preparation. There are several aspects to be considered in sample preparation for ITC analysis: optimal aptamer and ligand concentrations, choice of buffer and if needed, organic solvents. According to the VP-ITC manual (MicroCal), the optimal aptamer concentration should be 10 to 50 times the anticipated K_d value. A good starting concentration range for aptamer-small molecule interactions is 10-20 μM . These concentrations may be adjusted depending on the binding enthalpy of the interaction between aptamer and ligand, as well as the binding constant. For the ligand, its concentration should be 15-20 times the concentration of the aptamer in the sample cell. If the ligand concentration is much larger than the aptamer concentration, saturation will occur too soon producing a steep curve that saturates quickly and will yield an inaccurate fit. Based on theoretical analysis, Tellinghuisen⁹⁷ showed that the final excess of ligand over aptamer ($[X_0/M_0]$) could be calculated using equation (2):

$$R_m = \frac{6.4}{c^{0.2}} + \frac{13}{c} \quad (\text{Eq. 2})$$

where R_m is the ratio of total concentrations in the cell after the last injection and c is defined below. When choosing these initial concentration parameters, it also useful to consider the c -value (Eq. 3). This unitless parameter defines the shape of the binding curve (Figure 1-6) and is the product of the binding constant K_a , total aptamer concentration at the start of experiment M_{tot} and the stoichiometry parameter, n :

$$c = K_a M_{\text{tot}} n \quad (\text{Eq. 3})$$

An optimal c -value lies between 10 and 100, though there is discussion in the literature about this^{98-100,101}. High c -values (over 500) give binding curves too steep to accurately determine affinity, although stoichiometry and enthalpy are well determined. Data acquired at c -values below 10 results in a shallow titration curve where all three parameters (n , K_a and ΔH) are poorly determined. These three fitting parameters are directly proportional to ligand concentration accuracy, while aptamer concentration accuracy only affects stoichiometry value.

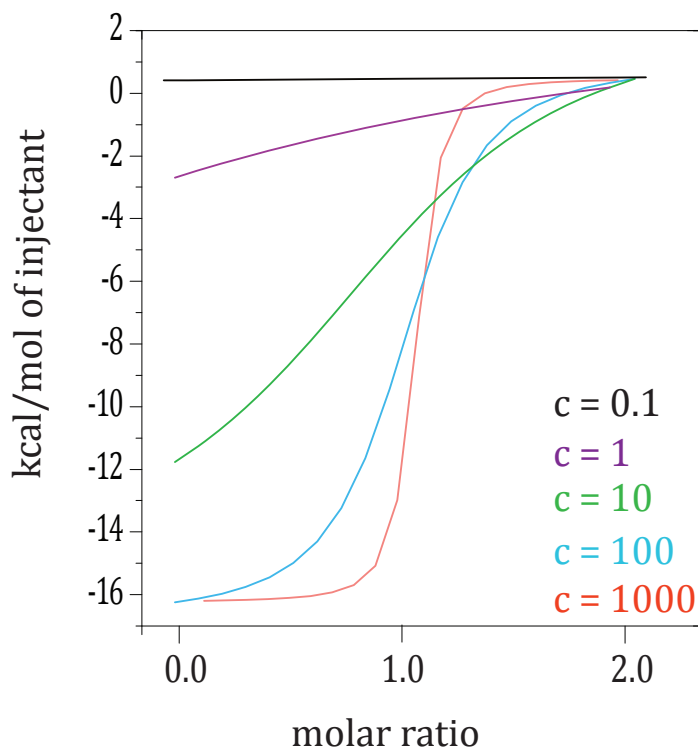


Figure 1-6: Illustration of the effect of the c -value on the shape of the titration curve.

The VP-ITC instrument requires a sample volume of ~ 2 mL of aptamer even though the cell measures 1.44 mL in volume. The injection syringe volume is 290 μL , but

600 μL of ligand should be prepared. These larger volumes are necessary in order to fill both sample cell and syringe in a bubble-free manner. Other ITC instruments have different cell and syringe volumes, this should be checked prior to sample preparation.

1.7.2 General ITC Experimental Setup. In a typical ITC experiment, the ligand is titrated into the aptamer. Reversing the contents of the cell and syringe typically does not change the fitted parameters but can be done to ensure there are consistent results. If solubility of the ligand is a concern, the aptamer should be titrated into ligand, i.e. the least soluble material is used as titrate (in the cell) and the more soluble as titrant (in the syringe). This is set at the start of an ITC experiment. Other instrumental parameters set by the user are number of injections, run temperature, reference power, initial delay, spacing, injection volumes and concentration of samples. Non-optimal or improper settings can have great impact on data quality.

The experimental temperature is determined by what the user desires and the stability of the aptamer. However, binding constants and the enthalpy of binding (ΔH) are temperature dependent. The temperature can be set between 2 to 80°C. Samples should be cooled prior to use to below the experimental temperature as it reduces ITC equilibration time. The total number of injections should be set to a total of 15-20 but this will also depend on each injection volume and the total volume of the syringe. If the aptamer and ligand interact in a 1:1 molar ratio, an

individual injection volume should be chosen such that this ratio is achieved in 8-12 injections. The volume of each injection is kept constant at 7-12 μL , with the exception of the first injection, which is usually set at 1-2 μL . Data from the first injection is discarded prior to data analysis as it has been shown that it results from a volumetric error due to the backlash in the motorized screw that drives the syringe plunger¹⁰². Feedback mode/gain is another parameter that is set by the user. For a typical ITC binding experiment, it is set to be high as it provides the fastest response time. For studies involving kinetics, this parameter is set at low or none.

Spacing refers to the time between consecutive injections. The time should be large enough to allow the signal to return back to baseline. This delay depends on the size of the peak – higher sample concentration produces larger peaks, which requires longer time between injections. Usually 300 second spacing is sufficient, but in some cases a longer time is required (Figure 1-7).

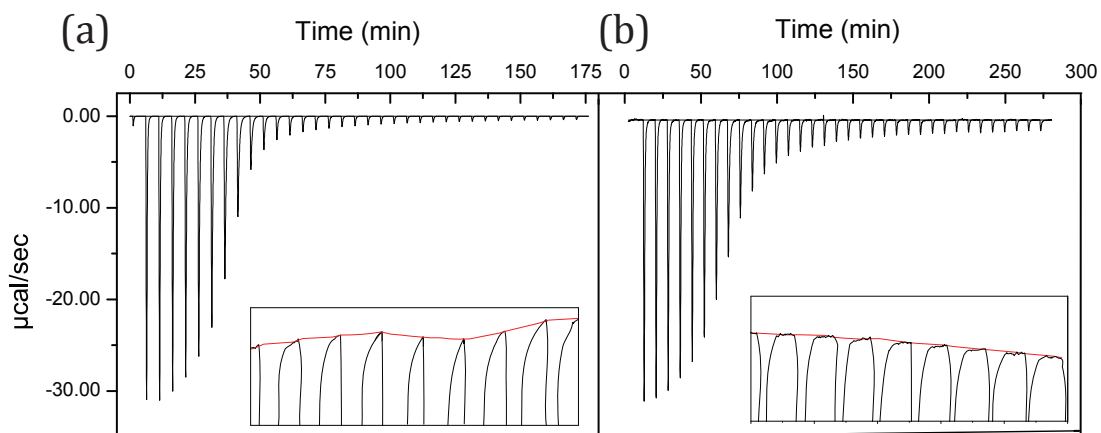


Figure 1-7: Adjustment of the time between injections. (a) An example of the interaction of the MN4 aptamer at 200 μM with quinine with the time between injections set at 300 s. The heat from an injection does not return to the baseline before the next injection takes place. In (b) the same experiment is performed with the spacing set at 480 s.

Reference power is the amount of power that is supplied to the heater in the reference cell. A typical setting is 25-30 $\mu\text{cal/sec}$ for exothermic reactions. Endothermic reactions require a lower reference power setting. Stirring speed is typically set at 300 rpm for aqueous solutions. Faster speeds will increase baseline noise levels, but it may be necessary if the sample is more viscous than water.

Measurement of the heat of dilution of the ligand is an important aspect of any ITC experiment as large or non-linear heats of dilution of ligand can sometimes mask binding. Depending on the ligand, there are two methods that can be used to perform this correction: external and internal heat of dilution. External heat of dilution involves performing a separate experiment where ligand is titrated into buffer using the same conditions as the binding experiment (Figure 1-8a, 1-8b). An

internal heat of dilution is obtained by extending the experiment by 5-10 injections after binding is complete (Figure 1-5c). Using a linear extrapolation of the heats of these injections a correction is applied to whole experiment. This method can be used only if heats of dilution are small and linear.

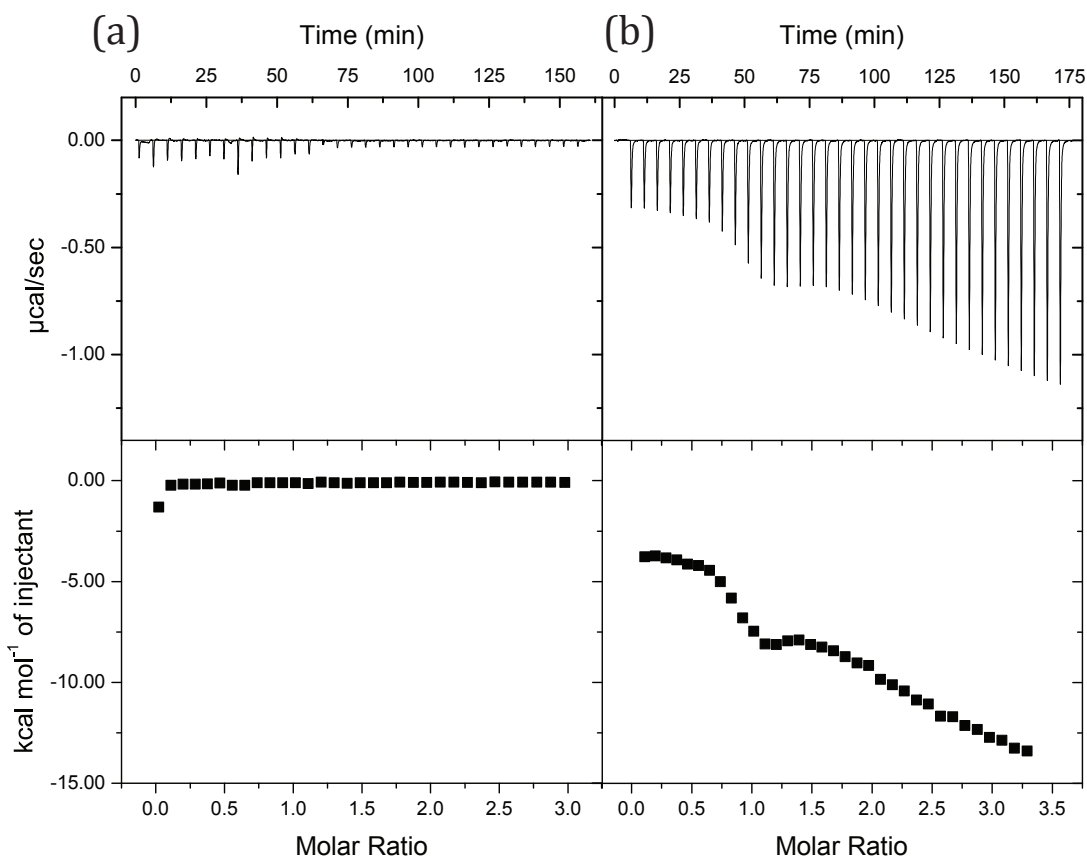


Figure 1-8: Examples of different possible heats of dilution. In (a) is a titration of quinine in buffer (20 mM TRIS (pH 7.4), 140 mM NaCl, 5 mM KCl) into a sample of the same buffer. This produces a small heat of dilution. The heat of dilution run in (b) is a sample of piperazine into same buffer as in (a) but produces large and non-linear heat of dilution.

1.7.3. Cell Cleaning. A critical step in obtaining quality ITC data is cleaning both sample cell and injection syringe before loading samples. While nucleic acid aptamers are usually quite soluble and not prone to contaminating the cell (unlike protein samples), the ligands involved in binding may be less soluble and can accumulate on the sample cell wall. There are two types of cleaning: standard and stringent cleaning.

Standard cleaning is performed before every use. It involves flushing both sample cell and injector syringe with ddH₂O, washing with 200 mL of 1% Contrad 70 solution and flushing with about 1 L of ddH₂O. Loading syringes should also be cleaned at this time. During an ITC experiment, raw data is plotted as differential power (DP) versus time. At the beginning of a titration, the user sets reference power, which is the amount of power continuously supplied to reference cell heater. If, for example, this value is set at 30 μ cal/sec, clean cell the baseline should be close to this value or 1-2 μ cal/sec lower. If the initial baseline is different from reference power, stringent cleaning is performed.

For stringent cleaning, the cell and injection syringe are flushed with 200 mL of 5% Contrad 70 then the cell is filled with the same 5% Contrad 70 cleaning solution and left to soak for overnight at 60-70°C. The sample cell and syringe should then be exhaustively flushed with ddH₂O (at least 1.5 L).

Finally, before filling with samples, both the cell and syringe should be rinsed with buffer and thoroughly emptied to avoid unwanted dilution. A useful check of instrument cleanliness is an ITC run of water into water (Figure 1-9). This run should produce very little heat and have the integrated heats very close to zero.

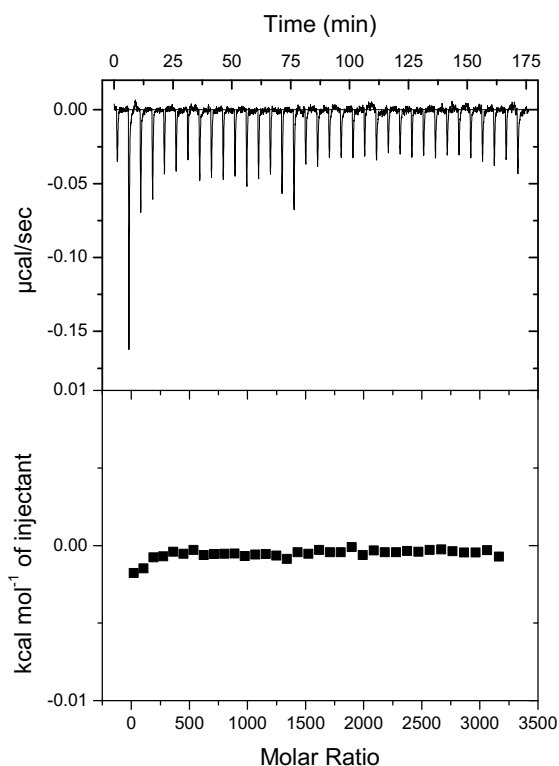


Figure 1-9: Titration of water into water is a good check of ITC cleanliness. A clean ITC sample cell and needle results in a very small heat signal with the integrated heats of ddH₂O titrated into ddH₂O being close to zero.

1.7.4. Data Analysis. Data analysis is typically performed with software supplied by the instrument manufacturer. For MicroCal instruments, the software employed is Origin. The software normalizes the heat of binding with respect to ligand concentration. It also sets the baseline and integrates each peak from the baseline. Most of the time the baseline is set appropriately automatically, but sometimes it

needs to be set manually to exclude integration of artifacts. The heat of dilution should then be subtracted and finally the data fitted to the appropriate binding model.

For ligand binding to an aptamer with single binding site the following equations are used:

$$K = \frac{f}{(1-f)[X]} \quad (\text{Eq. 4})$$

$$[X_t] = [X] + nf[M_t] \quad (\text{Eq. 5})$$

Combining equations (4) and (5) gives

$$f^2 - f \left[1 + \frac{X_t}{nM_t} + \frac{1}{nKM_t} \right] + \frac{X_t}{nM_t} = 0 \quad (\text{Eq. 6})$$

The total heat of binding is given by equation (7), where ΔH is the molar heat of ligand binding.

$$Q = nfM_t\Delta HV_c \quad (\text{Eq. 7})$$

Solving quadratic equation for f and substituting this into equation (7) gives

$$Q = \frac{nM_t\Delta HV_c}{2} \left[1 + \frac{X_t}{nM_t} + \frac{1}{nKM_t} - \sqrt{\left(1 + \frac{X_t}{nM_t} + \frac{1}{nKM_t} \right)^2 - \frac{4X_t}{nKM_t}} \right] \quad (\text{Eq. 8})$$

The integrated data is then used to determine n , K_a and ΔH by least squares minimization. Once these values are determined, the Gibb's free energy (ΔG) and entropy (ΔS) are determined according to the standard relationships (equations 8 and 9):

$$\Delta G = -R T \ln K_a \quad (\text{Eq. 9})$$

$$\Delta G = \Delta H - T\Delta S \quad (\text{Eq. 10})$$

where $R = 1.987 \text{ cal K}^{-1} \text{ mol}^{-1}$ is the gas constant, and T represents temperature in K.

For one set of sites binding model, n value should be very close to 1. If n , for a 1:1 interaction, is closer to 0.8 or 1.2 then there is an issue with inaccurate concentrations of either ligand or aptamer. Provided the concentrations are correct, but the n value is very low, it indicates a low c -value due to weak binding for the aptamer concentration used (Figure 1-6). In this case, the concentration of both aptamer and ligand should be increased to appropriately determine the three fitting parameters. Sometimes with small molecule-aptamer interactions the affinity of the interaction is quite weak and working at higher concentrations is not practical. In this case low- c ITC methods are available, provided the n value is known^{98,99}. More complicated binding models such as two-site independent binding and cooperative binding are also available and equations are shown in Appendix A^{103,104}.

If ligand binding is too tight, the affinity may be difficult to measure directly by ITC. In that case, it is possible to employ a displacement titration methodology where the aptamer is pre-bound to a weaker binding ligand and titration of the higher affinity ligand involves ligand exchange on the aptamer^{104,105}. This method requires knowledge of the binding affinity of the weaker ligand in advance. For simple 1:1 interactions, Origin software has a built-in competitive binding model where the

information for the weaker binding ligand (n , K_a and ΔH) can be entered and parameters for the tighter ligand determined.

1.7.5. Troubleshooting. The most common problems encountered when running ITC experiment are low binding heats, buffer mismatch, air bubbles, impurities and issues with the addition of organic solvents. If the observed binding enthalpy is low, the experiment can become heat limited. This can be overcome by increasing the aptamer concentration or injection volume as both will increase the heat detected per injection. In order to obtain best results, the first few injections should be at least 10 $\mu\text{cal/injection}$ and have an average of at least 5 $\mu\text{cal/injection}$. This corresponds to a peak height of about 0.5 $\mu\text{cal/sec}$. A low heat of binding produces an isotherm that is not well defined, as the heats of dilution are comparable to the binding heats. In this case, a series of experiments using the same aptamer and ligand and same conditions but at different temperatures can be performed. Increasing the experimental temperature typically increases the magnitude of the binding enthalpy. This increases the raw heats, which in turn gives greater signal to noise and a better-defined binding curve. The experiment can also be performed at a lower temperature. A measurement of binding enthalpy at several temperatures, in order to obtain the change in heat capacity (ΔC_p) can be used to predict binding enthalpy at a particular temperature.

An essential part of sample preparation is the buffer match between the aptamer and ligand. This is achieved by dialyzing the aptamer in the buffer of choice and

using the same buffer to prepare the stock solution of ligand. The same buffer must be used to dilute both aptamer and ligand to appropriate concentrations and fill the reference cell. The pH value of all components must be matched to avoid additional heats from pH mismatch. Difference in pH between aptamer, ligand and reference cell, gives large heat effect that show as artifacts or drift in baseline (Figure 1-10a). Another issue to consider is the ionization heats of different buffers. If binding involves protonation or deprotonation, binding enthalpy will vary widely between buffers¹⁰⁶. It is best to choose a buffer, which give minimal additional heat contribution such as phosphate, citrate or acetate.

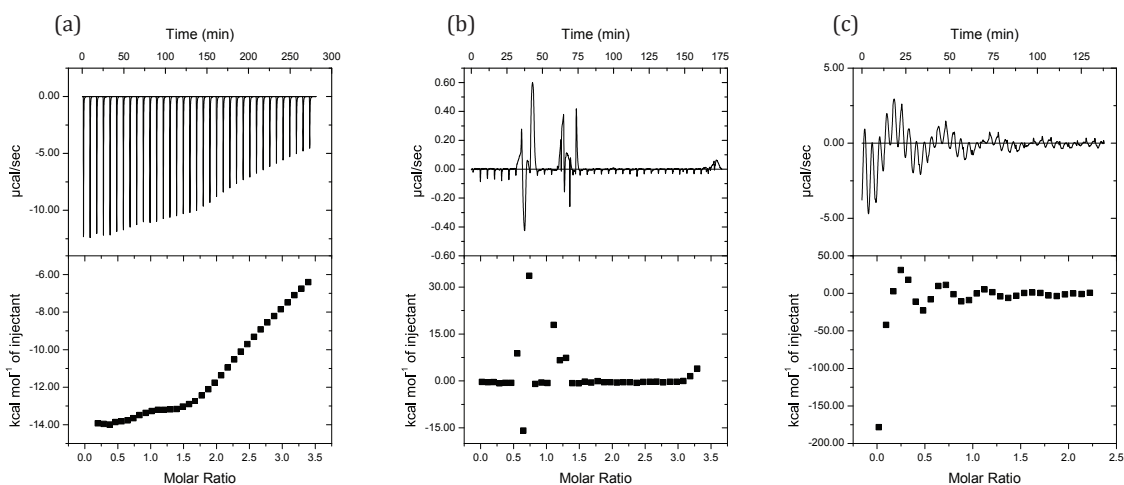


Figure 1-10: Examples of potential problems with ITC experiments. In (a) there is a pH mismatch between the aptamer in the sample cell and ligand injection syringe. In (b) there are large positive spikes indicating air bubbles in the sample cell. The negative spikes imply a possible impurity in the cell. In (c) there is an erroneous baseline. This indicates that both the sample cell and syringe require cleaning.

An additional problem that can be observed are large positive or negative spikes in the baseline (Figure 1-10b). The large positive spikes are usually indicative of air bubbles in the sample cell. The negative spikes can indicate that there are impurities

in the sample cell such as leftover cleaning solution from insufficient rinsing during the cleaning process. Finally, figure 1-10c is an example of a very poor baseline and results from the cell and syringe needing thorough cleaning. Figure 1-11 is an example of unstable baseline during final baseline equilibration, which occurs as a result of worn plastic part of injection syringe or bent needle.

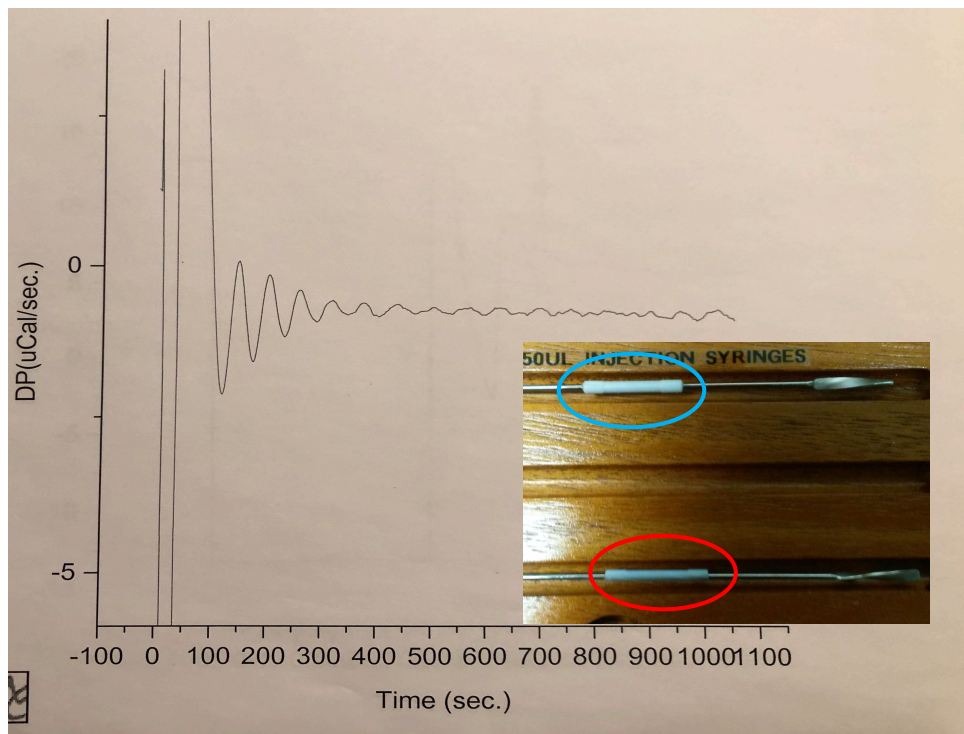


Figure 1-11: Baseline unable to equilibrate during final baseline equilibration. Plastic portion of injection syringe is worn (red circle). Blue circle shows plastic part of the new injection syringe.

Often, small molecule ligands require DMSO in order to solubilize. The final DMSO concentration should be minimal (up to 5% v/v) and added in the same amount to aptamer and ligand solution, as well as the reference cell. The heat of dilution run should also contain identical amounts of DMSO. Any mismatch in DMSO content will result in large heats produced (Figure 1-12a and 1-12b).

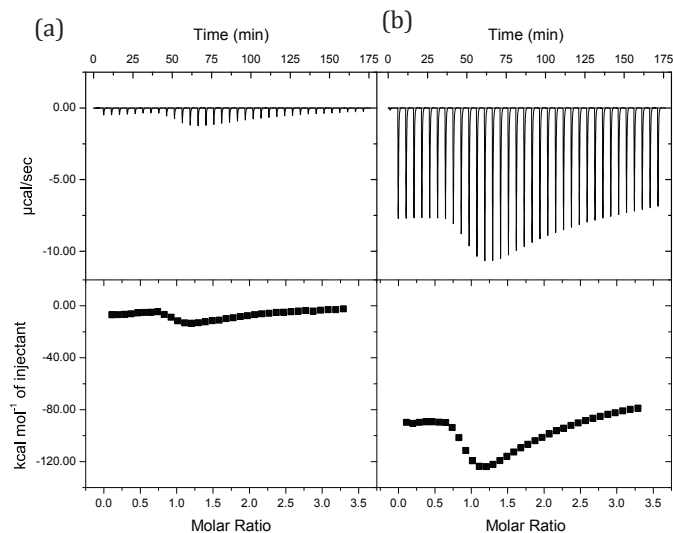


Figure 1-12: Example of a mismatch in DMSO concentration between the cell and needle. In (a) is a titration of a ligand into a DNA aptamer where both aptamer and ligand are prepared in buffer containing 3% (v/v) DMSO. In (b) is the same titration except there is 6% (v/v) DMSO in the syringe and 3% (v/v) DMSO in the cell. This mismatch in DMSO concentration produces very large apparent heats of binding.

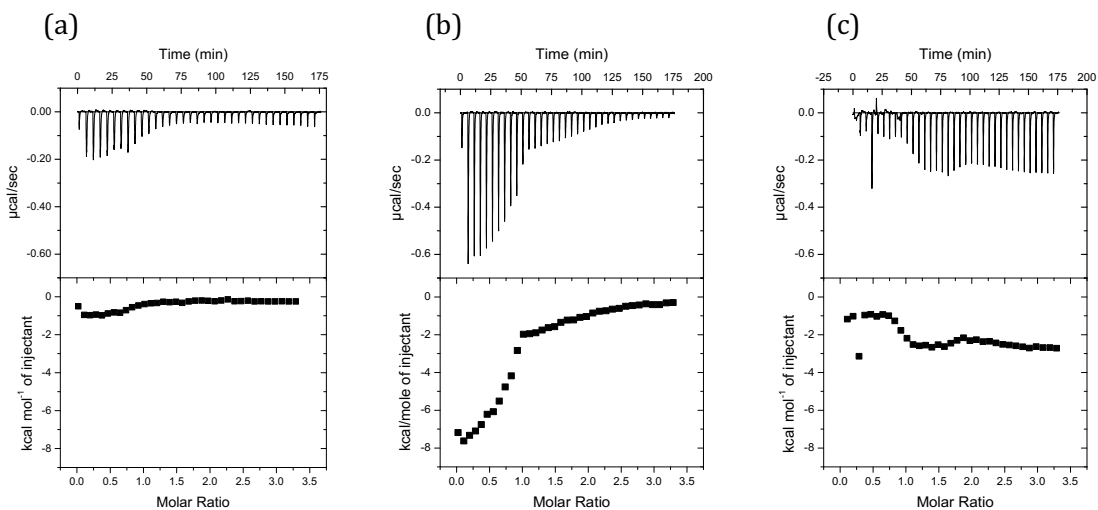


Figure 1-13: Examples of different solvent effect. In (a) is a titration of a amodiaquine into buffer containing 1% (v/v) methanol. In (b) is a titration of amodiaquine into buffer containing 1% (v/v) acetonitrile. In (c) is a titration of amodiaquine into buffer containing 1% (v/v) DMSO.

Other organic solvents can also be used to help solubilize ligands, but their concentration should be kept to a minimum. As the case with DMSO, these solvents should be added to both aptamer and ligand solutions and the reference cell at the same concentration. Different solvents produce non-linear heat of dilution as seen in Figure 1-13 and external heat of dilution should always be applied to whole experiment. ITC cells are inert to most solutions, however strong acids must be avoided, as they will damage instrument cells.

1.8 Thesis project

Aptamer technology has existed for over three decades; however, it is still poorly understood how aptamers function. They are selected for a specific target still, more often than not, they are incapable of selecting between common analogues. The goal of the work presented in this thesis is to understand aptamer-ligand interactions. The cocaine-binding aptamer was selected as the model system due to its ligand binding promiscuity and its ability to optimize length of stem 1 to improve the ligand selectivity. Isothermal titration calorimetry was chosen as it is a label free technique capable of determining the binding constant and thermodynamic parameters simultaneously. The work in this thesis explores binding of various quinine-based and non-quinine based ligands to the cocaine-binding aptamer in order to determine which parts of the ligand are essential for binding. The study included various quinine analogues and antimalarial compounds. Selectivity of the antimalarial compounds for the cocaine-binding aptamer is also probed. Different binding models are investigated to show that the ligand binding to the cocaine-binding aptamer follows independent binding model, while ATP and its analogues bind to the ATP-binding DNA aptamer cooperatively. Fine tuning of the binding affinity through use of the dangling nucleotide on either 5' or 3' end is also explored.

Chapter 2 **Methods and Materials**

2.1 Preface

This chapter includes general and specific methods for all subsequent chapters.

2.2. Aptamer preparation

All aptamer samples for ITC analysis have been purchased from Integrated DNA Technologies (IDT, Coralville, Iowa) with the standard desalting. The identity of aptamer samples was confirmed by mass spectrometry by the manufacturer. The DNA is dissolved in ~1 mL ddH₂O for a 1 micromole scale synthesis and then exchanged 3 times against 1 M NaCl using 3 kDa molecular weight cutoff Amicon-style concentrators to compete off any unwanted substances bound to the nucleic acid. The sample is then exchanged 4-6 times against ddH₂O and the final volume of this stock solution is ~0.25 mL from a 1 micromole scale synthesis. Aptamer is finally exchanged 3-4 times against appropriate buffer. The aptamer concentration is measured using UV spectroscopy and the known extinction coefficient provided by the manufacturer.

2.3. Ligand preparation

Unless otherwise stated all small molecule ligands were obtained from Sigma Aldrich. In all experiments, ligand solutions were prepared in the same buffer as the aptamer. Ligands dissolved in 100% DMSO were diluted to a final concentration

with appropriate buffer to a final DMSO concentration of 1 – 3% (vol/vol). The pH of buffers was adjusted at room temperature and not adjusted for temperature effects.

2.3.1. Cocaine, cocaine Analogues, quinine and quinine analogues

Stock solutions of compounds for binding experiments were prepared by dissolving the appropriate weight of each analogue in buffer containing 20 mM TRIS (pH 7.4), 140 mM NaCl, 5 mM KCl. Stock solutions of quinoline, 6-methoxyquinoline, 6-hydroxyquinoline, 6-aminoquinoline, acridine and benzo(h)quinoline were prepared by dissolving the appropriate weight of each analogue in buffer containing 1% DMSO, 20 mM TRIS (pH 7.4), 140 mM NaCl, 5 mM KCl.

2.3.2 Antimalarial compounds

Stock solutions of compounds for binding experiments were prepared by dissolving the appropriate weight of each antimalarial compound into either 100% DMSO or buffer containing 20 mM Tris (pH 7.4), 140 mM NaCl, 5 mM KCl. Amodiaquine, mefloquine, pyrimethamine, dapson, artemisinin and 2-deoxyartemisinin were diluted to experimental concentrations with buffer to a final DMSO concentration of 2 - 3% (v/v).

2.3.3 ATP, ADP, AMP, adenosine and adenine

Stock solution of ATP and its analogues for binding experiments were prepared by dissolving the appropriate weight into buffer consisting of 20 mM acetate (pH 5.5), 120 mM NaCl.

Adenosine used for dangling nucleotide study was dissolved in buffer containing 10 mM HEPES (pH 7.6), 100 mM NaCl, 2 mM MgCl₂.¹⁰⁷

2.4. Isothermal titration calorimetry experimental setup

2.4.1 General ITC setup

ITC binding experiments were performed using a MicroCal VP-ITC instrument in a manner similar to what was previously described⁹⁵. Samples were degassed before analysis with a MicroCal Thermo Vac unit for 5 minutes to avoid large spikes in the ITC baseline due to air bubble formation during the experiment. All experiments were corrected for the heat of dilution of the titrant. Titrations were performed with the aptamer samples in the cell and the ligand as the titrant, in the needle. All aptamer samples were heated in a 95°C water bath for 3-5 minutes and cooled in an ice water bath for at least 10 minutes prior to use in a binding experiment to allow the DNA aptamer to anneal in an intramolecular fashion (NOTE: aptamers where separate strands need to anneal should be left to cool to room temperature slowly). Unless otherwise noted, all binding experiments consisted of an initial delay of 60 s, first injection of 2 µL and 300 s delay. Subsequent 34 injections were 8 µL, spaced every 300 s. The first point was removed from all data sets due to the different injection volume and delay parameters.

2.4.2. Quinine analogues experiments

Binding experiments were performed at 15°C with the aptamer solution set at 20 µM and the small molecule concentration at 0.312 mM in a buffer of 20 mM TRIS

(pH 7.4), 140 mM NaCl, 5 mM KCl or 1% DMSO, 20 mM TRIS (pH 7.4), 140 mM NaCl, 5 mM KCl.

2.4.3. Cocaine and quinine two-site binding experiments

Cocaine binding experiments. These experiments were performed at 15°C with MN4 aptamer solutions of 56, 80 and 130 μM using ligand concentrations of 0.7, 1.4 and 2.8 mM in a buffer of 20 mM Tris (pH 7.4) with either 10 mM or 140 mM NaCl with a first injection of 30 μL .

Quinine binding experiments with varying c values. Experiments were performed at 15°C with MN4 and MN19 aptamer solutions of 11, 19, 42, 56, 80 and 130 μM using ligand concentrations of 0.156 to 3.12 mM in 5 mM Tris (pH 7.4).

Quinine binding experiments with varying NaCl concentrations. Experiments were performed at 15°C with MN4 aptamer solutions of 20 μM using a ligand concentration of 0.312 mM in 20 mM Tris (pH 7.4) with NaCl concentrations of 0, 25, 50, 75 and 140 mM.

2.4.4. The ATP-binding aptamer experiments

ATP3 binding experiments. The binding experiments used for global fitting were performed at 20°C with the aptamer solution at 10 to 100 μM using adenosine concentration of 0.312 to 2.8 mM. ATP, ADP and AMP binding experiments were performed at 70 μM aptamer concentration with 7 mM ligand concentration in 20 mM acetate (pH 5.5), 120 mM NaCl buffer. Adenine binding experiments were

performed at 70 μM aptamer concentration with 2.18 mM ligand concentration in the same buffer.

ATP6 binding experiments. All binding experiments were performed at 20°C with the aptamer solution at 100 μM using adenosine concentration of 5.4 mM in the above buffer.

ATP7 binding experiments. All binding experiments were performed at 20°C with the aptamer solution at 100 μM using ATP and adenosine concentration of 7 mM in the above buffer.

ATP9 and ATP10 binding experiments. All binding experiments were performed at 20°C with the aptamer solution at 100 μM using adenosine concentration of 2.18 mM in the above buffer.

ATP11 binding experiments. Binding experiments were performed at 20°C with the aptamer solution at 70 μM using adenosine concentration of 2.9 mM in the above buffer.

ATP17 binding experiments. All binding experiments were performed at 20°C with the aptamer solution at 100 μM using adenosine concentration of 3.12 mM in the above buffer.

2.4.5. Dangling nucleotide experiments

All ITC binding experiments were performed at 15°C. ITC experiments involving the cocaine-binding aptamer were performed with an aptamer concentration 98 μM

and using a quinine concentration of 1.12 mM. ITC experiments involving the ATP-binding aptamer were performed with an aptamer concentration 100 μ M and using an adenosine concentration of 3.12 mM.

2.4.6. Antimalarial compounds binding to the cocaine-binding aptamer experiments.

The binding experiments were performed at 15°C with the aptamer solution at 20 - 60 μ M using an antimalarial compound concentration of 0.312 to 0.936 mM. Chloroquine and primaquine were prepared in buffer containing 20 mM TRIS (pH 7.4), 140 mM NaCl, 5 mM KCl. Amodiaquine, mefloquine, pyrimethamine and dapsonsone were prepared in 100% DMSO and diluted to experimental concentrations with above mentioned buffer to a final DMSO concentration of 3% (v/v). Same concentration of DMSO was added to the aptamer solution and the reference cell to avoid buffer mismatch.

2.4.7. Various DNA structures binding to antimalarial compounds experiments.

The binding experiments were performed at 15°C with the aptamer solution at 20 μ M using ligand concentration of 0.312 mM. Chloroquine and quinine were prepared in buffer (20 mM TRIS (pH 7.4), 140 mM NaCl, 5 mM KCl). Amodiaquine and mefloquine were prepared in 100% DMSO and diluted to experimental concentration with above buffer to a final DMSO concentration of 3% (v/v). DMSO

was added to the aptamer solution and the reference cell at the same concentration to avoid buffer mismatch.

2.4.8. Artemisinin and 2-deoxyartemisinin binding experiments.

The binding experiments were performed at 15°C with the aptamer solution at 20 μ M using artemisinin and 2-deoxyartemisinin concentration of 0.312 mM. Both ligands were diluted to experimental concentration with 20 mM TRIS (pH 7.4), 140 mM NaCl, 5 mM KCl buffer to a final DMSO concentration of 2 – 3% (v/v). DMSO was added to the aptamer solution and the reference cell at the same concentration to avoid buffer mismatch.

2.5 Data fitting

ITC data following two-site binding model was fit to both cooperative and two-independent sites binding models developed by Freiburger *et al.*¹⁰³ using Matlab 14 software. Data following one-set of sites model was analyzed using manufacturer provided Origin 7.0 software.

Chapter 3 **Structure affinity relationship of the cocaine-binding aptamer with quinine derivatives**

3.1 Preface

All work presented in this chapter has been published in the article listed below⁹⁶.

- **Slavkovic S.**, Altunisik M., Reinstein O., and Johnson P.E. "Structure-affinity Relationship of the Cocaine-Binding Aptamer with Quinine Derivatives." *Bioorg. Med. Chem.* **23**, 2593-97 (2015)

3.2 Introduction

Ever since they were first developed, aptamers have been widely investigated and are used in numerous applications including medical treatments, pharmaceuticals and biosensors⁵². They bind to a variety of different ligands ranging from small molecules to whole cells³. However, it is not well understood how aptamers work. To study their structure and interaction with other molecules as well as biosensor applications^{75,76,84,108-114}, the cocaine-binding aptamer is often used as a model system. An important reason why the cocaine-binding aptamer has gained such wide usage is that it can be engineered to follow a structural switching or ligand-induced folding mechanism^{76,81,115,116}. The cocaine-binding aptamer is a DNA aptamer that contains 3 stems built around a 3-way junction containing a dinucleotide TC bulge with an adjacent pair of non-canonical GA base pairs. When stem 1 is shortened to three base pairs the free aptamer is loosely folded or unfolded and becomes more structured when it binds its target ligand⁷⁷. However, when stem 1 is longer the aptamer has its secondary structure formed in both the free and bound form⁷⁷. In addition, the aptamer can also be split into two or three

separate DNA strands with the annealing of the strands coupled with ligand binding^{78,85}. Of the many cocaine-binding aptamer constructs that have been studied, MN4 (Figure 3-1) is frequently used for detailed study as it displays excellent NMR spectra and binds cocaine slightly tighter than the originally reported aptamer⁷⁷.

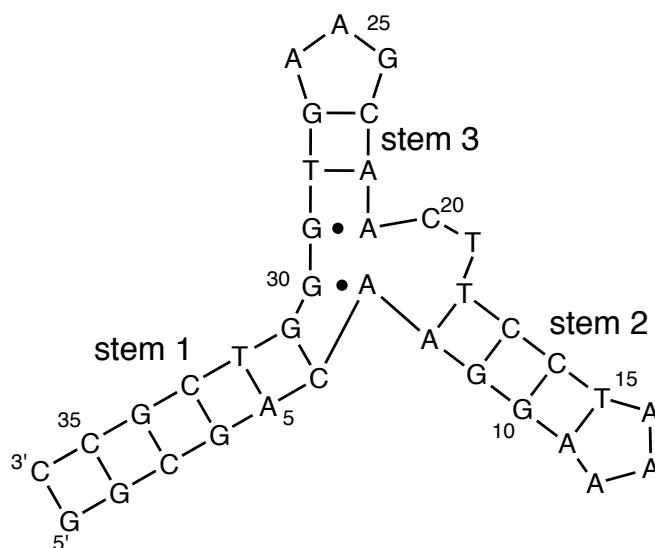


Figure 3-1: Structure of the MN4 cocaine-binding aptamer. Dashes indicate Watson-Crick base pairs while dots indicate non Watson-Crick base pairs.

Despite being selected for cocaine affinity, the cocaine-binding aptamer binds alternate molecules, including other alkaloids as well as steroids. Studies where the identity of the nucleotides at the three-way junction have been changed have taken advantage of this changed binding selectivity to build a sensor array^{80,117}.

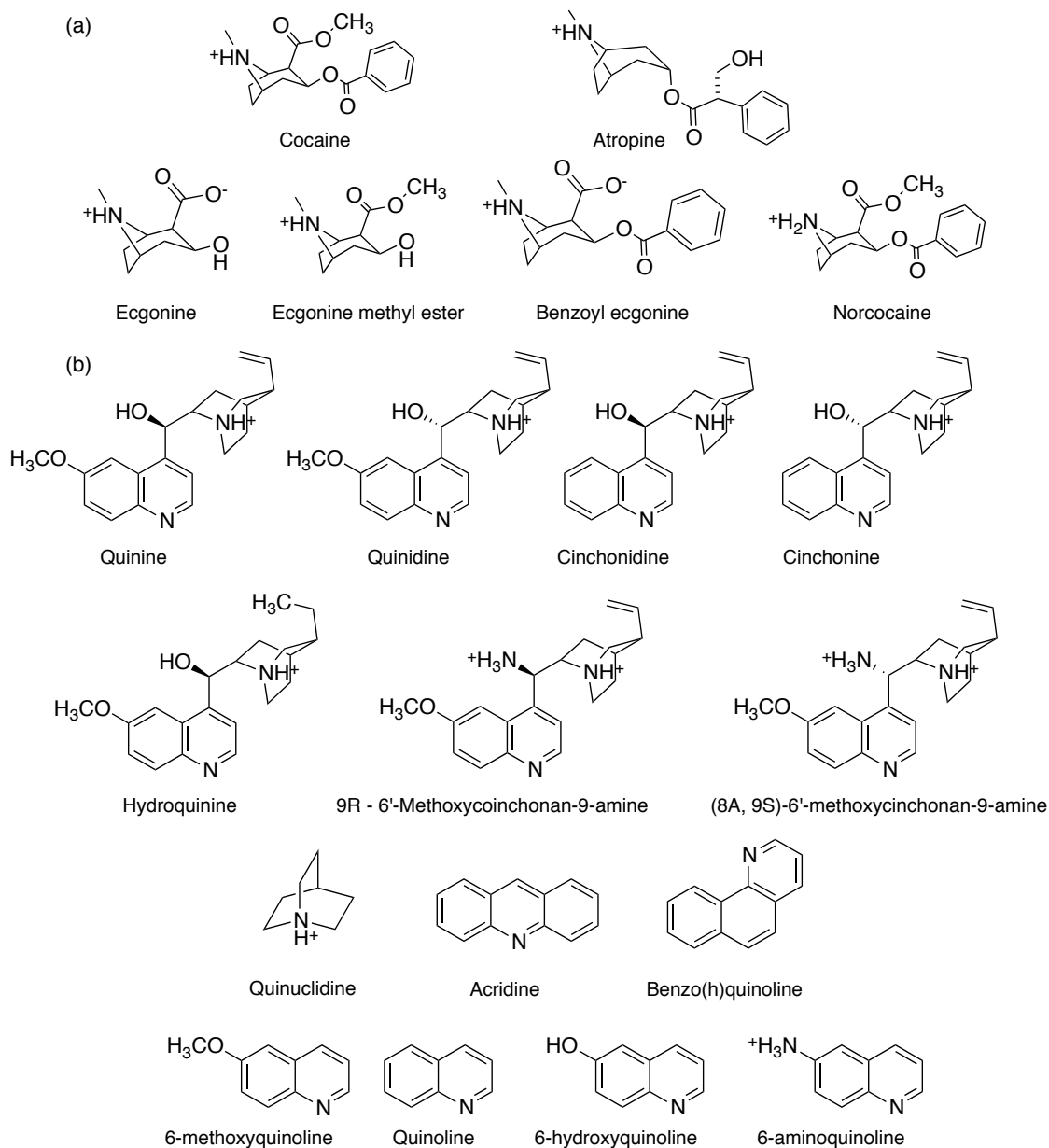


Figure 3-2: Structures of quinine, cocaine and their analogues used in this study. In (a) cocaine and its analogues are presented. In (b) quinine and its analogues are presented.

Even though it was selected for cocaine, the cocaine-binding aptamer exhibits almost 30-fold stronger affinity for quinine than cocaine^{82,83}. This adaptability in ligand specificity is not common among aptamers and prompted investigation to

determine what regions in the structure of the ligand are important for aptamer binding. To achieve this, isothermal titration calorimetry (ITC) technique is used to compare the binding affinity and thermodynamics of thirteen quinine analogues, a set of cocaine metabolites and the alkaloid atropine (Figure 3-2) for the MN4 cocaine-binding aptamer to that of quinine and cocaine. Results suggest that the presence of the fused aromatic rings and methoxy group in the quinine structure play an important role in the tight binding of ligands to the cocaine-binding aptamer.

3.3 Results

3.3.1. Binding affinity and thermodynamics of quinine and cocaine. Isothermal titration calorimetry was used to determine which regions of the cocaine-binding aptamer ligands are important for high-affinity binding. To achieve this, binding affinity and thermodynamics of thirteen quinine analogues along with four cocaine metabolites for the cocaine-binding aptamer MN4 was compared to that of quinine and cocaine. Figure 3-3 provides a sample ITC thermogram of the MN4 aptamer binding to quinine as well as an example of a case, for atropine, where no detectable binding to MN4 was observed. The binding affinity and the thermodynamic properties of all ligands used in this study for the MN4 aptamer are shown in Table 3-1. The data presented here for the binding of quinine and cocaine to MN4 agree with the results published previously^{78,82}.

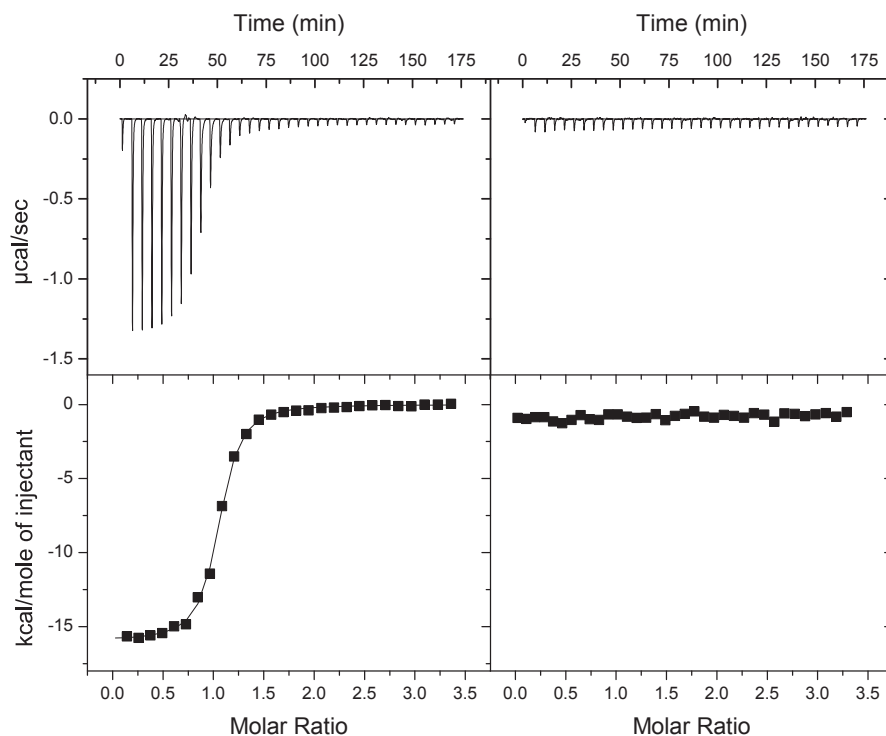


Figure 3-3: Sample ITC data showing the interaction of MN4 with (a) quinine and (b) atropine. On top is the raw titration data showing the heat resulting from each injection into the aptamer solution. On the bottom is the integrated heat after correcting for the heat of dilution. In (a) the binding experiment was performed at 15°C in a buffer of 20 mM TRIS (pH 7.4), 140 mM NaCl, 5 mM KCl. In (b) the binding experiment was performed at 15 °C in the same buffer as (a) that also contained 1% DMSO.

Both cocaine and quinine consist of an aromatic and an aliphatic region (Figure 3-2). As a first guess as to what may be required for binding by the cocaine-binding aptamer alkaloid atropine (Figure 3-2a) was assayed for binding to MN4. Despite containing both aromatic and aliphatic regions, atropine is not bound by the MN4 aptamer (Table 3-1).

Table 3-1: Binding affinities and thermodynamic parameters of ligands used in this study.

Ligand	K_d (μM)	ΔH (kcal mol^{-1})	$-\Delta S$ (kcal mol^{-1})
Cocaine	5.5 ± 0.4	-11.2 ± 1.1	4.2 ± 1.2
Norcocaine	4.4 ± 1.2	-11.3 ± 0.3	4.3 ± 0.4
Quinine	0.11 ± 0.04	-13.6 ± 0.5	4.4 ± 0.6
Quinine (1% DMSO)	0.16 ± 0.04	-12.7 ± 1.3	4.7 ± 0.9
Quinidine	0.25 ± 0.04	-23.5 ± 0.1	14.7 ± 0.1
Hydroquinine	0.10 ± 0.04	-13.0 ± 2	3.7 ± 1.6
Cinchonidine	1.2 ± 0.5	-9.0 ± 2	1.2 ± 1.4
Cinchonine	3.3 ± 0.1	-7.9 ± 0.2	0.7 ± 0.2
(9R)-6'-methoxycinchonan-9-amine	1.3 ± 0.1	-11.7 ± 0.1	3.9 ± 0.1
(8A,9S)-6'-methoxycinchonan-9-amine	1.7 ± 0.1	-11.2 ± 0.4	3.6 ± 0.4
Quinoline	3.5 ± 0.1	-10.2 ± 0.7	3 ± 1
6-methoxyquinoline	0.5 ± 0.1	-16.72 ± 0.01	8.5 ± 0.1
6-hydroxyquinoline	1.4 ± 0.1	-12.1 ± 0.7	4.4 ± 0.8
6-aminoquinoline	2.6 ± 0.5	-11.2 ± 1.6	3.9 ± 1.5
Atropine		NB	
Quinuclidine		NB	
Acridine		NB	
Benzo(h)quinoline		NB	
Ecgonine		NB	
Benzoyl Ecgonine		NB	
Ecgonine Methyl Ester		NB	

¹Data acquired at 15°C in buffer containing 20 mM TRIS (pH 7.4), 140 mM NaCl, 5 mM KCl. Data for quinoline and its analogues collected at 15°C in the same buffer containing 1% DMSO. The values reported are averages between 2 – 6 individual experiments. NB denotes no binding.

Table 3-1 also shows that DMSO does not affect binding of quinine to the cocaine-binding aptamer as binding affinities and thermodynamic properties are within the experimental error both in presence and absence of DMSO.

3.3.2. Cocaine metabolites. ITC was also used to determine which regions of cocaine are important for aptamer recognition. To study binding, four cocaine metabolites were used: ecgonine, benzoyl ecgonine, ecgonine methyl ester and norcocaine (Figure 3-2). Results show that all metabolites, except for norcocaine, do not exhibit affinity to the cocaine-binding aptamer MN4. In contrast, norcocaine exhibits slightly tighter binding to the MN4 aptamer than cocaine (Table 3-1).

3.3.3. The importance of fused ring. To study the role that the aromatic ring plays in quinine binding by MN4, the aliphatic region is separated from the aromatic portion and affinity measured. Initially, quinine was divided roughly in half with a molecule representing the aliphatic region, quinuclidine (Figure 3-2b), showing no detectable binding. Quinoline, on its own, binds to the cocaine-binding aptamer about 30-fold weaker than quinine (Figure 3-4a, Table 3-1). Surprisingly, a molecule representing the aromatic portion of quinine, 6-methoxyquinoline (Figure 3-2b), was bound by MN4 with significant affinity. The affinity of MN4 for 6-methoxyquinoline was $0.5 \pm 0.1 \mu\text{M}$ (Table 3-1), only 5 times weaker than for intact quinine. To further test the impact of fused aromatic rings on the binding affinity of the MN4 aptamer, aromatic ligands with three fused 6-membered rings, acridine

and benzo(h)quinoline (Figure 3-2b), were tested. Neither of the two molecules are bound by MN4 (Figure 3-4b, Table 3-1).

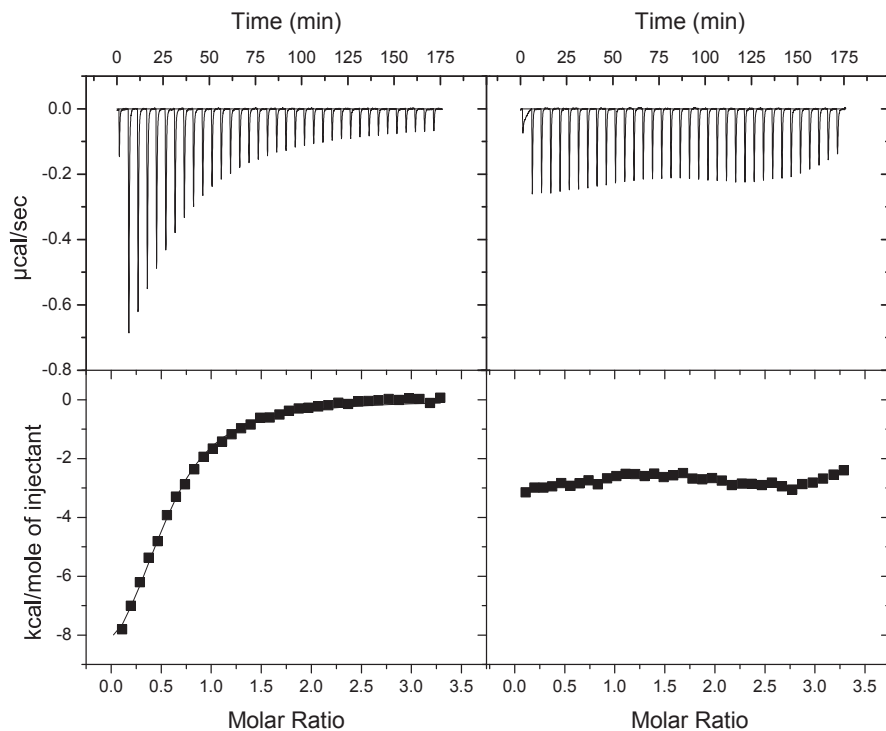


Figure 3-4: ITC data showing the interaction of MN4 with (a) quinoline and (b) benzo(h)quinoline. On top is the raw titration data showing the heat resulting from each injection into the aptamer solution. On the bottom is the integrated heat after correcting for the heat of dilution. Both binding experiments were performed at 15°C in a buffer of 20 mM TRIS (pH 7.4), 140 mM NaCl, 5 mM KCl that also contained 1% DMSO.

3.3.4. Methoxy variants. The importance of the methoxy group on the aromatic ring of quinine for aptamer binding was investigated. The affinity of compounds with the methoxy group was compared to those that had methoxy group replaced by hydrogen, an alcohol group, and an amino group. In each case studied, changing the methoxy group reduced ligand affinity. First, the methoxy group was replaced with hydrogen in intact quinine and studied the binding of cinchonidine (Figure 3-

2b). The affinity of MN4 for cinchonidine is ~10 fold weaker than MN4 for quinine. Additionally, binding of quinoline (Figure 3-2b) was compared to that of 6-methoxyquinoline. For this pair of ligands, replacing the methoxy with a hydrogen reduces the affinity seven-fold (Table 3-1). Next, the methoxy group on 6-methoxyquinoline was replaced with an alcohol and an amino group. The affinity of the MN4 aptamer for both 6-hydroxyquinoline and 6-aminoquinoline (Figure 3-2b), was reduced by 3 and 5 fold, respectively, when compared with the affinity for 6-methoxyquinoline (Table 3-1).

3.3.5. Isomerism. The effect of changing the position around the stereogenic carbon connecting the aliphatic and aromatic portions of quinine was studied using three pairs of optical isomers.

In the first pair, quinine and quinidine (Figure 3-2b), changing the stereochemistry at position 2 from S in quinine to R in quinidine results in a 2.3 fold reduction in MN4 binding affinity (Table 3-1). Similarly, changing the stereochemistry at the same location from S in cinchonidine to R in cinchonine reduces the ligand affinity by MN4 by 2.8 fold (Table 3-1).

Binding of another pair of optical isomers, (9*R*)-6'-Methoxycinchonan-9-amine and (8 α ,9*S*)-6'-Methoxycinchonan-9-amine (Figure 3-2b) to the MN4 aptamer was studied. This pair of molecules has an amino group instead of an alcohol group at the carbon between the aliphatic and aromatic parts of quinine. At the pH studied,

7.4, this amino should be protonated. Making the switch from an -OH to the -NH₃⁺ reduces the affinity of MN4 for the ligand by approximately 10-fold (Table 3-1) with binding by the 9S isomer 1.3 fold weaker than for the 9R isomer.

3.3.6. Effect of saturating the vinyl group. The final quinine analog tested has a change in the aliphatic portion of the molecule. Hydroquinine differs from quinine in that the double bond in quinine has been saturated to a methyl group in hydroquinine (Figure 3-2b). This change has no significant effect on the affinity of the ligand by MN4 (Table 3-1).

3.4 Discussion

All the compounds studied here that are bound by MN4 have binding driven by favorable enthalpy contribution that is balanced by an unfavorable binding entropy (Table 3-1). It is worth noting that all ligands have a lower logP value, suggesting that binding is not strongly dominated by the hydrophobic effect. When the enthalpy is plotted against entropy for the ligands that bind the data follow a straight line (Figure 3-5). There are different views on what an observed linearity of enthalpy-entropy compensation means¹¹⁸⁻¹²¹. However, having a correlation does show that the correlated ligands follow a similar binding mechanism. Ligands that are bound by MN4 are expected to follow a similar binding mechanism, which is consistent with previous finding that both quinine and cocaine compete for the same binding site in MN4⁸².

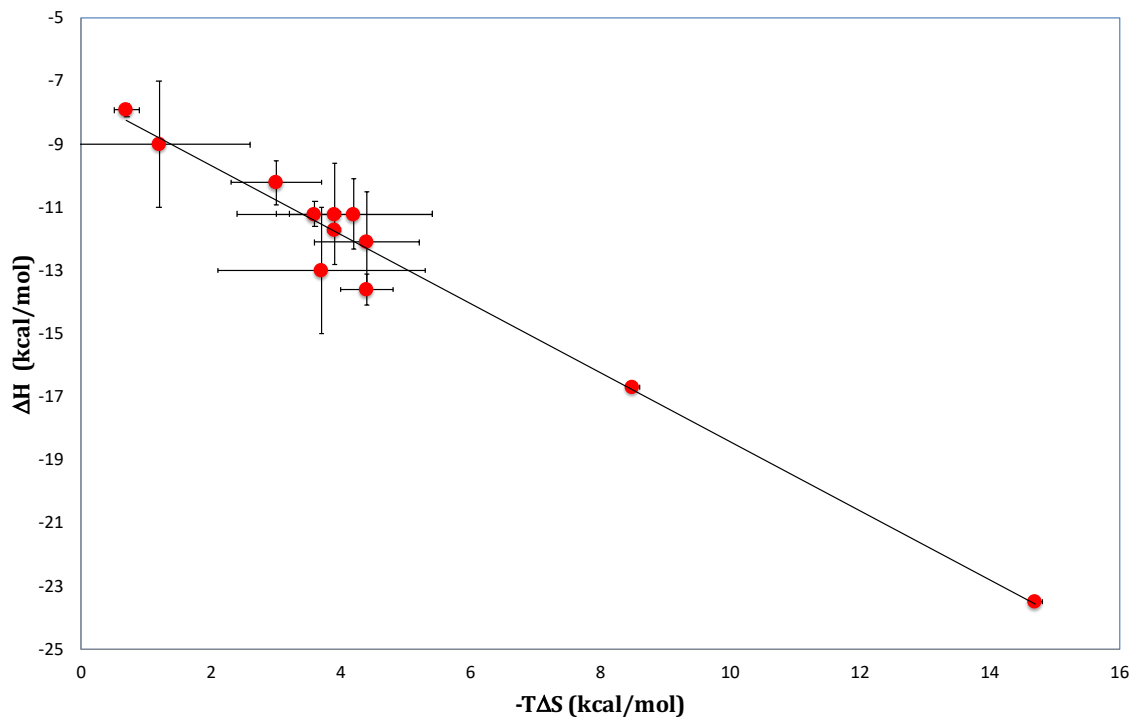


Figure 3-5: Plot for binding enthalpy versus entropy for the ligands used in this study that are bound by the MN4 cocaine binding aptamer with error bars for both axes.

The ability of the cocaine-binding aptamer to bind quinine tighter than the molecule it was originally selected, cocaine, for is unusual. A clear similarity between these ligands is that there is an aromatic portion of the molecule and an aliphatic region containing basic nitrogen. In order to see if having these two components is the sole requirement for aptamer binding, the ability of MN4 to bind atropine (Figure 3-2a) was examined. Like quinine and cocaine, atropine has an aromatic and aliphatic region that contains basic nitrogen. Unlike cocaine and quinine, atropine is not bound by MN4 (Figure 3-1). This indicates that there are some other features in ligands necessary for binding to MN4 than having an aromatic and nitrogen-containing aliphatic portion.

Cocaine metabolites binding to MN4 were also studied. Binding of these metabolites has previously been studied, though not by ITC methods. Apart from norcocaine, which is bound by MN4 with the same affinity as cocaine, ecgonine, ecgonine methyl ester and benzoyl ecgonine are not bound by MN4 (Table 3-1). These results are consistent with previously published studies^{75,76,84,109,110,112,122}. The minor change of removing a methyl group from cocaine to give benzoyl ecgonine (Figure 3-2a) results in the loss of binding. This removal of a methyl results in creating a negatively charged carboxylate that likely interferes with binding by the negatively charged DNA aptamer. Nevertheless, this subtle change reflects the high specificity of the MN4 aptamer for cocaine over modified cocaine molecules and is striking in light of the high affinity MN4 has for quinine and related compounds.

The ability of the cocaine-binding aptamer to bind a molecule tighter than the one it has been selected for is an unusual feature for an aptamer. The tight binding of quinine by MN4 has been reported previously^{82,83,123,124}. The aim of this study is to determine what structural and chemical features of the ligand are important for recognition. From the analysis of the binding results for different compounds investigated (Fig 3-2; Table 3-1) a number of conclusions can be made about what regions of quinine are important for high affinity binding.

Firstly, the aromatic region of the ligand is the key for tight binding. The non-binding of quinuclidine, the aliphatic region of quinine and observation that the change in the aliphatic portion of quinine to hydroquinine does not result in any

significant change in affinity. The importance of the aromatic ring portion is emphasized by the fact that 6-methoxyquinine alone is bound at an affinity of 0.5 ± 0.1 μM , a level still 10-fold tighter than MN4 has for cocaine.

This demonstrates that the bicyclic aromatic portion of quinine alone can be bound by MN4. However, when the ligand was expanded to 3 fused rings, such as in acridine and benzo(h)quinoline, there was no detectable binding, likely because the ligand is now too large to fit into the binding site. This importance of the aromatic region of an MN4 ligand is consistent with the thermodynamic signature of binding falling into the intercalating region as defined by Chaires¹²⁵. These data also indicate that the optimum ring size for MN4 binding is two fused six-membered rings as the aptamer does not bind ligands with three fused aromatic rings.

The substituents on the aromatic rings are also important for recognition. Having a methoxy group at the 6-position, as found in quinine and 6-methoxyquinoline, appears to be the optimum configuration. Removing the methoxy group reduces affinity as seen in cinchonidine and quinoline when compared to quinine and 6-methoxyquinoline, respectively (Table 3-1). Additionally, substitutions of a hydroxyl and an amino group at the 6 position in quinoline reduce affinity compared to having a methoxy group, but do not reduce affinity as much as having a hydrogen only in this position. This indicates that retaining some sort of hydrogen bond acceptor is important at this position.

Finally, the importance of the stereogenic center at carbon 9, the carbon that connects the aromatic and aliphatic rings in quinine, was investigated. In all cases studied, the 9R configuration, as found in quinine, results in the tightest binding. This is shown when comparing the pairs quinine and quinidine, cinchonidine and cinchonine and 9R-6'-methoxycinchonan-9-amine and (8 α ,9S)-6'-methoxycinchonan-9-amine (Table 3-1). It is interesting to also note in this last pair that when an amino group is introduced into the molecule and this amino should be protonated at the pH studied, that binding is reduced 10-fold from that of quinine. This indicates that adding an extra positive charge at position 9 does not add to affinity and that removing the hydrogen bond acceptor results in a decreased affinity.

3.5 Concluding remarks

In summary, presence of fused aromatic ring and methoxy group on the aromatic ring are important for tight binding of ligand to cocaine-binding aptamer. 6-methoxyquinoline on its own is bound tightly by the MN4 aptamer, while the aliphatic portion of quinine, represented by quinuclidine, does not show detectable binding. Larger aromatic molecules that contain three fused rings are also not bound by the aptamer. The presence of a methoxy group at the 6-position of the quinoline ring is important for binding as changing it to hydrogen, an alcohol or an amino group all result in lower binding affinity. For all ligands that bind, association is driven by a negative enthalpy compensated by unfavorable binding entropy.

Chapter 4 **Salt-Mediated Two-Site Ligand Binding by the Cocaine-Binding Aptamer**

4.1 Preface

All work presented in this chapter has been published in the article listed below¹²⁶.

- Neves, M. A. D.*, **Slavkovic, S.***, Churcher, Z. R. & Johnson, P. E. "Salt-mediated two-site ligand binding by the cocaine-binding aptamer." *Nucleic Acids Res.* **45**, 1041–1048 (2017).

Note: * denotes co-first authorship

4.2 Introduction

Controlling biomolecular function is an important area of chemical biology. In nature, there are many ways in which the activity of proteins and nucleic acids are controlled including genetic control, allosteric effectors and covalent modification. For rationally designed biosystems, having control over the function of molecules is a desired, but difficult to achieve capability. Aptamers have been used in a modular manner to control nucleic acid-based enzymes and molecular devices^{127,128} typically in a fashion where aptamer binding leads to a structural change that activates an associated enzyme or receptor molecule. However, more subtle examples of biomolecular control where, for example, changes in solution composition leading to a change in activity or function, are rare or not currently known.

The cocaine-binding aptamer, originally reported in the early 2000s, has become a model system routinely implemented in the study and development of small

molecule sensing and aptamer-based technologies^{75,76,132,84-86,111,114,129-131}. The widespread use of the cocaine-binding aptamer continues despite the fact the aptamer was revealed to bind quinine and quinine analogs with up to 50 fold higher affinity than cocaine, the target the aptamer was initially selected to bind^{82,83,96,133}. The reason for the continued utilization of the cocaine-binding aptamer likely lies in the ability to engineer the aptamer with a structure switching binding mechanism. The secondary structure of the MN4 aptamer (Figure 4-1) is pre-formed in the absence of ligand and upon binding its target there is no observable change in secondary structure⁷⁷. However, if the length of stem one is shortened to three base pairs, such as MN19 (Figure 4-1), the aptamer is loosely structured in the absence of target and upon binding the secondary structure rigidifies in a ligand-induced folding process^{76,77}. This ligand-induced folding mechanism is retained with quinine binding and when the sequence is altered to allow for binding of the steroid deoxycholic acid (DCA)^{81,82}. The cocaine-binding aptamer has also been shown to function when separated into two strands, referred to as a split-aptamer^{75,78,85}. The majority of published cocaine-aptamer based technologies rely on the use of the structure-switching or split-aptamer sequence variants.

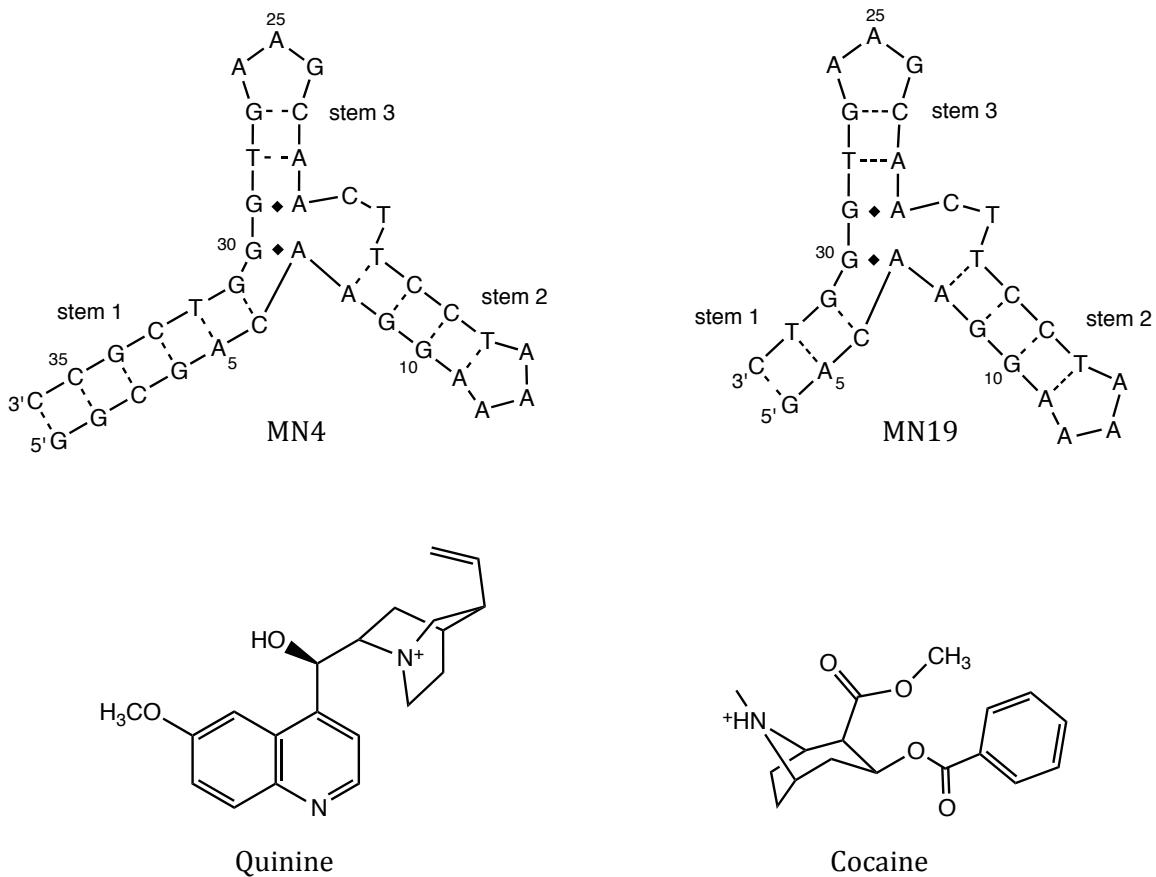


Figure 4-1: Secondary structure of the MN4 and MN19 cocaine-binding aptamer and chemical structures of the cocaine and quinine ligands. Dashes between nucleotides indicate Watson–Crick base pairs while dots indicate non-Watson–Crick base pairs.

Multisite ligand binding is commonly observed in proteins but less frequently observed in functional nucleic acids such as aptamers and riboswitches. Multisite ligand binding can be independent or cooperative, with both positive and negative cooperativity possible. A classic example of multisite binding occurring in nature is the binding of oxygen to hemoglobin, which occurs in a positively cooperative manner. Despite the prevalence of multisite ligand binding in proteins and enzymes, it is rare to find examples of multisite binding among functional nucleic acids. One

example is the tetrahydrofolate (THF) riboswitch that binds two ligands in a cooperative manner¹³⁴. Another example is the ATP-binding DNA aptamer that binds two ATP molecules at separate sites^{8,135}. An RNA aptamer for neomycin B was demonstrated to bind one neomycin B ligand at a high affinity site and have two additional low affinity sites at which binding can be disrupted by addition of NaCl¹³⁶. In a slightly different example the activity of a ribozyme was controlled by engineering an FMN and a theophylline aptamer into the structure of the hammerhead ribozyme to produce a ribozyme whose activity was controlled by the binding of these two different ligands¹³⁷.

In this study we show that the cocaine-binding aptamer binds two molecules of its ligand in buffer conditions of low NaCl concentration. Additionally, we demonstrate that binding at the second site can be controlled by varying the NaCl concentration of the buffer, a feature that, to the best of our knowledge, has not been observed in any other aptamer. Ligand binding at the first site continues to occur in all buffer conditions studied. Buffer-controlled binding could be utilized in applications employing this aptamer where an increased affinity or aptamer rigidity could be beneficial, such as in sensing, by simply changing the NaCl concentration of the buffer.

4.3 Results and Discussion

4.3.1. Salt-controlled two-site binding of cocaine. The ability of the cocaine-binding aptamer to bind more than one ligand is clearly demonstrated by the shape of the ITC thermogram when cocaine is titrated into a solution of aptamer in the absence of NaCl (Figure 4-2). The non-sigmoidal-shaped binding curve observed when MN4 binds cocaine with no NaCl present contrasts sharply with the binding thermogram for MN4 in the presence of 140 mM NaCl and indicates that more than one binding event is taking place. The ITC data indicates that the stoichiometry of this multi-site interaction is two-site binding as the thermogram saturates after the addition of two molar equivalents of cocaine.

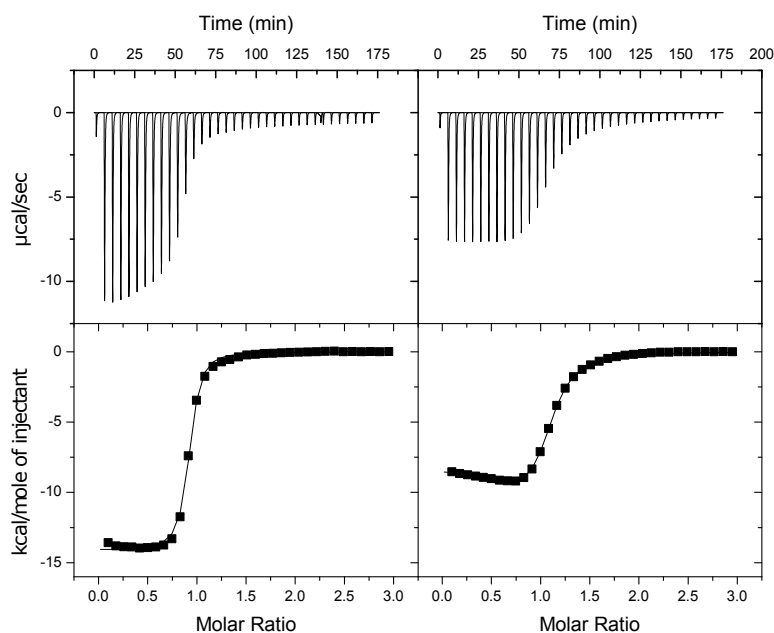


Figure 4-2: Titrations of cocaine into MN4 aptamer with buffer conditions of (a) 140 mM NaCl and (b) 0 mM NaCl. The non-sigmoidal nature of the binding curve in (b) indicates that more than one binding event is occurring. On top is the titration data showing the heat resulting from each injection of cocaine into an aptamer solution. On bottom are the integrated heats after correcting for the heat of dilution. Both binding experiments were performed at 15°C and also contained 20 mM TRIS (pH 7.4).

This two-site binding data was then fit to a two-independent site binding model in order to determine the affinity and binding enthalpy of each of the two sites¹³⁸. A feature of this binding model is that the ITC isotherms analyzed vary as a function of aptamer concentration. Results are presented in Table 4-1, which includes the average of the fits from ITC experiments performed at three different MN4 concentrations.

Table 4-1: Individual two-site independent fits of cocaine bound to MN4 aptamer¹

MN4 Conc. (μM)	K_{d1} (μM)	ΔH_1 (kcal mol^{-1})	$-T\Delta S_1$ (kcal mol^{-1})	K_{d2} (μM)	ΔH_2 (kcal mol^{-1})	$-T\Delta S_2$ (kcal mol^{-1})
50	1.2 ± 0.1	-11.3 ± 0.1	3.5 ± 0.1	8 ± 3	-18 ± 32	11 ± 32
86	0.9 ± 0.5	-10.7 ± 0.5	2.7 ± 0.3	16 ± 3	-21 ± 8	15 ± 8
130	1.3 ± 0.4	-8.9 ± 0.1	1.3 ± 0.3	23 ± 6	-20 ± 3	13 ± 3
Average	1.3 ± 0.4	-10.3 ± 1.2	2.5 ± 1.2	16 ± 8	-20 ± 2	13 ± 2

¹Data collected at 15°C in 20 mM TRIS (pH 7.4).

The other potential binding models of identical independent and identical cooperative binding¹³⁹ were not considered as it is not possible to have two identical binding sites within the monomeric cocaine-binding aptamer. The high affinity site is slightly tighter with no added NaCl than previously reported in 140 mM NaCl ($5.5 \pm 0.4 \mu\text{M}$) at the same pH value and temperature⁹⁶. This higher affinity in the absence of NaCl is consistent with electrostatic interactions playing a role in the affinity of the positively charged ligand to the polyanionic DNA^{78,82} as reducing the salt concentration will decrease shielding of the charge-charge interactions, increasing the electrostatic attractions yielding higher affinity.

4.3.2. Salt-mediated two-site binding of quinine. The low NaCl-dependent two-site binding phenomenon of the cocaine-binding aptamer was assayed for quinine binding. MN4 was previously shown to bind quinine about 50 fold tighter than cocaine^{82,83,96}. The K_d value for MN4 binding quinine in 140 mM NaCl is 0.20 ± 0.05 μM with a ΔH of -14 ± 1 kcal mol^{-1} also at a temperature of 15 °C. This higher affinity makes it possible to perform ligand binding experiments at a wide range of c-values ($c=[\text{aptamer}]/K_d$) in order to better define the independent two-site binding model using global fitting, where all c-values are fit to the same parameters simultaneously¹³⁸. Results of six ITC experiments at varying aptamer concentrations ranging from 11 to 130 μM are presented in Table 4-2.

Table 4-2: Individual two-site independent fits of quinine bound to MN4 aptamer¹

MN4 Conc. (μM)	K_{d1} (μM)	ΔH_1 (kcal mol^{-1})	$-T\Delta S_1$ (kcal mol^{-1})	K_{d2} (μM)	ΔH_2 (kcal mol^{-1})	$-T\Delta S_2$ (kcal mol^{-1})
11	0.05 ± 0.02	-9.1 ± 0.3	-0.6 ± 0.4	0.34 ± 0.07	-19 ± 16	10 ± 16
19	0.14 ± 0.09	-11.9 ± 0.1	2.9 ± 0.3	2.29 ± 0.76	-60 ± 26	53 ± 26
42	0.28 ± 0.09	-10.5 ± 0.1	1.9 ± 0.2	2.58 ± 0.47	-35 ± 92	28 ± 92
56	0.57 ± 0.20	-10.6 ± 0.1	2.3 ± 0.2	6.80 ± 1.06	-23 ± 28	16 ± 28
80	0.41 ± 0.13	-10.2 ± 0.1	1.8 ± 0.2	4.52 ± 0.68	-29 ± 22	22 ± 22
130	0.33 ± 0.14	-11.4 ± 0.1	2.9 ± 0.3	4.26 ± 0.66	-20 ± 4	13 ± 4

¹Data collected at 15°C in 20 mM TRIS (pH 7.4).

Using global fitting, the affinity of MN4 for quinine at both sites has been determined and results agree within the error range with the average of the individual fits (Table 4-3)

Table 4-3: Average individual fits and global fits comparison¹

Fit	K_{d1} (μM)	ΔH_1 (kcal mol^{-1})	$-T\Delta S_1$ (kcal mol^{-1})	K_{d2} (μM)	ΔH_2 (kcal mol^{-1})	$-T\Delta S_2$ (kcal mol^{-1})
Average	0.3 ± 0.2	-10.6 ± 0.9	1.9 ± 0.5	3 ± 2	-31 ± 15	24 ± 4
Global	0.2 ± 0.1	-10.8 ± 0.5	1.9 ± 0.8	1.2 ± 0.6	-26 ± 3	19 ± 9

¹Data collected at 15°C in 20 mM TRIS (pH 7.4).

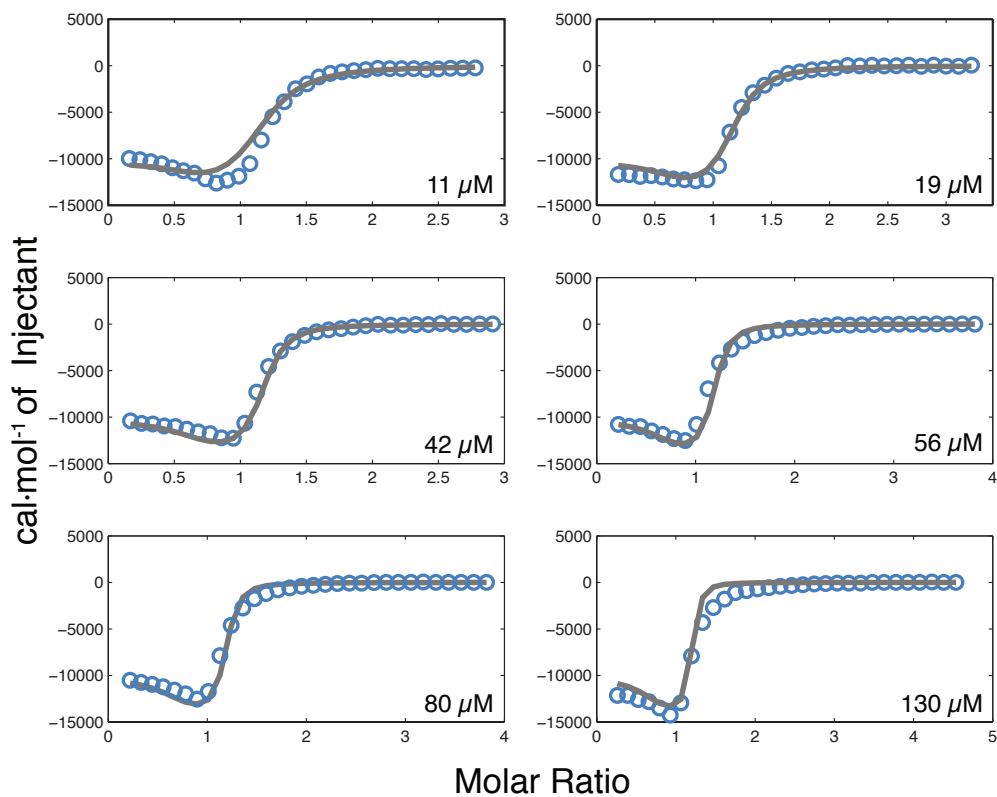


Figure 4-3: ITC data for MN4 binding quinine acquired at various aptamer concentrations at 0 mM NaCl. Shown in blue circles are the experimental data with the global fit of the data to an independent sites model shown as a solid grey line.

4.4.3. Salt mediated binding of quinine to MN19 aptamer. Many of the applications of the cocaine-binding aptamer rely on the structure-switching binding mechanism of a short stem 1 sequence variant. We analyzed the interaction of the

cocaine-binding aptamer construct MN19 (Figure 4-1) in order to assess a short stem 1 variant for two-site binding. ITC experiments were performed at both high and low NaCl concentrations and, as seen with the long stem 1 construct, MN19 binds two quinine molecules at 0 M NaCl (Figure 4-4). The affinity of MN19 for quinine at 20 mM Tris pH 7.4, 0 mM NaCl has a K_{d1} value of $0.28 \pm 0.12 \mu\text{M}$ and an enthalpy of $-8.5 \pm 0.2 \text{ kcal mol}^{-1}$ at the high affinity site; while the low affinity site has a K_{d2} value of $5 \pm 1 \mu\text{M}$ and an enthalpy of $-68 \pm 42 \text{ kcal mol}^{-1}$. At 140 mM NaCl, MN19 binds quinine only at a single site with an affinity of $0.38 \pm 0.09 \mu\text{M}$ and a ΔH of $-15.2 \pm 3.2 \text{ kcal mol}^{-1}$. These values match within the error range with what we reported earlier for quinine binding with the same buffer conditions, though at slightly different temperatures (17.5°C versus 15°C)⁸².

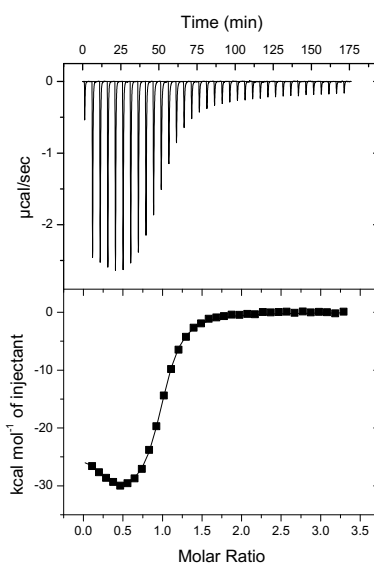


Figure 4-4: Two-site binding of the short stem 1, MN19 cocaine-binding aptamer using ITC. Shown is the titration of quinine into a 20 μM solution of the MN19 aptamer with buffer conditions of 0 mM NaCl, 20 mM TRIS (pH 7.4). On top is the titration data showing the heat resulting from each injection of quinine into an aptamer solution. On the bottom are integrated heats after correcting for the heat of dilution. The binding experiment was performed at 15°C .

4.4.4. Effect of NaCl concentration in buffer on binding. In order to investigate the effect of NaCl concentration on MN4-quinine binding, ITC experiments were performed at NaCl concentrations ranging from 0 to 140 mM. Figure 4-5 shows the raw thermograms acquired at different concentrations of NaCl. The shape of the thermograms clearly demonstrates the shift from two-site to one site binding as the concentration of NaCl increases. Presumably, at higher Na⁺ concentrations the cation shields electrostatic interactions between the negatively charged DNA aptamer and the positively charged quinine (or cocaine) ligand. It is likely that electrostatic interactions play a greater role in ligand binding at the low affinity site as Na⁺ reduces binding at high concentrations. This increased role of electrostatics at the low affinity site is consistent with the ITC determined enthalpy at this site being more exothermic than at the high affinity site.

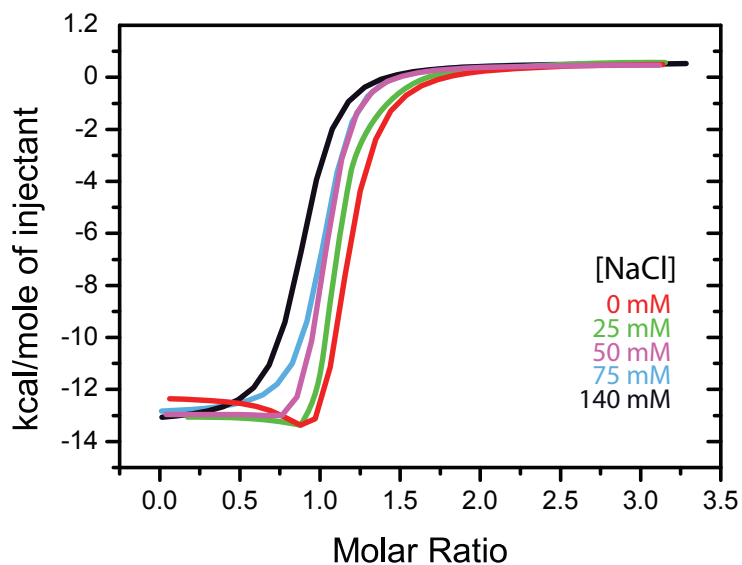


Figure 4-5: Ligand binding at the second site is controlled by the concentration of NaCl. Shown are the ITC data for the titration of MN4 with quinine at different NaCl concentrations. Represented in red is data at 0 mM; green at 25 mM; purple at 50 mM; blue at 75 mM and black at 140 mM NaCl. Experiments were performed at 15°C and also contained 20 mM TRIS (pH 7.4).

4.4 Concluding Remarks

It can be concluded that the cocaine-binding aptamer has the ability to bind two copies of its ligand at low NaCl concentrations. Both cocaine and quinine binding at the second site have a lower affinity than at the first site and increasing the concentration of NaCl can eliminate binding at the second site. Previous studies have looked at binding by the aptamer at relatively high NaCl concentrations and consequently binding at this second site was not previously observed. A benefit of this second binding site to biosensor design could be to extend the dynamic range of a cocaine sensor. By working at a low NaCl concentration the two sites with two different binding affinities should act in a similar fashion as using oligonucleotide inhibitors to alter the dynamic range of the cocaine-binding aptamer¹⁴⁰. The ability to control ligand binding at the second site by adjusting the NaCl concentration is unique among aptamers. What is demonstrated here is the first NaCl controlled binding by an aptamer to ligands not known to bind nucleic acids nonspecifically. Other functional nucleic acid molecules, such as the ATP DNA aptamer^{8,135} and the aptamer domain from the THF riboswitch¹³⁴ bind two copies of their ligand, but they do not have the ability to control the switch from single to two-sided binding by such a simple change, as the buffer concentration of NaCl, that is seen with the cocaine-binding aptamer. This ability to one of two binding events by changing the NaCl concentration may prove useful in different biotechnology applications such as aptamer controlled cargo release¹⁴¹ and aptamer based materials and sensing applications. This work also demonstrates that *in vitro* selected molecules can have as complex a function as those found in nature.

Chapter 5 Analysis of cooperative ligand binding by the ATP aptamer

5.1. Preface

- The work presented in this chapter is taken from the manuscript titled “*Thermodynamic Analysis of Cooperative Ligand Binding by the ATP-binding Aptamer*” by Sladjana Slavkovic, Yanrui Zhu, Zachary Churcher, Aron A. Shoara and Philip E. Johnson. Currently awaiting submission to a peer reviewed journal.

5.2 Introduction

One of the most studied aptamers since its development is the 27 nucleotide long ATP DNA aptamer selected by Huizenga and Szostak in 1995 that binds ATP with micromolar affinity¹³⁵. This ATP aptamer has a highly recurring sequence and has been re-developed using different selection method in biosensor development¹⁴². It has been used as model study and many studies have been employed to understand binding dynamics and cooperativity¹⁴³⁻¹⁴⁶. In 1997, Lin and Patel have solved the structure of the ATP aptamer by nuclear magnetic resonance (NMR) using AMP as the binding ligand⁸. The structure shows two binding pockets each one binding one molecule of AMP. The binding site is in a zipped up internal loop formed by a sheared G•A, and a reverse Hoogsteen G•G mismatch with the unpaired G at the binding site pairing with the AMP ligand (Figure 5-1a). Interestingly, the ATP-binding DNA aptamer binds two molecules unlike the ATP-binding RNA aptamer selected to bind only one AMP molecule even though the two aptamers have the same mode of binding even though they have different architectures⁴⁷. The ATP-

binding aptamer has been used for an effector binding domain of allosteric sensors and deoxyribozymes¹⁴² and for probe sensing adenine nucleotides by fluorescence labeling¹⁴⁷. It has been shown that it also binds ADP, adenosine as well as adenine^{8,135,148}. Methods for binding detection of ATP, AMP and adenosine to the ATP DNA aptamer have been developed previously and include chromatography, fluorescence, bioluminescence and electrochemical biosensors^{146,149,150}. Here we use isothermal titration calorimetry and global fitting method of ITC data^{103,138} obtained over a range of ATP aptamer concentrations to determine whether adenosine binding to ATP aptamer follows independent or cooperative binding model.

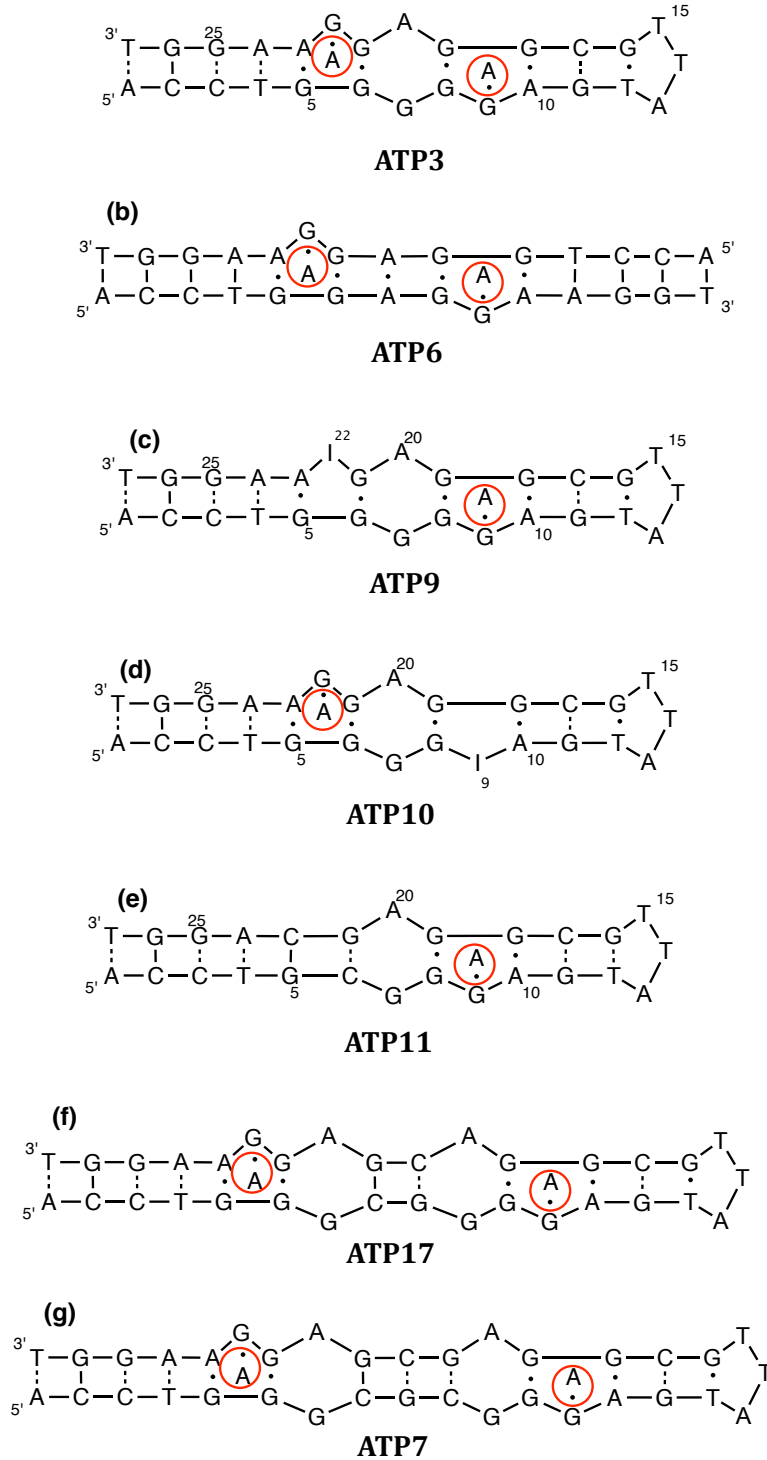


Figure 5-1: Secondary structures of the (a) original ATP-binding aptamer and (b-g) variants. (b) Self-complementary 14mer (ATP6) (c) and (d) ATP aptamer variants that have inosine substitution at position 22 (ATP9) and position 9 (ATP10). (e) One site removed (ATP11). (f) ATP-binding aptamer with two sites removed by extra three base pairs (ATP17). (g) ATP-binding aptamer with two sites separated by extra four base pairs (ATP7).

5.3 Results

5.3.1. Ligand binding to ATP3 aptamer. The originally selected 27-nucleotide long ATP-binding aptamer¹³⁵ (Figure 5-1a) was chosen to look at binding of the aptamer to a variety of adenine-based ligands. Binding of the ATP3 aptamer to ATP, ADP, AMP, adenosine and adenine was observed (Figure 5-2). The ITC data for these ligands were fit to both a cooperative and an independent binding model with the model that provided the lowest residual sum of squared differences (RSS) between the experimental and calculated data points being judged as the best fit (Table 5-1). Adenosine was then chosen for more detailed analysis as it provided the best quality ITC data in terms of signal to noise.

Table 5-1: Binding affinities and thermodynamic parameters of adenine-based ligands to the ATP-binding aptamer and comparison of fits¹.

	Aptamer	K_{d1} (μM)	ΔH_1 (kcal mol^{-1})	$-\text{T}\Delta S_1$ (kcal mol^{-1})	K_{d2} (μM)	ΔH_2 (kcal mol^{-1})	$-\text{T}\Delta S_2$ (kcal mol^{-1})	RSS
Cooperative	ATP	133 ± 55	-1.8 ± 0.1	-3.4 ± 0.3	498 ± 123	-6.0 ± 1.7	1.5 ± 1.6	9.69×10^6
Independent		1.9 ± 1.9	-0.83 ± 0.02	-6.8 ± 0.6	186 ± 28	-1.3 ± 0.1	-3.7 ± 0.1	2.85×10^{11}
Cooperative	ADP	101 ± 33	-2.7 ± 0.1	-2.7 ± 0.2	254 ± 37	-13 ± 1	8 ± 1	1.02×10^7
Independent		1.3 ± 0.8	-1.5 ± 0.1	-6.4 ± 2.6	87 ± 10	-2.8 ± 0.2	-2.6 ± 0.1	2.15×10^{11}
Cooperative	AMP	86 ± 26	-6.7 ± 0.1	1.2 ± 0.1	127 ± 9	-16 ± 1	15 ± 1	1.27×10^7
Independent		0.8 ± 0.4	-3.7 ± 0.1	-4.5 ± 0.3	89 ± 3	-6.7 ± 0.2	0.9 ± 0.4	4.37×10^{11}
Cooperative	Adenosine	42 ± 13	-11 ± 3	4.9 ± 3.2	43 ± 2	-27 ± 2	21 ± 2	5.63×10^7
Independent		0.7 ± 0.3	-4.5 ± 1.2	-3.7 ± 1.3	24 ± 1	-10 ± 1	4.1 ± 0.2	2.87×10^{11}
Cooperative	Adenine	39 ± 14	-5.5 ± 0.2	-0.5 ± 0.3	218 ± 114	-35 ± 18	30 ± 18	3.32×10^8
Independent		0.9 ± 0.4	-2.4 ± 0.2	-5.8 ± 0.3	37 ± 6	-5.0 ± 0.4	-1.0 ± 0.4	2.58×10^{11}

¹Data collected at 20°C in 10 mM acetate (pH 5.5), 120 mM NaCl, at 70 μM aptamer concentration and 1.96 mM ligand concentration.

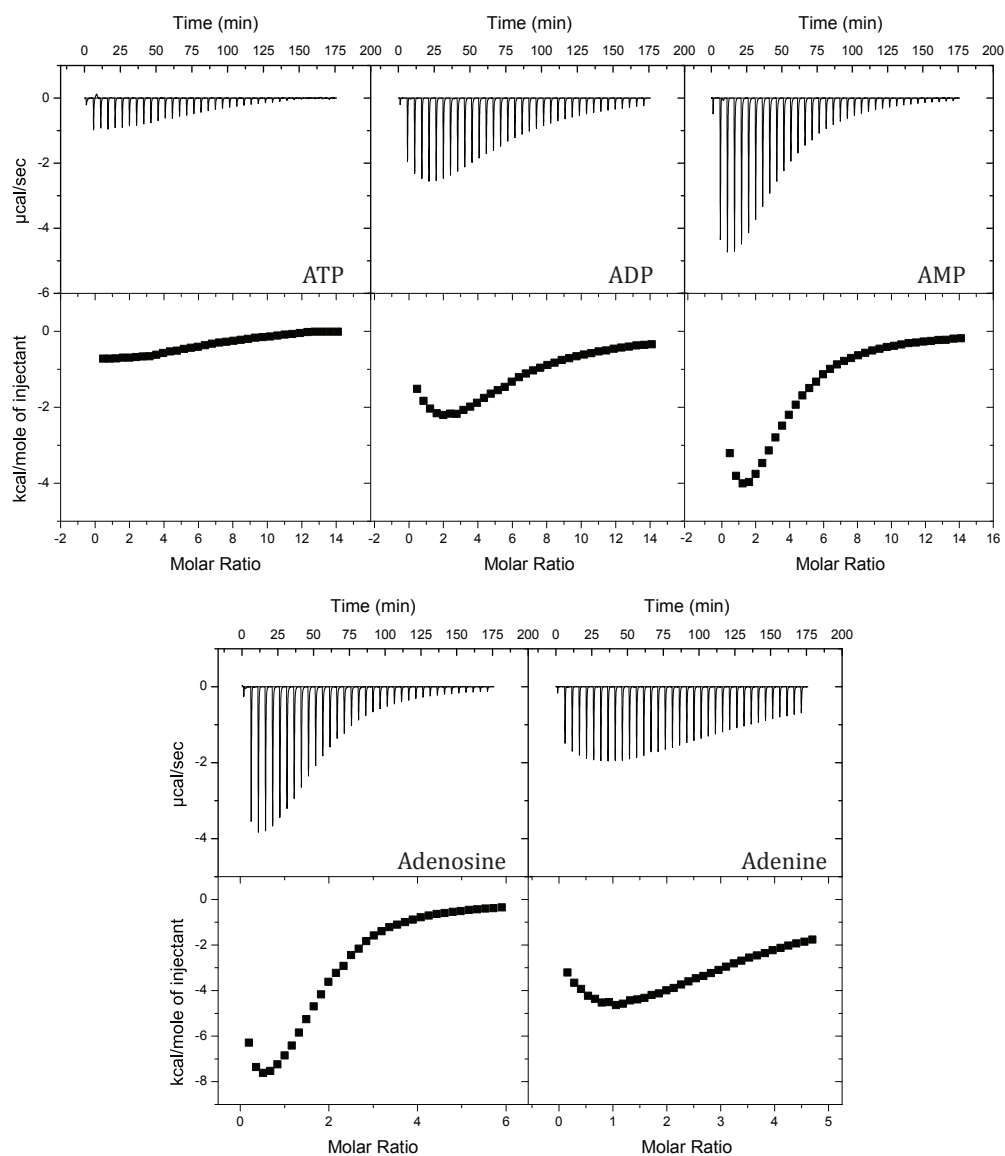


Figure 5-2: Binding of ATP, ADP, AMP, adenosine and adenine by the ATP3 aptamer. On top is the titration data showing the heat resulting from each injection of ligand into an aptamer solution. On the bottom are integrated heats after correcting for the heat of dilution. The binding experiment was performed at 20°C in 10 mM acetate (pH 5.5), 120 mM NaCl.

5.3.2. Binding Mechanism of Adenosine to ATP3 Aptamer. In order to confirm that ATP3 binds two molecules of ligand in a cooperative and not independent manner, ITC binding data was acquired at six aptamer concentrations ranging from 10 – 100 μM . Data were fit both individually and globally to an independent and a cooperative binding model with the model providing the lowest sum of residual squared differences (RSS) between the experimental and calculated data points being judged as the best fit. For all six aptamer concentrations, the cooperative model provided the best fit of the experimental data to the calculated fit (Table 5-2).

Table 5-2: Individual independent and cooperative fits comparison of adenosine binding to ATP3 aptamer¹.

	Aptamer Conc. (μM)	K_{d1} (μM)	ΔH_1 (kcal mol^{-1})	$-\text{T}\Delta S_1$ (kcal mol^{-1})	K_{d2} (μM)	ΔH_2 (kcal mol^{-1})	$-\text{T}\Delta S_2$ (kcal mol^{-1})	RSS ²
Cooperative	10	6.1 ± 1.4	-1.7 ± 0.1	-5.3 ± 0.2	50 ± 33	-17 ± 11	11 ± 12	1.29×10^9
Independent		1.5 ± 2.5	-0.2 ± 0.6	-7.5 ± 1.1	21 ± 32	-4.7 ± 4.4	-2.1 ± 4.5	1.33×10^{12}
Cooperative	20	17 ± 9	-3.5 ± 0.2	-2.9 ± 0.3	32 ± 11	-24 ± 6	19 ± 6	9.79×10^8
Independent		0.6 ± 0.5	0.3 ± 17	-8.7 ± 17	12 ± 1	-5.2 ± 0.6	-1.4 ± 0.6	1.61×10^{12}
Cooperative	30	15 ± 2	-4.1 ± 0.7	-2.4 ± 0.1	26 ± 2	-21 ± 1	15 ± 1	1.80×10^8
Independent		0.7 ± 0.3	-1.9 ± 0.4	-6.4 ± 0.5	15 ± 1	-7.4 ± 0.4	0.9 ± 0.4	3.40×10^{11}
Cooperative	50	26 ± 3	-5.2 ± 0.6	-0.9 ± 0.6	57 ± 18	-23 ± 2	18 ± 2	1.60×10^7
Independent		1.9 ± 0.9	-1.9 ± 2.7	-5.8 ± 2.8	35 ± 1	-8.2 ± 0.7	2.2 ± 0.2	2.28×10^{11}
Cooperative	70	42 ± 13	-11 ± 3	4.9 ± 3.2	43 ± 2	-27 ± 2	21 ± 2	5.63×10^7
Independent		0.7 ± 0.3	-4.5 ± 1.2	-3.7 ± 1.3	24 ± 1	-10 ± 1	4.1 ± 0.2	2.87×10^{11}
Cooperative	100	45 ± 4	-11 ± 2	4.8 ± 1.5	50 ± 7	-26 ± 2	20 ± 2	6.02×10^7
Independent		0.6 ± 0.2	-4.4 ± 1.0	3.9 ± 1.0	35 ± 1	-8.7 ± 0.1	2.7 ± 0.1	1.86×10^{12}

¹Data collected at 20°C in 10 mM acetate (pH 5.5), 120 mM NaCl. ²RSS value obtained from MATLAB.

Table 5-3: Average of the individual fits comparison¹

	K_{d1} (μM)	ΔH_1 (kcal mol^{-1})	$-T\Delta S_1$ (kcal mol^{-1})	K_{d2} (μM)	ΔH_2 (kcal mol^{-1})	$-T\Delta S_2$ (kcal mol^{-1})	RSS ²
Cooperative	25 ± 15	-6 ± 3	-0.3 ± 0.4	43 ± 12	-23 ± 4	17 ± 4	2.6×10^9
Independent	1.0 ± 1.0	-2.1 ± 2.1	-6 ± 2	24 ± 9	-8 ± 3	1.1 ± 2.4	4.2×10^{12}

¹Data collected at 20°C in 10 mM acetate (pH 5.5), 120 mM NaCl. ²RSS value obtained from MATLAB.

The ITC data from the experiments performed at the six different concentrations were also analyzed using a global fit to both the independent and cooperative binding models (Figures 5-3 and 5-4). Again, the cooperative model provided the best fit as judged by the lowest RSS values (Table 5-4). The thermodynamic parameters for adenosine binding at each aptamer concentration are shown in Table 5-2 with the average of the individual fits shown in Table 5-3. The thermodynamic binding parameters from the global fit are shown in Table 5-4. There is an agreement between the average of the individual fits and the global fits to within the reported error range for all values except for the $-T\Delta S_1$ value.

Table 5-4: Global fits for cooperative and independent binding model comparison

	K_{d1} (μM)	ΔH_1 (kcal mol^{-1})	$-T\Delta S_1$ (kcal mol^{-1})	K_{d2} (μM)	ΔH_2 (kcal mol^{-1})	$-T\Delta S_2$ (kcal mol^{-1})	RSS
Cooperative	28 ± 5	-7.0 ± 0.3	1.0 ± 0.3	36 ± 4	-22 ± 1	16 ± 1	4.20×10^7
Independent	1.2 ± 0.7	4.7 ± 0.2	-12 ± 0.4	45 ± 18	-11 ± 11	5 ± 11	2.23×10^{11}

¹Data collected at 20°C in 10 mM acetate (pH 5.5), 120 mM NaCl. RSS value obtained from MATLAB

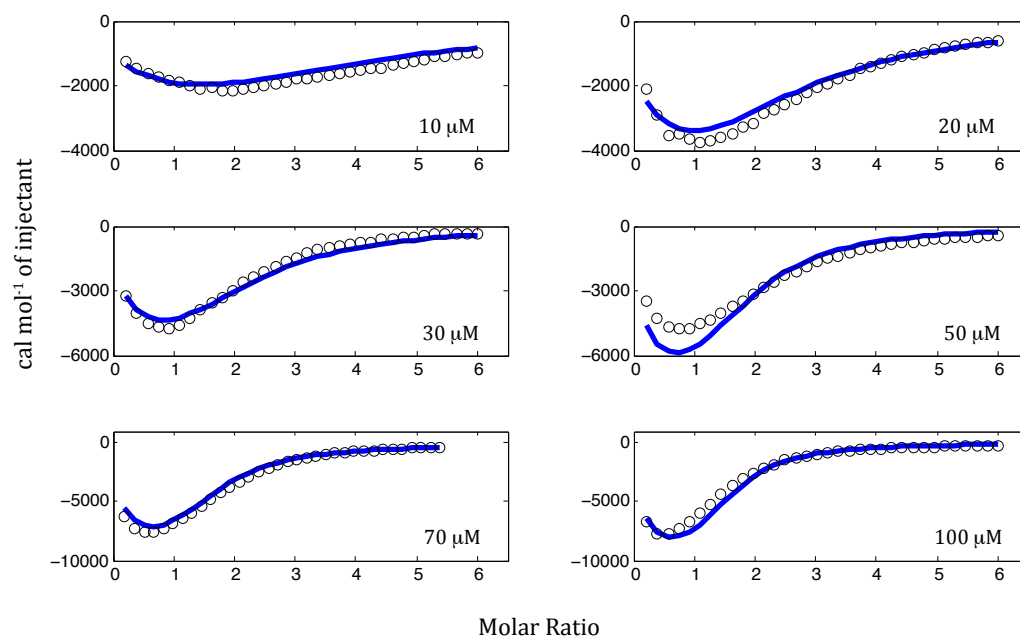


Figure 5-3. Global cooperative fit showing binding of adenosine to ATP3 aptamer acquired at various aptamer concentrations. Shown in green circles are the experimental data. Blue solid line shows global fit of the data to a cooperative binding model.

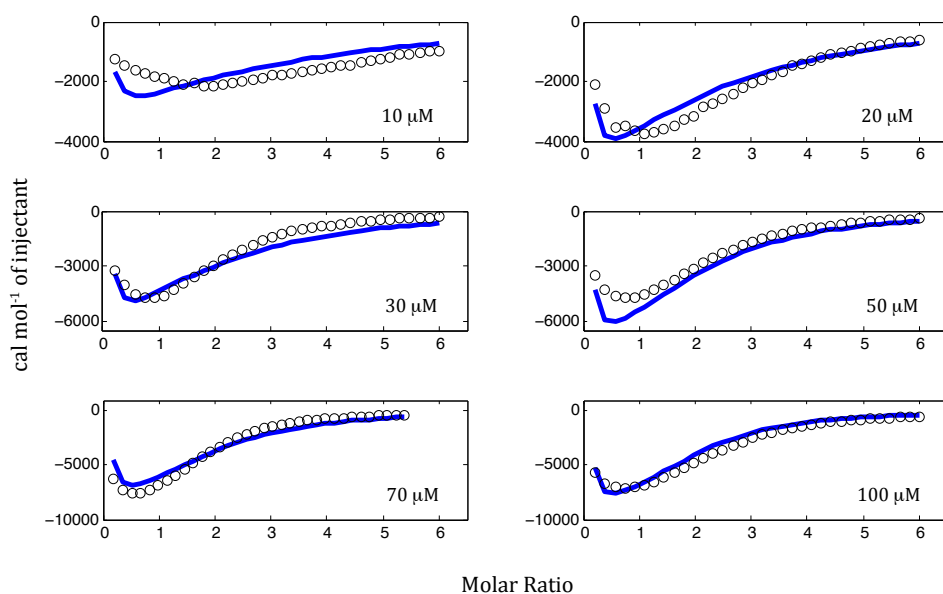


Figure 5-4: Global independent fit showing binding of adenosine to ATP3 aptamer acquired at various aptamer concentrations. Shown in green circles are the experimental data. Blue solid line shows global fit of the data to a cooperative binding model.

5.3.3. Relationship between two binding sites. To study how two binding sites are affected by mutations, guanine at positions 9 and 22 was replaced with inosine (Figure 5-1c and 5-1d). Thermograms for two ATP constructs are shown in Figure 5-5 and indicate that only one site is bound when guanine is replaced with inosine. Results presented in Table 5-5 indicate that adenosine binds to ATP9 and ATP10 weakly to the active site of the aptamer. Data was fit to a one site binding model.

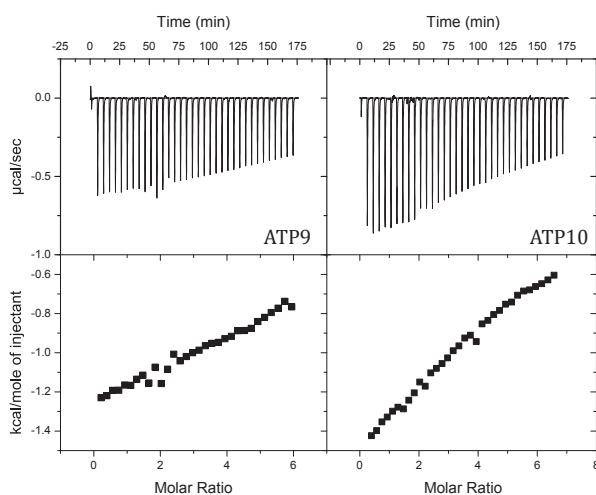


Figure 5-5: ITC thermograms showing binding of adenosine to (left) ATP9 and (right) ATP10.

Table 5-5: ATP9 and ATP10 aptamers binding to adenosine¹

	K_{d1} (µM)	ΔH₁ (kcal mol⁻¹)	-TΔS₁ (kcal mol⁻¹)
ATP9	212 ± 69	-1.7 ± 0.1	-3.9 ± 0.2
ATP10	188 ± 37	-2.1 ± 0.1	-3.9 ± 0.2

¹Data collected at 20°C in 10 mM acetate (pH 5.5), 120 mM NaCl.

5.3.4. ATP aptamer variants with one binding site. To compare to two-site ATP aptamer, three one-site ATP-binding aptamers were engineered (Figures 5-1e and 5-7). In the case of ATP11 (Figure 5-1e), new base pairs were introduced, and non-canonical base pairs replaced by Watson-Crick base pairs. This resulted in a binding affinity of $12 \pm 4 \mu\text{M}$, an enthalpy of $-133 \pm 1 \text{ cal mol}^{-1}$ and $-T\Delta S$ of $-7 \pm 1 \text{ kcal mol}^{-1}$ (Figure 5-6).

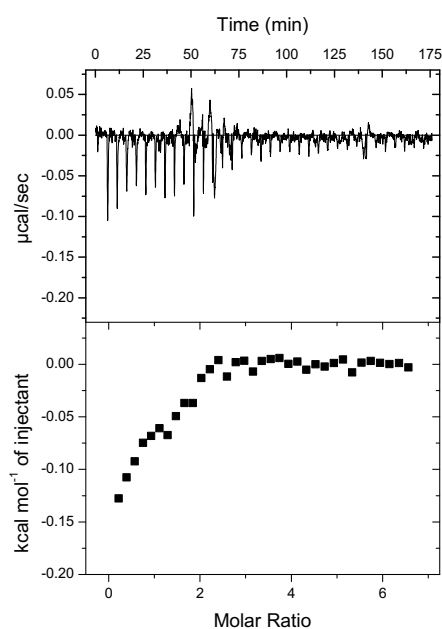


Figure 5-6: Thermogram showing binding of adenosine to the ATP11 aptamer. On top is the titration data showing the heat resulting from each injection of ligand into an aptamer solution. On the bottom are integrated heats after correcting for the heat of dilution. The binding experiment was performed at 20°C in 10 mM acetate (pH 5.5), 120 mM NaCl with aptamer concentration of $70 \mu\text{M}$ and adenosine concentration of 2.18 mM.

Next, a different one-site ATP aptamer, ATP1d was studied. This aptamer has been used in previous studies and binding affinity obtained matches the one obtained by

Zhang et al.¹⁰⁷ Replacing G16 with C16 (Figure 5-7b) and A7 with C7 (Figure 5-7c) disrupts binding as evident in ITC thermograms (Figure 5-8).

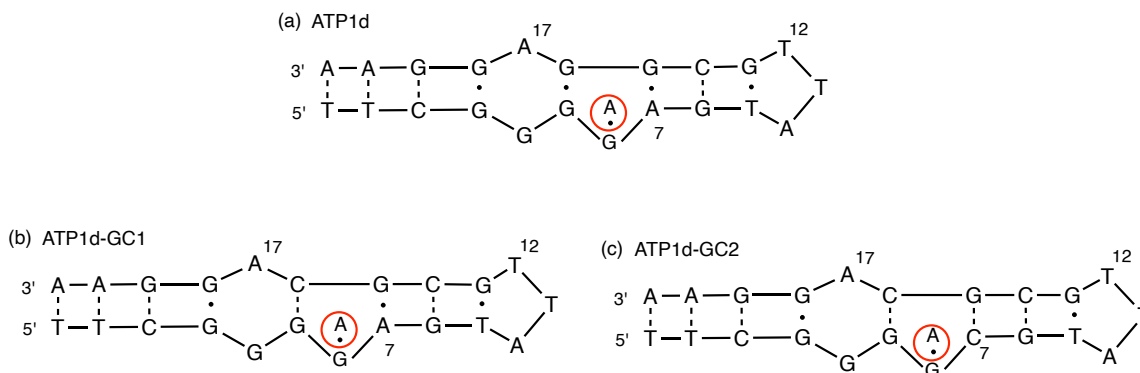


Figure 5-7: Structures of one-site ATP aptamer variants.

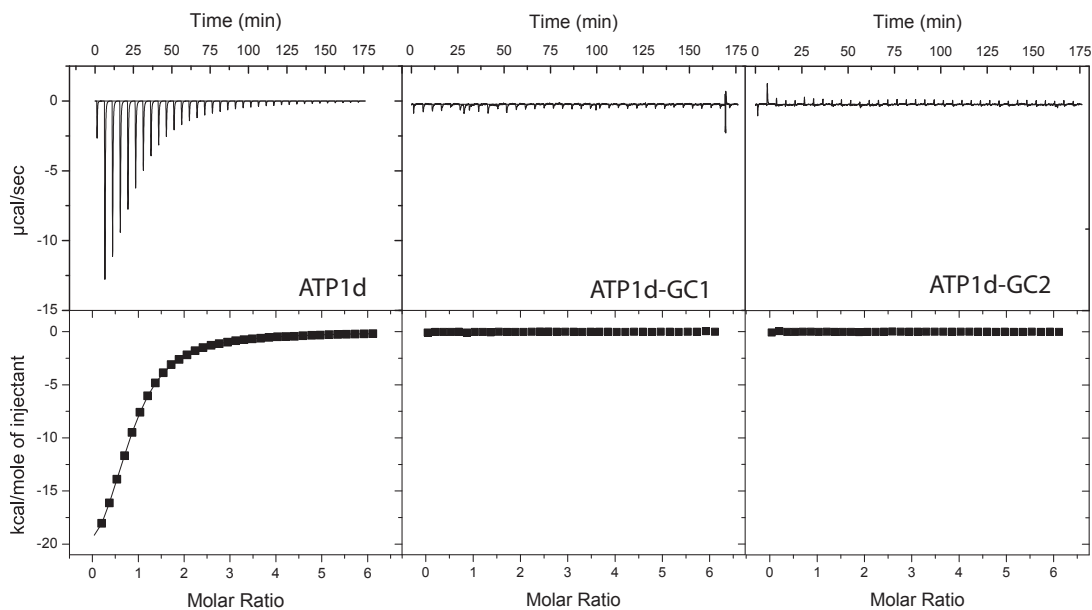


Figure 5-8: Thermograms showing interaction of one-site aptamers binding to adenosine. On top is the titration data showing the heat resulting from each injection of ligand into an aptamer solution. On the bottom are integrated heats after correcting for the heat of dilution. The binding experiment was performed at 20°C in 10 mM HEPES (pH 7.6), 100 mM NaCl, 2 mM MgCl₂ with aptamer concentration of 100 μM and adenosine concentration of 2.9 mM.

5.3.5. Adenosine binding to ATP6 aptamer. Another ATP aptamer variant, ATP6 (Figure 5-1b) was tested for binding to adenosine. This ATP aptamer variant consists of two palindromic strands and is 14 base pairs long. Each strand base pairs with its homologous strand to form a double helix conformation. ATP6 aptamer binds to adenosine and data was fit to both independent and cooperative binding model. Results best fit the cooperative binding model based on RSS value determined (Table 5-6). Figure 5-9 shows ITC thermogram of adenosine binding to ATP6 aptamer and MATLAB fits for both models.

Table 5-6: ATP6 binding to adenosine fit comparison¹

	K_{d1} (μM)	ΔH_1 (kcal mol^{-1})	$-\text{T}\Delta S_1$ (kcal mol^{-1})	K_{d2} (μM)	ΔH_2 (kcal mol^{-1})	$-\text{T}\Delta S_2$ (kcal mol^{-1})	RSS
Cooperative	91 ± 42	-3.0 ± 0.1	-2.9 ± 0.3	279 ± 18	-57 ± 21	-50 ± 21	4.38×10^8
Independent	0.9 ± 0.8	-3.7 ± 0.1	-4.5 ± 0.6	226 ± 27	-9 ± 1	3 ± 1	1.05×10^{12}

¹Data collected at 20°C in 10 mM acetate (pH 5.5), 120 mM NaCl. RSS value obtained from MATLAB

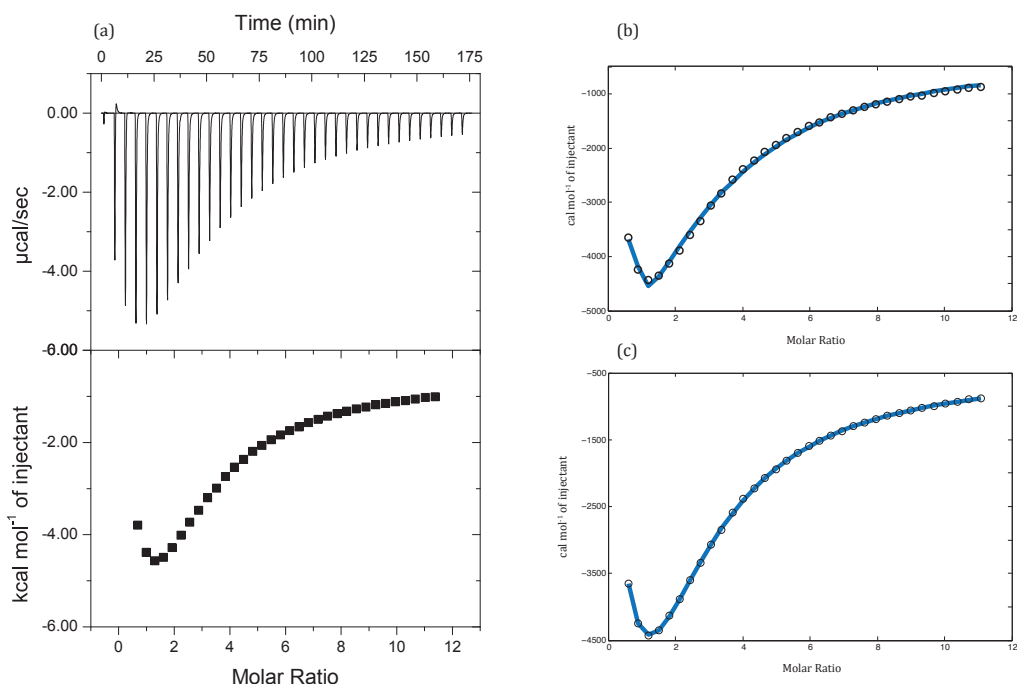


Figure 5-9: (a) ITC figure showing binding of adenosine to the ATP6 aptamer. MATLAB figure showing (b) independent binding fit and (c) cooperative binding fit. Black circles represent experimental data obtained by ITC. Blue solid line represents MATLAB fit.

5.3.6. ATP and adenosine binding to ATP7 aptamer. From binding results of the ATP-binding aptamer to the adenine-based ligands (Table 5-1) it can be noticed that, as the number of phosphates on the ligand is reduced, the affinity at both binding sites increases. Additionally, in the structure of the ATP3 aptamer the two binding sites are adjacent on the same side of the helical structure⁸. The binding probably became tighter with fewer phosphate groups present due to electrostatic repulsion between the ligands, and this repulsion could be minimized if the binding sites were on opposite sides of the helical structure. In order to test this, ATP7 aptamer was introduced, where three G•C base pairs and G•A mismatch between the 2 binding sites (5-1g). These 4 new base pairs should position the 2 binding sites

on opposite sides of the B-form helix. Binding results show that ATP7 aptamer binds two molecules of adenosine (Figure 5-10) with the data best fitting an independent binding model (Table 5-7).

Table 5-7: ATP7 binding to adenosine fit comparison¹

	K_{d1} (μM)	ΔH_1 (kcal mol^{-1})	$-T\Delta S_1$ (kcal mol^{-1})	K_{d2} (μM)	ΔH_2 (kcal mol^{-1})	$-T\Delta S_2$ (kcal mol^{-1})	RSS
Cooperative	0.6 ± 0.3	-7.7 ± 0.1	-1.1 ± 0.2	48 ± 6	-11 ± 2	4 ± 2	4.44×10^{11}
Independent	1.3 ± 0.5	-6.4 ± 0.1	-2.0 ± 0.6	32 ± 1	-12 ± 1	4 ± 1	9.33×10^{10}

¹Data collected at 20°C in 10 mM acetate (pH 5.5), 120 mM NaCl. RSS value obtained from MATLAB

Separating the two binding sites by 4 base pairs does not change the binding model in case of ATP binding to ATP7 however it affects binding affinity of one of the sites. Two molecules of ATP are bound by this aptamer (Figure 5-11) with the data best fitting a cooperative binding model (Table 5-8).

Table 5-8: ATP7 binding to ATP fit comparison¹

	K_{d1} (μM)	ΔH_1 (kcal mol^{-1})	$-T\Delta S_1$ (kcal mol^{-1})	K_{d2} (μM)	ΔH_2 (kcal mol^{-1})	$-T\Delta S_2$ (kcal mol^{-1})	RSS
Cooperative	13 ± 1	-1.3 ± 0.1	-5.1 ± 0.1	615 ± 97	-15 ± 2	10 ± 1	1.93×10^7
Independent	4 ± 2	-0.6 ± 0.9	-7.1 ± 0.3	145 ± 52	-3 ± 1	-3 ± 1	1.28×10^{10}

¹Data collected at 20°C in 10 mM acetate (pH 5.5), 120 mM NaCl. RSS value obtained from MATLAB

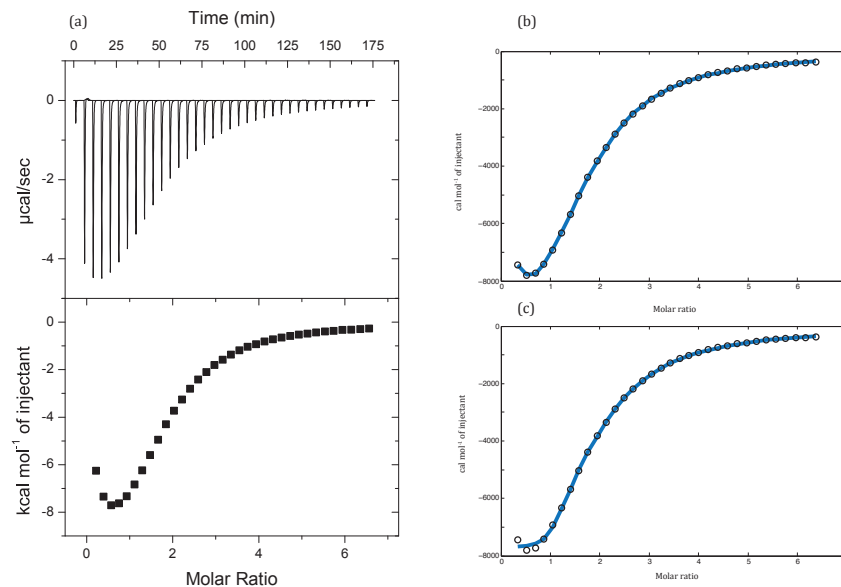


Figure 5-10: (a) ITC figure showing binding of adenosine to the ATP7 aptamer. MATLAB figure showing: (b) independent binding fit; (c) cooperative binding fit. Black circles represent experimental data obtained by ITC. Blue solid line represents MATLAB fit.

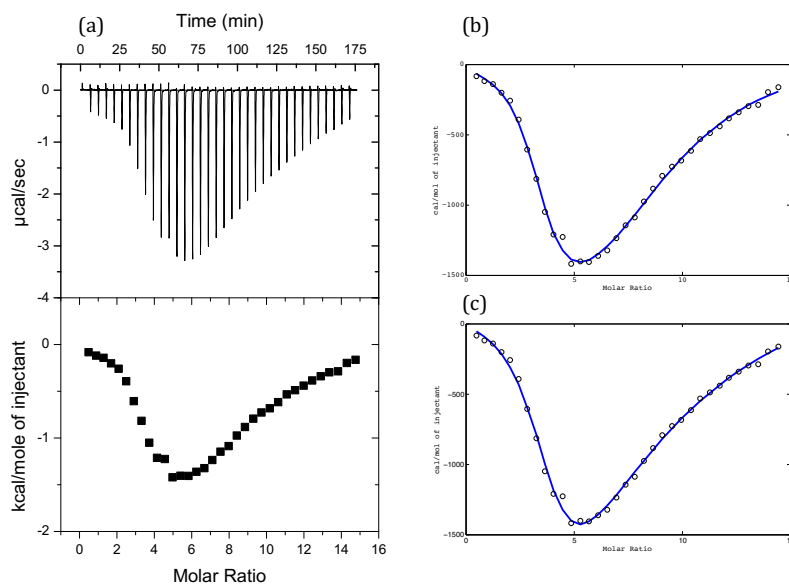


Figure 5-11: (a) ITC figure showing binding of ATP to ATP7 aptamer. MATLAB figure showing: (b) independent binding fit; (c) cooperative binding fit. Black circles represent experimental data obtained by ITC. Blue solid line represents MATLAB fit.

5.3.7. Adenosine binding to ATP17 aptamer. In order to determine the minimum number of base pairs between the two sites necessary to switch the binding model from cooperative to independent for adenosine, ATP17 aptamer was introduced. Here, the two binding sites are separated by two G•C base pairs and G•A mismatch (5-1f). Binding results show that ATP17 aptamer binds two molecules of adenosine (Figure 5-12) with the data best fitting a cooperative binding model (Table 5-9).

Table 5-9: ATP17 binding to adenosine comparison fits.¹

	K_{d1} (μM)	ΔH_1 (kcal mol^{-1})	$-\text{T}\Delta S_1$ (kcal mol^{-1})	K_{d2} (μM)	ΔH_2 (kcal mol^{-1})	$-\text{T}\Delta S_2$ (kcal mol^{-1})	RSS ²
Cooperative	44 ± 8	-1.0 ± 0.1	-4.7 ± 0.1	129 ± 71	-12 ± 2	7 ± 2	3.71×10^7
Independent	12 ± 2	0.1 ± 0.5	-7 ± 1	624 ± 206	-1.7 ± 0.3	-2.5 ± 0.5	1.33×10^{10}

¹Data collected at 20°C in 10 mM acetate (pH 5.5), 120 mM NaCl. ²RSS value from MATLAB

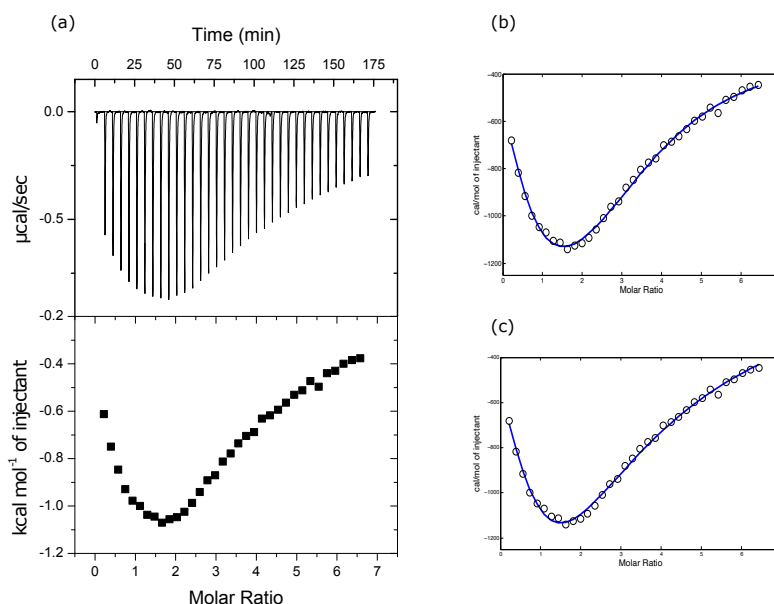


Figure 5-12: (a) ITC figure showing binding of adenosine to ATP17 aptamer. MATLAB figure showing (b) independent binding fit; (c) cooperative binding fit. Black circles represent experimental data obtained by ITC. Blue solid line represents MATLAB fit.

5.3.8. Hill coefficient analysis. ITC binding data acquired for ATP3, ATP7, ATP15 and ATP17 was analyzed to determine the Hill coefficient (n_H) for these aptamers and results presented in Table 5-10. Detailed calculation is shown in Appendix B.

Table 5-10: Hill coefficient results for ATP and adenosine binding to the ATP-binding aptamer constructs.

Aptamer	Ligand	n_H	Ligand	n_H
ATP3	ATP	1.19 ± 0.05	Adenosine	1.29 ± 0.08
ATP17	ATP	N/A	Adenosine	1.09 ± 0.02
ATP7	ATP	1.06 ± 0.02	Adenosine	1.01 ± 0.03

5.4 Discussion

Isothermal titration calorimetry (ITC) is a useful tool used in determination of binding constants and thermodynamic parameters of binding from a single experiment^{125,151-153}. ITC is often applied in the study of systems where an aptamer has a single binding site and only one molecule of ligand is bound. However, it can be applied in study of systems in which ligand binds to multiple sites independently or cooperatively^{103,126,154,155}. Determining which binding model is the correct one by ITC can be a challenge as different binding models can give the identical fit to the same set of data. If the binding mechanism is not known it can be difficult to determine which model is the correct one. In ITC, Wiseman parameter “c” plays an important role. This parameter is the product of aptamer concentration, binding affinity, K_a and stoichiometry parameter, n ¹⁵⁶. An optimal c-value lies between 10 and 100 where thermodynamic parameters are most accurately determined^{95,157}.

Different aptamer concentrations will give different shape of the curve. Low aptamer concentrations (c value close to 1) will give shallow curve from which affinity can be determined, but not enthalpy; while high concentrations of aptamer will give sigmoidal shape (in case of one site binding) and “u” or “v” shaped curve in case of two-site binding mechanism. Therefore, it is important to have some data sets at higher concentrations because if an aptamer possesses second binding site, at low aptamer concentrations second binding site may not be visible. In case of fitting, changing concentration of the aptamer should not affect the binding model, i.e. data should fit to the correct model regardless of the aptamer concentration.

Here, isothermal titration calorimetry is used to determine whether two molecules of adenosine bind cooperatively or independently of each other to ATP3 aptamer. Using a method developed by Freiburg et al.¹⁰³, ITC experiments were performed on six different samples of ATP3 aptamer with concentrations ranging from 10 to 100 μM . Each data set was fit individually to both independent and cooperative model with different binding parameters obtained for each sample. Lower concentrations of ATP3 aptamer did not provide good fit using independent model and had large uncertainties in values (Table 5-1), which was not evident in cooperative model. In order to determine which fit corresponds better to the binding mechanism, the residual sum of squared deviations (RSS) was determined. This value represents discrepancy between experimental data and an estimation model. Small RSS value indicates a tight fit of the model to the data and is used as criterion in model selection. Results indicate that cooperative global fitting model of

adenosine binding to ATP3 aptamer has lower RSS values (4.2×10^7) compared to independent model (2.23×10^{11}) (Table 5-3). Individual data fits were also averaged for each binding model and average individual cooperative fits agree within experimental errors with results obtained by global cooperative fitting model. The binding parameters for cooperative model are presented in Table 5-3 and although two adenosines bind with similar affinities ($K_{d1} = 28 \pm 5 \mu\text{M}$ and $K_{d2} = 36 \pm 4 \mu\text{M}$) they have different enthalpy and entropy of binding ($\Delta H_1 = -7.0 \pm 0.3 \text{ kcal mol}^{-1}$, $-T\Delta S_1 = 1.0 \pm 0.3 \text{ kcal mol}^{-1}$, $\Delta H_2 = -22 \pm 1 \text{ kcal mol}^{-1}$, $-T\Delta S_2 = 16 \pm 1 \text{ kcal mol}^{-1}$). In case of independent model large errors have been obtained for both enthalpy and entropy values of the second site (Table 5-3).

To further investigate the validity of the cooperative model, base substitution using inosine instead of guanine was performed. Guanine to inosine substitution is often used to study properties of nucleic acid. Inosine differs by loss of the N2 amino group, so this substitution is suited to probe structural and thermodynamic effects of single H-bonds¹⁵⁸. In the ATP3 aptamer, one of the binding sites was mutated by changing guanine at positions 9 and 22 (guanine that interacts with the ligand) with inosine (ATP9 and ATP10). It has been shown that inosine in this position inhibits binding as these two bases, G9 and G22, are part of binding pocket, a recognition alignment that involves AMP • G mismatch formation through a pair of hydrogen bonds between Watson-Crick edge of adenosine and minor groove edge of guanine⁸. Both ATP9 and ATP10 retain only very weak binding to adenosine (Table 5-5). In these aptamers the ligand does not bind at the mutated binding site, but the

unbound aptamer retains its disordered nature at the entire binding site. With binding at the one remaining site still possible, more of the binding free energy from that single ligand binding event needs to go into folding the aptamer with much weaker binding being observed.

To determine whether binding is retained after completely removing one site, several ATP aptamer variants were studied. In the case of ATP11 (Figure 5-1e), one binding site has been removed by incorporating Watson-Crick type base pairs in order to retain structural stability. This aptamer also binds adenosine with $K_d = 12 \pm 4 \mu\text{M}$ and enthalpy $-133 \pm 13 \text{ cal mol}^{-1}$. Long stem provides stability giving tighter binding but introducing Watson-Crick base pairs decreases enthalpy suggesting that free energy went into folding of the aptamer and only little into binding. ATP1d aptamer also retains structural stability, although it binds slightly weaker than ATP11, with $K_d = 21 \pm 2 \mu\text{M}$ and enthalpy $-23.6 \pm 0.4 \text{ kcal mol}^{-1}$.

As a further test of reducing the disorder at the binding site, two aptamers Apt1d-GC1 and Apt1d-GC2 were analyzed. These aptamers were constructed by changing the mismatched base pairs immediately adjacent to the G that interacts with the ligand to be Watson-Crick paired. This further reduction in binding site mobility resulted in no binding being observed. This indicates that these mismatched base pairs are required for binding, likely due to structural reasons, and consistent with G•G mismatched base pairs being found in both the DNA and RNA forms of AMP-binding aptamers^{8,159}.

A palindromic version of this aptamer can be generated through base pairing of two self-complementary strands that contain 14 base pairs. Binding of adenosine to ATP6 aptamer has been originally studied by Lin and Patel as it provided improved $^1\text{H-NMR}$ spectra compared to ATP3¹⁶⁰. Binding of adenosine to this self-complementary ATP6 still follows cooperative model with thermodynamic parameters shown in Table 5-6. Cooperative fit agrees better with experimental data unlike independent model as RSS value obtained for cooperative model (4.38×10^8) is lower compared to the one obtained for independent binding model (1.05×10^{12}).

In all ATP aptamer versions with two binding sites studied, the two sites are adjacent to each other. When two sites are separated by an additional four base pairs, as in ATP7 aptamer, they point away from each other. In this case, two adenosines bind independently of each other. Affinity of one site is about 20-fold higher than for ATP3 aptamer; however, binding affinity of the second site remains unchanged. Results are presented in Table 5-7 and RSS value obtained for cooperative model (4.44×10^{11}) is higher than one obtained for independent model (9.33×10^{10}). Also, Figure 5-10 shows that independent fit agrees better with the experimental data. On the other hand, ATP binds cooperatively to the ATP7 aptamer with RSS value for cooperative model (1.93×10^7) smaller than the one obtained for the independent model (1.28×10^{10}). Binding affinity of one site is about 10-fold tighter than for the ATP3 aptamer, while affinity of the second site remains the same (Table 5-8).

In order to determine how many base pairs are required to switch binding model for adenosine from cooperative to independent, ATP17 aptamer is introduced. Separating two binding sites by three base pairs does not change the binding model for adenosine. Results are presented in Table 5-11 with RSS value for the cooperative fit (3.71×10^7) being smaller than for independent fit (1.33×10^{10}). These findings show that for adenosine at least four base pairs are necessary to switch the binding model from cooperative to independent.

5.5 Concluding remarks

ATP-binding aptamer consistently follows a cooperative binding mechanism whether it is the original 27 nucleotide sequence or the duplex version and whatever ligand the aptamer binds (Table 1). What factor(s) in the aptamer that gives rise to the cooperativity is unknown, however the two binding sites need to be close together and this results in the two ligands binding on the same side of the helix. When the two sites are separated, as in ATP7, the two adenosine ligands bind independently (Table 6). It may be possible that the two binding sites need to be close for them to somehow communicate with each other or that the two ligands interact during the binding process. As first ligand binds, it organizes the second binding site, then second ligand binds this preorganized site higher than it would, which is evident in positive hill coefficient for both adenosine and ATP binding.

Chapter 6 **Designed Alteration of Binding Affinity in Structure-Switching Aptamers Through the Use of Dangling Nucleotides**

6.1 Preface

All work presented in this chapter has been published in the article listed below.

- **Slavkovic, S.,** Eisen, S., and Johnson, P.E. “Designed Alteration of Binding Affinity in Structure-Switching Aptamers Through the Use of Dangling Nucleotides.” *Biochemistry* **59 (5)**, 663 – 671 (2020).

6.2 Introduction

The ability to alter the function of biomolecules in a designed manner is an important goal in biotechnology. For functional nucleic acids, altering nucleic acid structure and thereby its function, is greatly aided by the known thermodynamic contributions to stability of adding or changing base pair identity¹⁶¹. Important class of functional nucleic acids are structure-switching aptamers. For these aptamers, ligand binding is coupled with a structural transition from an unfolded or loosely folded ligand-free structure, to a folded ligand-bound structure^{162,163}. Structure-switching aptamers are important in biosensor development where the structural change is converted into a measurable signal of the binding event to a folded have the advantage are more amenable to introducing controlled changes in their function^{144,164-166}.

The cocaine-binding aptamer is a useful model system for aptamer design^{64,75,85,86,115,167}. This aptamer is structured as a three-way junction centered

near a tandem AG mismatch (Fig. 1)⁷⁷. Two facets of this aptamer that make it particularly interesting are that it transitions between having a ligand-induced folding mechanism when stem 1 is three base pairs long or shorter and being pre-structured with a four base pair or longer stem 1^{77,79}. Additionally, the cocaine-binding aptamer has substantial binding promiscuity in that it binds quinine-based ligands much tighter than cocaine, the ligand it was originally selected for^{82,96,168}. Previously, we introduced binding selectivity for tighter binding ligands into this aptamer by altering the length of stem 1. By shortening stem 1 to have two base pairs (OR8, Figure 6-1) instead of three (MN19, Figure 6-1), more free energy from ligand binding is needed to fold the aptamer with only the tighter binding ligand, quinine, able both fold and bind the OR8 aptamer while cocaine is not capable of binding OR8.

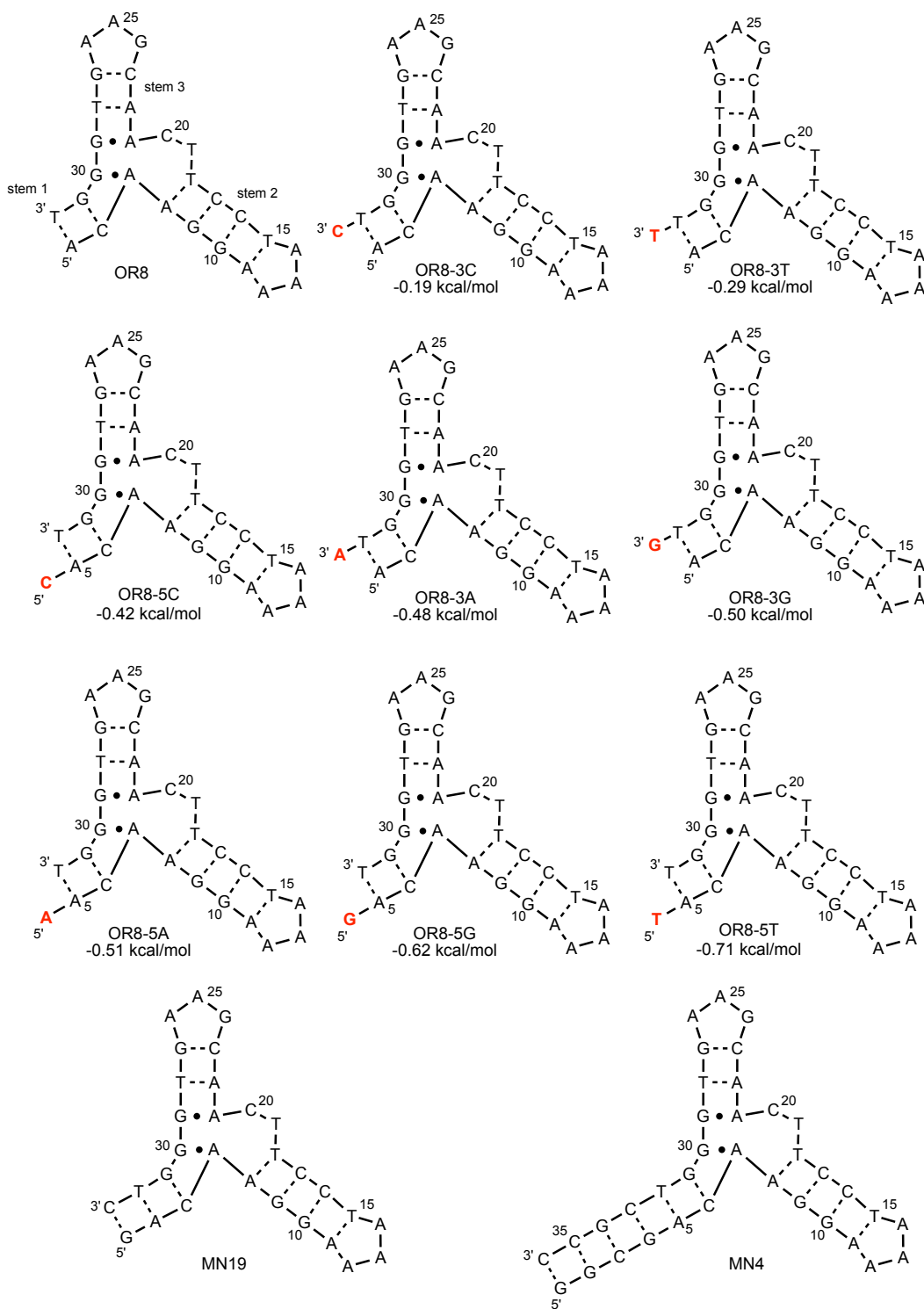


Figure 6-1: Secondary structures of the cocaine-binding aptamers containing dangling nucleotides as well as the OR8 and MN19 aptamers. The numbering of the nucleotides matches what we have used previously and is derived from the MN4 construct. Dashes between nucleotides indicate Watson–Crick base pairs while dots indicate non-Watson–Crick base pairs.

In this study, the binding affinity of the structure switching cocaine-binding aptamer is fine tuned in a designed manner by introducing unpaired, or dangling 3' or 5' nucleotides. Unpaired nucleotides can stack against the terminal base pair¹⁶⁹⁻¹⁷¹ and stabilize, or even destabilize, a nucleic acid structure by a known ΔG°_{37} value¹⁷². For structure-switching aptamers, or aptamers that undergo a ligand-induced folding mechanism, adding a stabilizing dangling nucleotide should reduce the free energy needed to fold the molecule, as this free energy is obtained from the ligand-binding free energy, more free energy would be left over for the apparent ΔG of binding, and observed in the K_d value measured.

6.3 Results

6.3.1. Cocaine-binding aptamer dangling nucleotide constructs. The quinine binding thermodynamics of eight different cocaine-binding aptamer constructs (Figure 6-1) with dangling nucleotides were determined using ITC methods. For comparison, both the OR8 and MN19 constructs, comprised of stem 1 lengths of 2 and 3 base pairs, respectively, were also measured. These dangling nucleotide constructs were chosen to give as large a range of ΔG° values as possible while preserving the terminal AT base pair of OR8. The terminal AT base pair must be maintained as switching the AT base pair to be a TA base pair causes reduction in affinity for cocaine to 31 μM from 7 μM ⁷⁷.

The thermograms for all ten constructs are shown in Figure 6-2. With the exception of MN19 all binding curves were fit to a 1:1 binding model. For MN19, the thermogram shows a distinct non-sigmoidal shape indicative of two-site binding as observed previously at lower aptamer and NaCl concentrations¹²⁶. The data for MN19 were therefore fit to a two-site independent binding model. The thermodynamic binding parameters for these cocaine-binding aptamer constructs are shown in Tables 6-1 and 6-2.

Table 6-1: Binding affinities and free energy of quinine binding by aptamers used in this study.¹

	K_d (μM)	ΔG (kcal mol^{-1})	$\Delta\Delta G$ (kcal mol^{-1})	ΔG (cal mol^{-1}) ³
OR8	111 ± 4	-5.2 ± 0.2	-	-
OR8 – 3C	66 ± 4	-5.5 ± 0.4	-0.29 ± 0.43	-190
OR8 – 3T	57 ± 1	-5.6 ± 0.1	-0.38 ± 0.23	-290
OR8 – 5C	43 ± 1	-5.8 ± 0.1	-0.55 ± 0.23	-420
OR8 – 3A	22 ± 1	-6.2 ± 0.1	-0.94 ± 0.23	-0.48
OR8 – 3G	21 ± 1	-6.2 ± 0.2	-0.94 ± 0.27	-0.50
OR8 – 5A	8.7 ± 0.3	-6.7 ± 0.2	-1.46 ± 0.38	-510
OR8 – 5G	8.3 ± 0.1	-6.7 ± 0.1	-1.49 ± 0.22	-620
OR8 – 5T	7.2 ± 0.1	-6.8 ± 0.1	-1.57 ± 0.21	-710
MN19 ²	0.4 ± 0.1	-8.4 ± 1.2	-3.22 ± 1.25	-1150

¹Data acquired at 15°C in 20 mM TRIS (pH 7.4), 140 mM NaCl, 5 mM KCl. The values reported are averages of 2 to 5 individual experiments. ²Data were fit to a 2-site independent binding model with the fits for the high affinity site reported here. ³Values from Bommarito *et al.*(28).

Table 6-2: Thermodynamic parameters of aptamers used in this study upon binding to quinine.¹

	ΔH (kcal mol ⁻¹)	$-T\Delta S$ (kcal mol ⁻¹)
OR8	-10.1 ± 0.1	4.9 ± 0.3
OR8 – 3C	-15.2 ± 2.1	9.7 ± 2.1
OR8 – 3T	-16.9 ± 0.2	11.3 ± 0.2
OR8 – 5C	-16.4 ± 2.8	10.6 ± 2.9
OR8 – 3A	-16.6 ± 0.1	10.5 ± 0.1
OR8 – 3G	-19.8 ± 0.1	13.6 ± 0.2
OR8 – 5A	-20.2 ± 2.7	13.5 ± 2.8
OR8 – 5G	-21.0 ± 1.5	14.3 ± 1.5
OR8 – 5T	-25.7 ± 0.1	19.0 ± 0.1
MN19 ²	-17.4 ± 1.1	8.9 ± 1.6

¹Data acquired at 15°C in 20 mM TRIS (pH 7.4), 140 mM NaCl, 5 mM KCl. The values reported are averages of 2 to 5 individual experiments. ²Data were fit to a 2-site independent binding model with the fits for the high affinity site reported here.

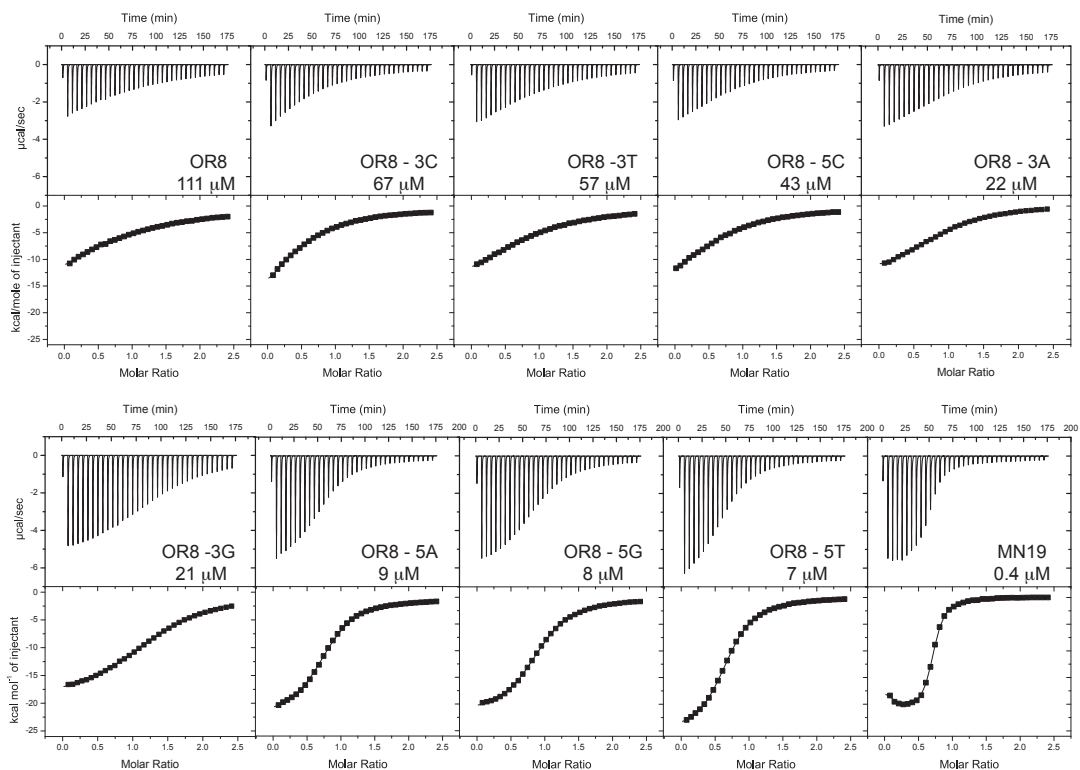


Figure 6-2: ITC data showing the interaction of the different cocaine-binding aptamers binding quinine. On top is the raw titration data showing the heat resulting from each injection of ligand into aptamer solution. The bottom shows the integrated heat plot after correcting for the heat of dilution. Data were acquired at 15 °C in 20 mM Tris (pH 7.4), 140 mM NaCl, 5 mM KCl.

6.3.2. ATP-binding aptamer dangling nucleotide constructs. In order to test the generality of introducing dangling nucleotides into structure-switching aptamers to alter binding affinity, dangling nucleotides were introduced into a single site version of the ATP-binding aptamer (Figure 6-3)¹⁰⁷. The adenosine binding thermodynamics of two different ATP-binding aptamer constructs with dangling nucleotides were determined using ITC methods.

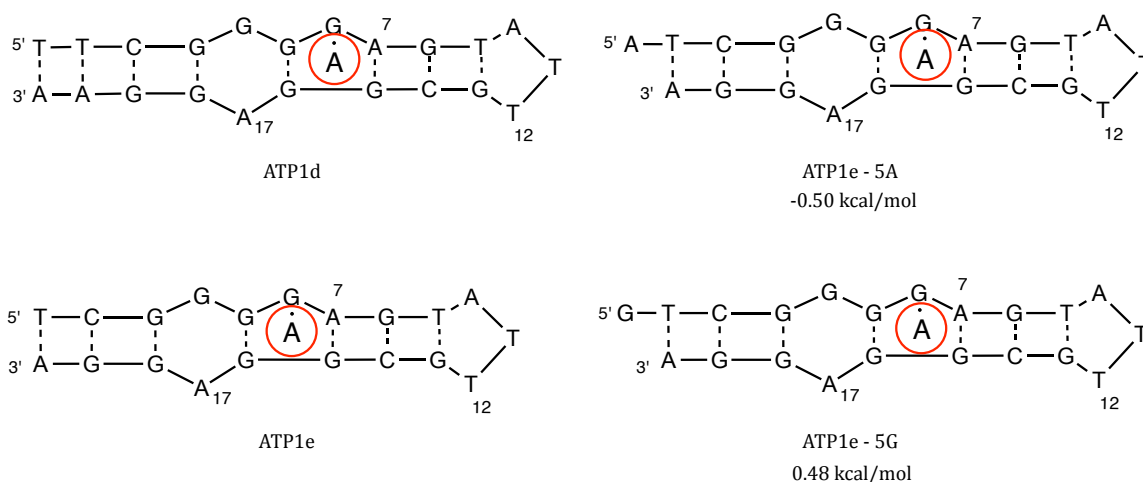


Figure 6-3: Secondary structures of the ATP-binding aptamers containing dangling nucleotides as well as the ATP1d and ATP1e aptamers. Dashes between nucleotides indicate Watson–Crick base pairs while dots indicate non-Watson–Crick base pairs.

To provide a comparison with the dangling nucleotide constructs, both the ATP1d and ATP1e aptamers, comprised of stem lengths that differed by 1 base pair were also analyzed (Figure 6-3). The two dangling nucleotide constructs were chosen as their unpaired nucleotides are the most stabilizing and destabilizing possible combinations for a terminal TA base pair¹⁷². These two dangling nucleotide constructs have a stability difference of $1213 \text{ cal mol}^{-1}$ which is similar to the $1150 \text{ cal mol}^{-1}$ range of stability in the cocaine-binding aptamer dangling nucleotide constructs analyzed. Additionally, the dangling 5'-G in ATP1e-5G against a TA base pair is the most destabilizing possibility reported of all potential combinations. The thermograms for all four ATP-binding aptamer constructs are shown in Figure 6-4. All binding curves were fit to a 1:1 binding model. The thermodynamic binding parameters for the ATP-binding aptamer constructs for adenosine are shown in Tables 6-3 and 6-4.

Table 6-3: Binding affinities and free energy of adenosine binding by the ATP-binding aptamers used in this study.¹

	K_d (μM)	ΔG (kcal mol^{-1})	$\Delta\Delta G$ (kcal mol^{-1})	ΔG°_{37} (cal mol^{-1}) ²
ATP1e	57 ± 5	-5.6 ± 0.5	-	-
ATP1e-5A	37 ± 3	-5.9 ± 0.5	-0.3 ± 0.8	-500
ATP1e-5G	81 ± 7	-5.5 ± 0.2	0.1 ± 0.6	480
ATP1d	21 ± 2	-6.2 ± 0.6	-0.6 ± 0.8	-733

¹Data acquired at 15°C in 10 mM HEPES (pH 7.6), 100 mM NaCl, 2 mM MgCl₂. The values reported are averages of 2 to 3 individual experiments. ²Values from Bommarito *et al.*¹⁷².

Table 6-4: Thermodynamic parameters of adenosine binding by the ATP-binding aptamers used in this study.¹

	ΔH (kcal mol^{-1})	$-T\Delta S$ (kcal mol^{-1})
ATP1e	-8.1 ± 0.8	3 ± 1
ATP1e-5A	-17.3 ± 0.2	11.5 ± 0.2
ATP1e-5G	-8 ± 2	3 ± 2
ATP1d	-23.6 ± 0.4	17.4 ± 0.4

¹Data acquired at 15°C in 10 mM HEPES (pH 7.6), 100 mM NaCl, 2 mM MgCl₂. The values reported are averages of 2 to 3 individual experiments.

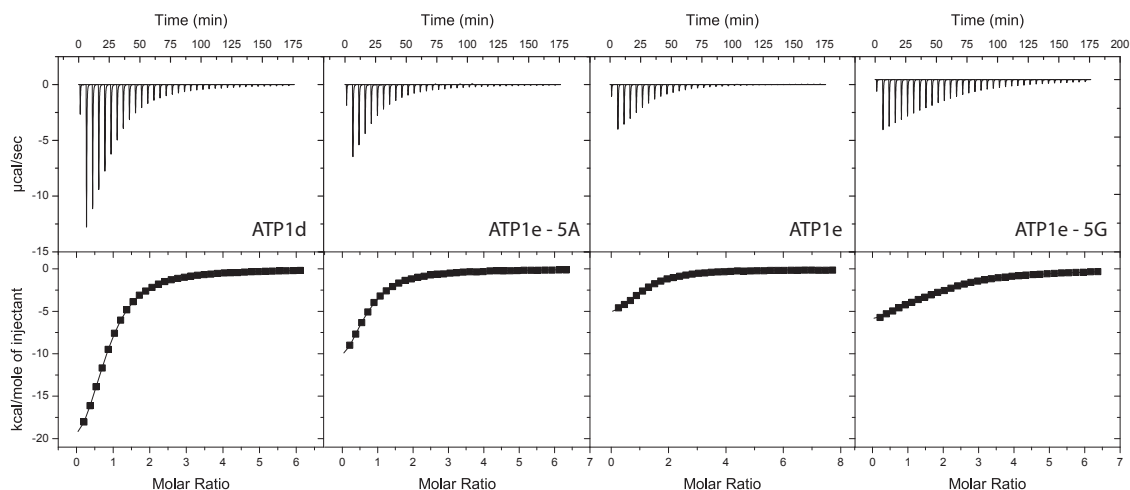


Figure 6-4: ITC data showing the interaction of the different ATP-binding aptamers interacting with adenosine. On top is the raw titration data showing the heat resulting from each injection of ligand into aptamer solution. The bottom shows the integrated heat plot after correcting for the heat of dilution. Data were acquired at 15 °C in 10 mM HEPES (pH 7.6), 100 mM NaCl, 2 mM MgCl₂.

6.4 Discussion

The addition of dangling nucleotides to structure-switching aptamers increases or decreases the affinity of the aptamer depending on whether the dangling nucleotide stabilizes or destabilizes the DNA structure (Tables 6-1 and 6-3). All the different constructs of the same aptamer type bind the ligand with the same amount of free energy. For the cocaine-binding aptamer binding quinine, this amount is $\Delta G_{QN,bind}$ (Figure 6-5). This binding free energy is the same for the different constructs as the nucleotide composition at the ligand binding site is the same in all aptamers while the changes to the aptamer that effect stability are located away from the binding site. Interaction of quinine with an aptamer results in some of the $\Delta G_{QN,bind}$ going into folding the aptamer, with the remaining binding free energy manifesting itself

as an apparent binding affinity, $\Delta G^{\text{app}}_{\text{QN,bind}}$ (Figure 6-5). This apparent ΔG value is what is measured by the ITC and manifested in the observed affinity.

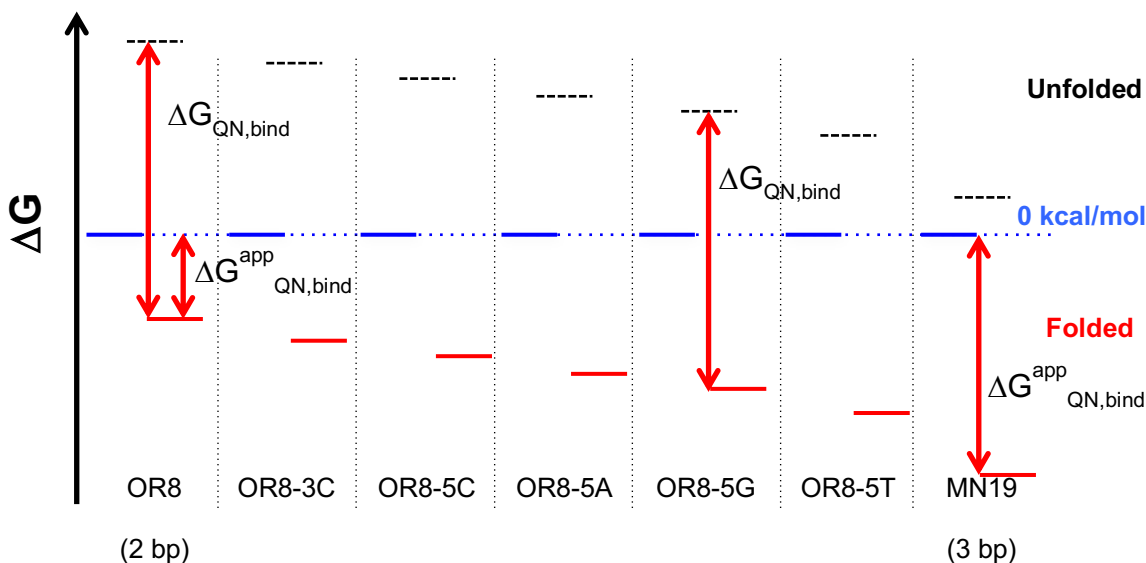


Figure 6-5: Free energy diagram of ligand binding by selected dangling nucleotide cocaine-binding aptamer constructs. Each aptamer has solid blue, dotted black and solid red line representing the unfolded free state, the hypothetical folded free state and the folded bound state, respectively.

Similar concept was demonstrated with the cocaine-binding aptamer by altering the length of stem 1 in order to obtain an aptamer (OR8) that only bound the tighter-binding ligand quinine, and not the weaker-binding ligand cocaine⁷⁹. This demonstrated that quinine binding is tight enough to both fold and bind OR8, but the binding of cocaine does not have enough free energy to fold OR8, so no binding is observed. This analysis was extended for the quinine derivative amodiaquine, the tightest binding ligand for the cocaine-binding aptamer reported to date¹⁶⁸. Amodiaquine can fold and bind a cocaine-binding aptamer (OR7) comprised of only

one base pair in stem 1, therefore requiring even more free energy from ligand binding to fold than does OR8 which has 2 base pairs in stem 1. Quinine, a weaker binding ligand than amodiaquine, does not bind OR7.

Incorporation of dangling nucleotides into a structure-switching aptamer alters the binding affinity in a more fine-grained manner than by adding or removing base pairs (Figure 6-5). Dangling nucleotides can stabilize or destabilize a nucleic acid structure in a known manner depending on the identity of the 5' or 3' added nucleotide and the identity of the terminal base pair^{172,173}. If the dangling nucleotide is stabilizing, as almost all possibilities are, less free energy from the binding affinity is needed to fold the aptamer and consequently the observed binding affinity increases (Figure 6-5). This is what is observed with all the cocaine-binding aptamer dangling nucleotides constructs (Table 6-1). The binding thermodynamics for the OR8 and MN19 aptamers match what was observed previously when corrected for temperature. Additionally, two-site binding for the MN19 construct at 140 mM NaCl concentration is not observed at low aptamer concentrations. However, at the high aptamer concentration used here, 98 μ M, binding of quinine at the weaker second site is observed.

As a confirmation of the trend seen with the cocaine-binding aptamer, and to extend results to include a destabilizing dangling nucleotide construct, dangling nucleotides were incorporated into the single-site version of the ATP-binding aptamer developed by Zhang and Liu¹⁰⁷. The ATP aptamer is also recognized as undergoing a

structure switching transition from an unstructured, or loosely structured free state to a structured bound state⁸. A large change in affinity between the 2 and 3 base pair aptamers ATP1d and ATP1e represent a limitation of the amount of free energy available from adenosine binding to fold the destabilized aptamer ATP1e being reached. Therefore, this construct was chosen to which to add dangling nucleotides. Adenosine binding results for ATP1d (Tables 6-3 and 6-4) match what was previously reported¹⁰⁷. For ATP1e, affinity is significantly tighter than previously reported for the same conditions due to working at a much higher aptamer concentration of 100 μM rather than 10 μM . The binding curve is better defined because of the higher Wiseman “c” parameter (c-value)^{152,156}.

The binding affinity of the two dangling nucleotide ATP-binding aptamers were measured using ITC methods and match the trends observed with the cocaine-binding aptamer. ATP1e-5A, which is more stable than ATP1e has a tighter affinity for adenosine than ATP1e (Table 6-3). ATP1e-5G, which has the destabilizing dangling 5'G has a weaker affinity for adenosine than ATP1e (Table 6-3).

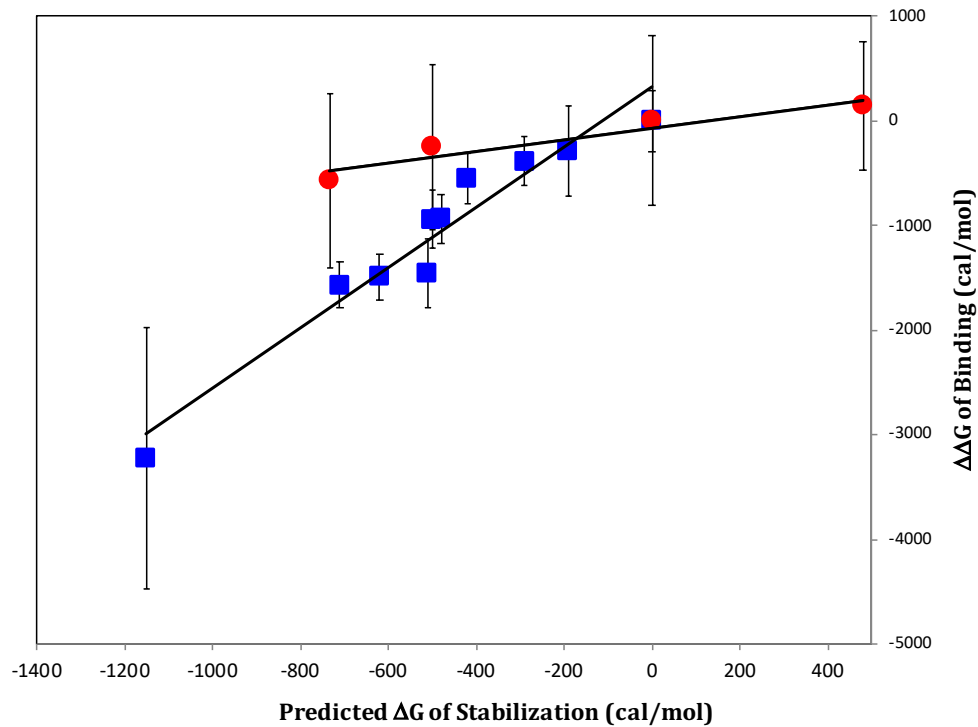


Figure 6-6: Plot of the predicted ΔG°_{37} values of adding a dangling nucleotide versus the observed change in ΔG of binding ($\Delta\Delta G$). The blue filled squares are the data for the cocaine-binding aptamer series while the open red circles are for the ATP-binding aptamers.

For both the cocaine-binding and ATP-binding aptamers, dangling nucleotides with the largest contributions to stabilization display the largest increase in observed binding affinity (Tables 6-1 and 6-3). Figure 6-6 shows the difference in the free energy of binding ($\Delta\Delta G$), obtained from the K_d values, against the predicted ΔG°_{37} values for the added dangling nucleotide. Also plotted are the data for aptamer constructs extended by a base pair. Both the cocaine-binding aptamer and ATP-binding aptamer data follow separate straight-line relationships. Neither data set has a slope of 1 likely arising from the fact that the predicted stabilization data are tabulated for 37 °C while both binding data sets were acquired at 15 °C.

6.5 Concluding remarks

In conclusion, the two data sets do not fall on the same straight line as the addition of a dangling nucleotide in these two separate aptamer systems results in different contributions to decrease the required free energy of folding for each system. One difference between these two aptamers is that the ligand binding sites in the aptamers are at a different distance from the site of stabilization by the dangling nucleotide. For the cocaine-binding aptamer, the high affinity ligand binding site is at the three-way junction close to nucleotides T19, C20, G30 and G31⁷⁷. This is 2–3 bp from the site of stabilization by the addition of dangling nucleotides at the terminal base pair in OR8 (Figure 6-1). For the ATP-binding aptamer, the binding site is at the sole unpaired G nucleotide (G7; Figure 6-3) located 5 bp away from where the addition of dangling nucleotide stabilizes the free aptamer structure. Another factor that could contribute to the different effect of adding dangling nucleotides would be the different three-dimensional structure formed by the two aptamers. Other factors that may influence how the addition of dangling nucleotides affects these two systems differently could involve the difference in the nature of how the two ligands interact with the aptamers due to factors such as the size and shape of the ligand and the role played by the different non-covalent forces involved in ligand binding. Finally, different types of forces could drive the folding of the two different aptamers, with the added dangling nucleotides affecting the different folding events in different ways. It is likely that a combination of these factors results in the different effect on ligand affinity that adding dangling nucleotides has in the cocaine-binding and ATP-binding aptamer systems.

Chapter 7 Nanomolar Binding Affinity of Quinine-Based Antimalarial Compounds by the Cocaine-Binding Aptamer

7.1 Preface

All work presented in this chapter has been taken from the article listed below.¹⁶⁸

- **Slavkovic, S.**, Churcher, Z.R. and Johnson, P.E. “Nanomolar Binding Affinity of Quinine-Based Antimalarial Compounds by the Cocaine-Binding Aptamer.” *Bioorganic & Medicinal Chemistry* 26(20), 5427-5434 (2018).

7.2 Introduction

Aptamers are usefully employed in many biosensor and biotechnology applications for a number of reasons including their stability compared to protein-based antibodies, the cost effectiveness of their manufacture and the fact that, once selected, they are usually highly specific for a particular ligand¹⁷⁴⁻¹⁷⁸. The advantage of binding specificity is only partly true for the cocaine-binding aptamer. While this aptamer binds cocaine, it binds very weakly to the common cocaine metabolites ecgonine, benzoyl ecgonine and ecgonine methyl ester^{75,76,84,96,129,133}. The cocaine-binding aptamer also displays high affinity for quinine and several quinine analogues^{82,83,93,96,133}. This “off-target” binding is unusual as it is approximately 50-fold tighter than for cocaine, the ligand used in selection of the aptamer. The ability of this aptamer to bind quinine has recently been exploited to develop a biosensor for quinine in wastewater⁸⁸.

The cocaine-binding aptamer was originally reported by Stojanovic *et al* in 2000⁷⁵ and has subsequently become a model system for both developing new applications of aptamers in biotechnology and for aptamer-focused functional studies. The secondary structure of the aptamer contains three stems arranged around a three-way junction that contains a tandem AG mismatch (Figure 7-1)⁷⁷. This AG mismatch is essential for binding, as making any sequence change, even to a GA mismatch eliminates ligand binding^{81,93}. The aptamer contains two binding sites for its ligand, a high-affinity and a low-affinity site¹²⁶. Ligand binding at the low-affinity site is often not observed as its affinity decreases as NaCl concentration increases. Two variations of the cocaine-binding aptamer are often studied. In the first, stem 1 (Figure 7-1) has 6-7 base pairs and the secondary structure is formed in the ligand-free state. In the second form, stem 1 is shortened to have 3 base pairs and the ligand-free form is dynamic or unstructured and the aptamer becomes structured upon ligand binding^{77,79,179,180}. It is this second “structure switching” version of the cocaine-binding aptamer that is most often used in biosensor development^{86,111,114,181,182}.

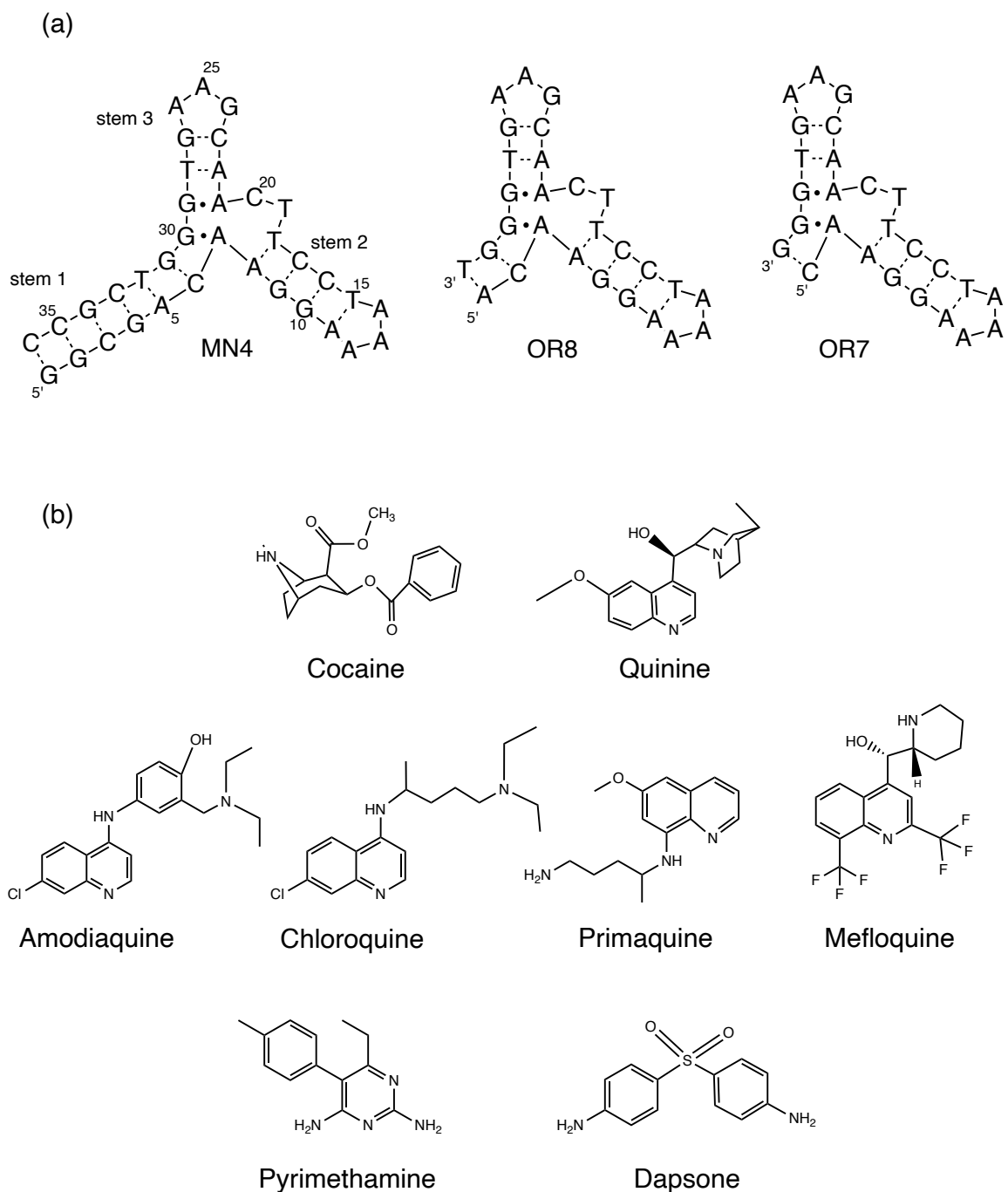


Figure 7-1: (a) Secondary structure of the different cocaine-binding aptamer constructs used in this study. Dashes between nucleotides indicate Watson–Crick base pairs and dots indicate the location of non-Watson–Crick base pairs. (b) Chemical structures of the compounds investigated in this study.

Quinine is found in the bark of some trees of the genus *Cinchona*, and extracts from the bark have been traditionally used in South America to stop shivering, which led to its use as a treatment for malaria. The use of quinine as an antimalarial agent has led to the development of a series of compounds derived from quinine such as amodiaquine, mefloquine and chloroquine. The mode of action of this set of compounds is not yet fully understood, but is thought to inhibit heme polymerization through an association with heme¹⁸³. Often, one of these quinine-based compounds is used in conjunction with artemisinin in antimalarial combination treatment¹⁸⁴.

Here, the range of ligands bound by the cocaine-binding aptamer is expanded to include a number of quinine-based antimalarial compounds. Using isothermal titration calorimetry (ITC) it can be demonstrated that all of the quinine-based compounds are bound by the cocaine-binding aptamer, that these compounds share common high and low-affinity binding sites and that some compounds, such as amodiaquine, are bound by the cocaine-binding aptamer in the single-digit nanomolar range. This affinity is much tighter than previously observed for quinine.

7.3 Results and Discussion

7.3.1. Binding affinity and thermodynamics of antimalarial compounds. ITC experiments were performed to determine if the quinine-based antimalarial compounds primaquine, amodiaquine, chloroquine and mefloquine (Figure 7-1) are bound by the cocaine-binding aptamer. As seen by their thermograms (Figure 7-2)

all of these compounds are bound by the MN4 cocaine-binding aptamer and their binding affinity and thermodynamics are given in Table 7-1. It is notable that, with the exception of primaquine, these compounds bind 5-29 fold tighter than quinine. Amodiaquine binds the tightest of all currently known cocaine-binding aptamer ligands, having an affinity of (7 ± 4) nM. Also reported in Table 7-1 are binding results for MN4 to both cocaine and quinine acquired at the same conditions.

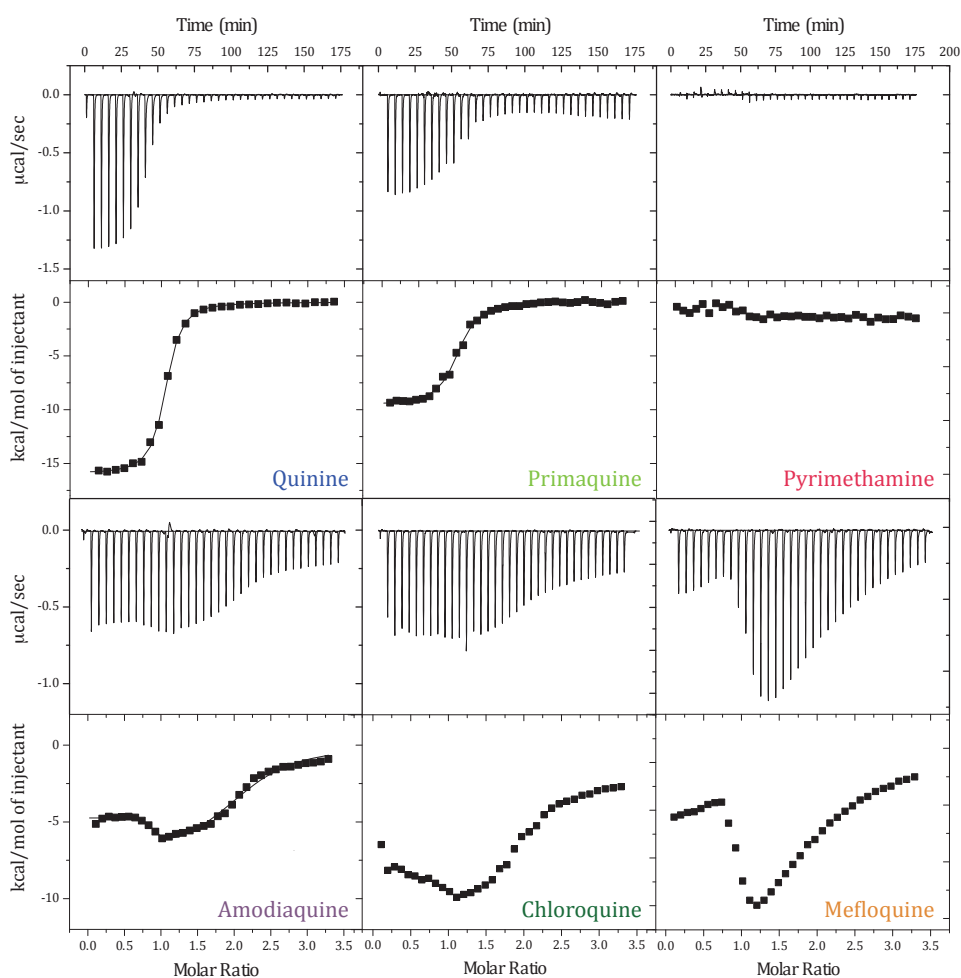


Figure 7-2: ITC analysis of ligand binding by the MN4 cocaine-binding aptamer. On top is the titration data showing the heat resulting from each injection of ligand into an aptamer solution. On bottom are the integrated heats corrected for the heat of dilution. Binding experiments were performed at 15°C in 20 mM Tris (pH 7.4), 140 mM NaCl, 5 mM KCl.

Table 7-1: Binding affinities and thermodynamic values for the binding between the MN4 cocaine-binding aptamer and ligands in high salt buffer (140 mM NaCl, 5 mM KCl, 20 mM Tris, pH 7.4).

Ligand	K_{d1} (μM)	ΔH_1 (kcal mol^{-1})	$-\text{T}\Delta S_1$ (kcal mol^{-1})	K_{d2} (μM)	ΔH_2 (kcal mol^{-1})	$-\text{T}\Delta S_2$ (kcal mol^{-1})
Cocaine ^a	5.5 ± 0.4	-11.1 ± 1	2.4 ± 0.8	-	-	-
Quinine ^a	0.20 ± 0.05	-14.1 ± 1	5.7 ± 0.7	-	-	-
Primaquine	0.48 ± 0.1	-9.5 ± 0.1	1.2 ± 0.2	-	-	-
Amodiaquine ^b	0.007 ± 0.004	-2.8 ± 0.9	-8.0 ± 1.1	2.1 ± 0.5	-5.1 ± 1.6	-2.4 ± 1.6
Chloroquine	0.037 ± 0.002	-3.5 ± 1.8	-6.3 ± 1.8	1.6 ± 0.4	-7.4 ± 1.1	-0.2 ± 0.1
Mefloquine ^b	0.035 ± 0.005	-6.3 ± 1.8	-3.5 ± 1.8	15 ± 3.1	-29.0 ± 1.1	22 ± 1.1
Dapsone ^b			NB			
Pyrimethamine ^b			NB			

The values reported are averages between 2 – 3 individual experiments. NB denotes no binding detected at these experimental conditions. Data acquired at 15°C. ^aData taken from Neves *et al.*¹²⁶ ^bData acquired in the same buffer with 3% DMSO.

The binding thermodynamics for amodiaquine, chloroquine and mefloquine by MN4 show that these ligands bind with both a favorable enthalpy and entropy. For cocaine, quinine and primaquine binding is enthalpically favorable, but counterbalanced by an unfavorable binding entropy (Table 7-1). Having both enthalpy and entropy as a driving force for binding likely contributes to the reason why amodiaquine, chloroquine and mefloquine bind so much tighter than quinine. The reason why these ligands are entropically favorable may be due to their higher hydrophobicity as their logP values (octanol/water partition coefficient) are higher than for the ligands that have an unfavorable binding entropy. However, there are likely other factors involved including molecular shape as well as hydration and solvation effects.

The non-sigmoidal nature of the ITC thermograms for amodiaquine, chloroquine and mefloquine are due to these three compounds binding at both the high and low-affinity sites in the cocaine-binding aptamer at 140 mM NaCl at 20 μM DNA aptamer

concentration. This behaviour is in contrast to that seen with quinine and primaquine that display no significant amount of second site binding at 140 mM NaCl, also at 20 μM aptamer concentration. The data for amodiaquine, chloroquine and mefloquine were fit to a two-site independent binding model in a similar fashion as described previously for cocaine and quinine two-site binding in low salt buffer¹²⁶. The thermodynamic parameters for binding at the second, low-affinity, site are provided in Table 7-1.

As a control for ligand binding the ability of the cocaine-binding aptamer to bind dapson and pyrimethamine was assayed. Both of these compounds have been used as antimalarial agents and both of these compounds have two 6-member aromatic rings, like cocaine, but not the quinoline ring system (Figure 7-1). Neither of these compounds displays binding by MN4 as observed by ITC (Figure 7-2; Table 7-1).

Due to the very tight binding of amodiaquine by MN4 the binding of two structural components of amodiaquine, 7-chloroquine and triethylamine (Figure 7-1) was analyzed. The thermogram of 7-chloroquine titrated into MN4 shows that this bicyclic ring is bound by MN4 with a K_d value of $(0.92 \pm 0.04) \mu\text{M}$ (Figure 7-3) In contrast, no binding of triethylamine by MN4 was observed (Figure 7-3). These results mirror what we observed previously with quinine where we looked at the binding of the aromatic (6-methoxyquinoline) and the aliphatic (quinuclidine) portions individually and binding of $(0.5 \pm 0.1) \mu\text{M}$ and no binding were observed, respectively. We note that even though amodiaquine binds much tighter than

quinine, 6-methoxyquinoline binds tighter than 7-chloroquinine. Similarly, for this and our previous study⁹⁶, we observe no binding for the aliphatic portion of the ligand, even though the triethylamine would be positively charged at the pH value studied. These results are consistent with our proposed mechanism of binding being driven by stacking interactions between the aromatic portion of the ligand and a base or base pair(s) in the aptamers⁹³.

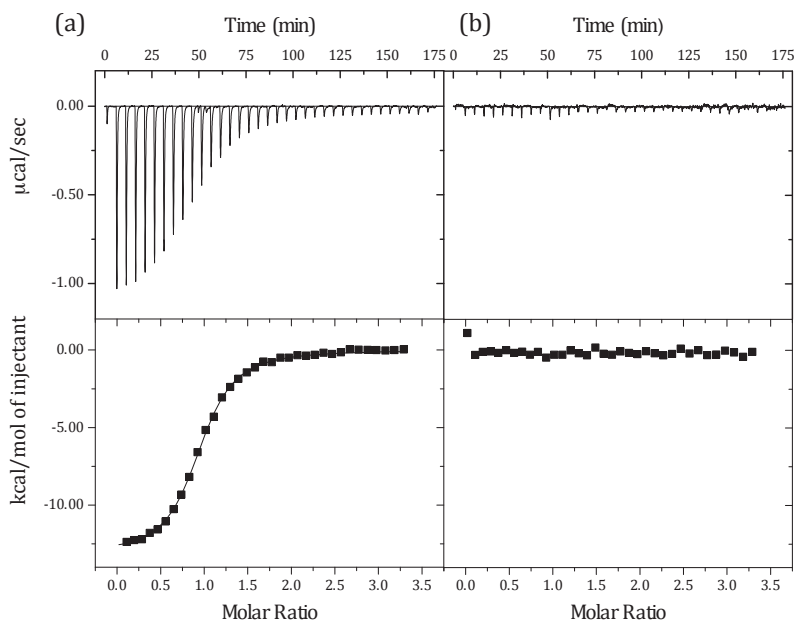


Figure 7-3: ITC analysis of the binding of structural pieces of amodiaquine by the MN4 cocaine-binding aptamer. In (a) is the binding of 7-chloroquinoline and in (b) is the addition of triethylamine to MN4 where no binding is observed. On top is the titration data showing the heat resulting from each injection of ligand into an aptamer solution. On bottom are the integrated heats corrected for the heat of dilution. Binding experiments were performed at 15°C in 20 mM Tris (pH 7.4), 140 mM NaCl, 5 mM KCl.

7.3.2. Competition binding experiments. In order to see if quinine and these quinine-based compounds share a common binding site on the cocaine-binding aptamer an ITC-based competition binding experiment with amodiaquine and

quinine was performed. In the first experiment, quinine was bound to the cocaine-binding aptamer (3:1 molar ratio ligand:MN4) and then titrated in amodiaquine (Figure 7-4a). In this case, the tighter binding ligand, amodiaquine, displaces quinine and two-site binding is observed. In a second experiment, amodiaquine was bound to the cocaine-binding aptamer (3:1 molar ratio ligand:MN4) and quinine was titrated. As seen in Figure 7-4b, no binding was observed for the addition of quinine into amodiaquine-bound aptamer. These results show that both ligands share the same high-affinity binding site. Previously, both ITC and NMR-based competition experiments showed that cocaine and quinine compete for the same binding site in MN4⁸² and it can be concluded that all the quinine-based antimalarial compounds here compete for the same high affinity binding site in the cocaine-binding aptamer.

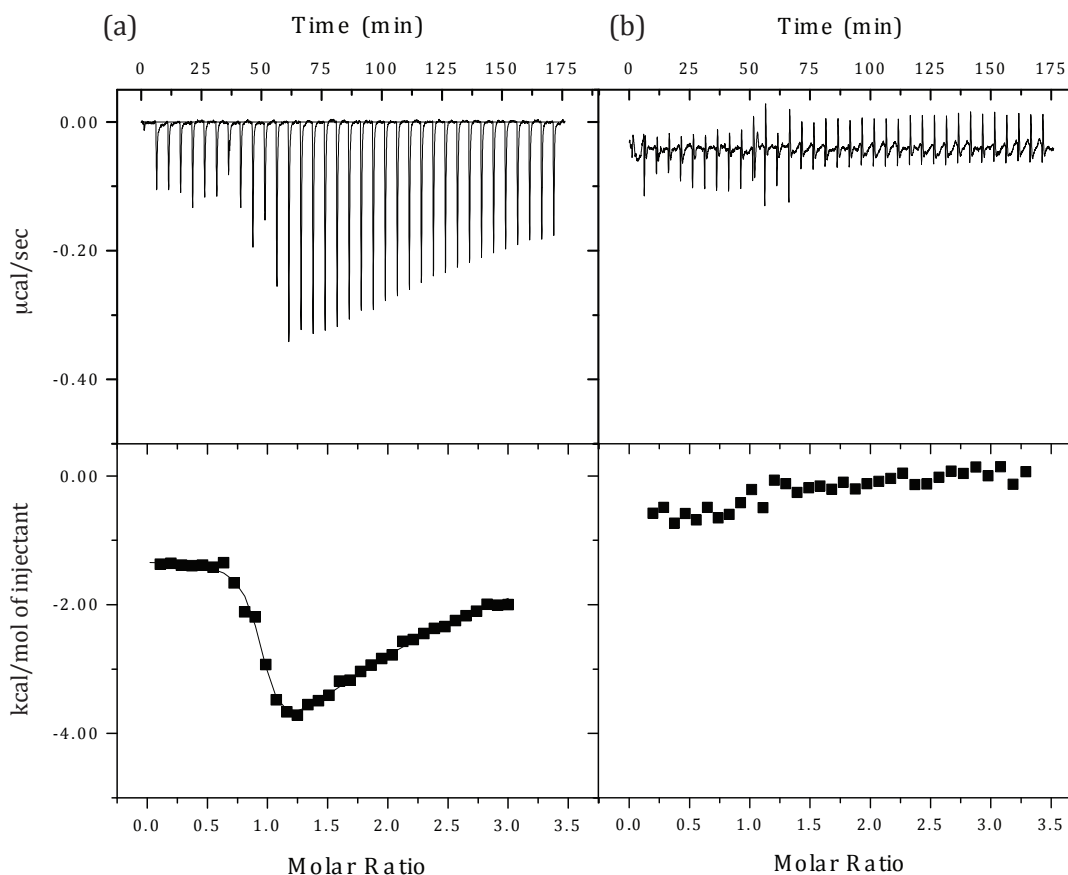


Figure 7-4: ITC-based competition binding experiments. Shown are the interaction of (a) amodiaquine with quinine-bound MN4 and (b) quinine into amodiaquine-bound MN4. On top of each part is the raw titration data showing the heat resulting from each injection of ligand into aptamer solution. On the bottom is the integrated heat plot after correcting for the heat of dilution. All binding experiments were performed at 15 °C in a buffer of 20 mM Tris (pH 7.4), 140 mM NaCl, 5 mM KCl.

7.3.3. Binding at different NaCl concentrations. The two-site binding of amodiaquine, chloroquine and mefloquine by MN4 at 20 μ M aptamer and 140 mM NaCl distinguishes the binding of these ligands from the observation of one-site binding of cocaine, quinine and primaquine at the same NaCl concentration (Figure 7-2). To further investigate this difference binding data at different NaCl concentrations was acquired. First, binding data in 20 mM Tris buffer with no added

NaCl (Table 7-2) was obtained. Primaquine behaves similarly to cocaine and quinine and binding becomes slightly tighter and binding at the low affinity site is observed in the absence of added NaCl (Figure 7-5). In contrast, amodiaquine, chloroquine and mefloquine are bound weaker at both the high-affinity and low-affinity site by MN4 with no NaCl added.

Table 7-2: Binding affinities and thermodynamic values for the binding between the MN4 cocaine-binding aptamer and ligands in low salt buffer (20 mM Tris, pH 7.4).

ligand	K_{d1} (μM)	ΔH_1 (kcal mol^{-1})	$-\text{T}\Delta S_1$ (kcal mol^{-1})	K_{d2} (μM)	ΔH_2 (kcal mol^{-1})	$-\text{T}\Delta S_2$ (kcal mol^{-1})
Cocaine ^a	1.3 ± 0.4	-10.8 ± 1	2.5 ± 1.1	16 ± 8	-20 ± 2	13 ± 2
Quinine ^a	0.17 ± 0.07	-10 ± 1	1.9 ± 0.8	1.2 ± 0.6	-26 ± 2	19 ± 9
Primaquine	0.30 ± 0.02	-6.9 ± 1.9	-1.7 ± 0.9	8 ± 2	-20 ± 3	13 ± 3
Amodiaquine ^b	0.21 ± 0.05	-0.9 ± 0.1	-7.9 ± 0.3	5.6 ± 0.9	-3.7 ± 2.1	-3.2 ± 2.1
Chloroquine	0.39 ± 0.13	-5.3 ± 1.1	-3.1 ± 1.1	19 ± 7	-20 ± 2	14 ± 2
Mefloquine ^b	1.7 ± 0.7	-10.4 ± 1.4	2.8 ± 1.5		vwb	

The values reported are averages between 2 – 3 individual experiments. vwb denotes very weak binding observed that was not quantifiable. Data acquired at 15°C. ^aData taken from Neves *et al.*¹²⁶ ^bData acquired in the same buffer with 3% DMSO.

NaCl concentration was increased and amodiaquine binding at 500 mM and 750 mM NaCl was measured (Table 7-3; Figure 7-6). At both these concentrations, binding affinity at both the high and low affinity sites decreased as the NaCl concentration increased.

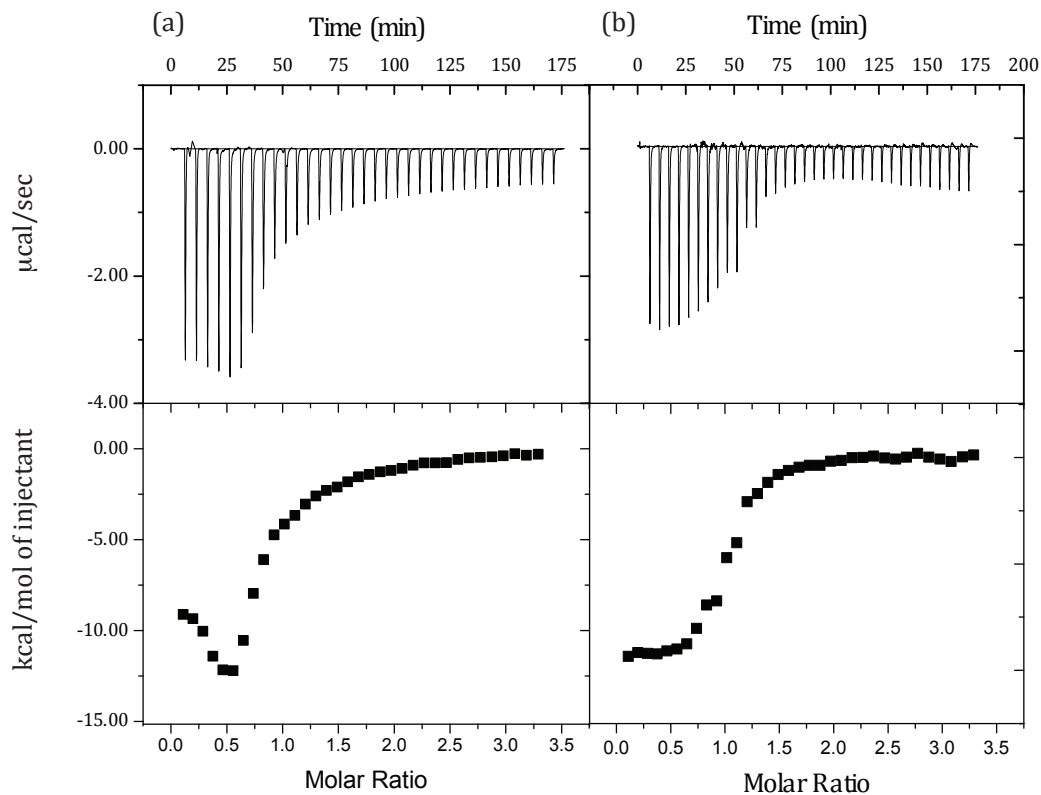


Figure 7-5: ITC analysis of the binding of primaquine by the MN4 cocaine-binding aptamer in (a) the presence and (b) the absence of 140 mM NaCl. As shown by the non-sigmoidal binding curve in (a), two-site binding is observed. In (b) binding follows a 1:1 model. On top is the titration data showing the heat resulting from each injection of ligand into an aptamer solution. On bottom are the integrated heats corrected for the heat of dilution. Binding experiments were performed at 15°C in 20 mM Tris (pH 7.4) with the concentration of NaCl indicated.

Table 7-3: Binding affinities and thermodynamic values for the interaction between the MN4 cocaine-binding aptamer and amodiaquine at different NaCl concentrations.

[NaCl] (mM)	K_{d1} (μM)	ΔH_1 (kcal mol ⁻¹)	$-\text{T}\Delta S_1$ (kcal mol ⁻¹)	K_{d2} (μM)	ΔH_2 (kcal mol ⁻¹)	$-\text{T}\Delta S_2$ (kcal mol ⁻¹)
0	0.21 ± 0.05	-0.9 ± 0.1	-7.9 ± 0.3	5.6 ± 0.9	-3.7 ± 2.1	-3.2 ± 2.1
140	0.007 ± 0.004	-2.8 ± 0.9	-8.0 ± 1.1	2.1 ± 0.5	-5.1 ± 1.6	-2.4 ± 1.6
500	0.23 ± 0.11	-2.3 ± 0.1	-6.4 ± 0.5	18 ± 2	-6.8 ± 0.6	0.5 ± 0.2
750 ^a	1.5 ± 0.4	-3.2 ± 0.2	-4.5 ± 0.3		vwb	

Data acquired at 15°C in 20 mM Tris (pH 7.4), 3% DMSO at NaCl concentrations indicated with an aptamer concentration of 60 μM . The values reported are averages of between 2 – 3 individual experiments. vwb denotes very weak binding observed but not quantified. ^aAptamer concentration used was 20 μM in order to best define binding at high-affinity site.

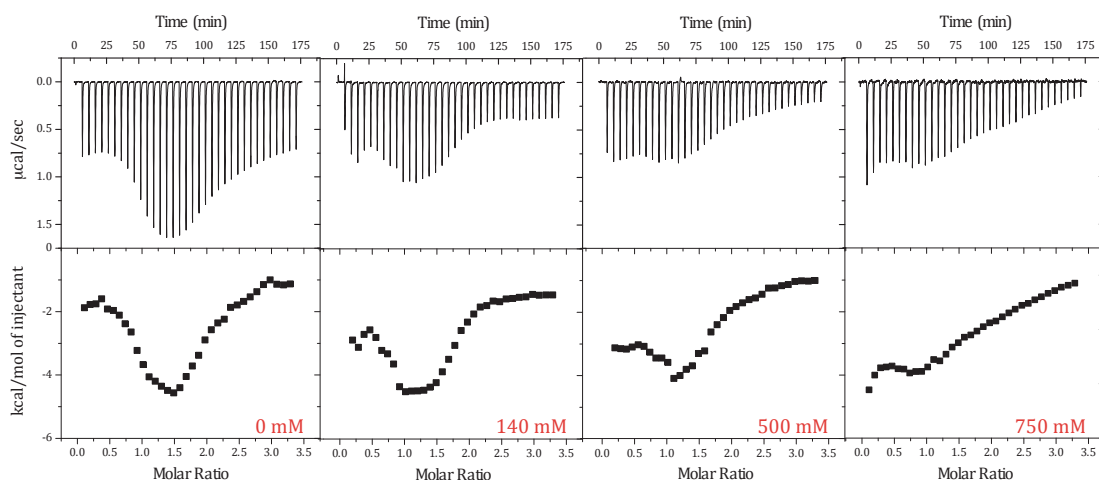


Figure 7-6: ITC analysis of the binding of amodiaquine by the MN4 cocaine-binding aptamer in different concentrations of NaCl. As shown by the non-sigmoidal binding curves, two-site binding is observed in all conditions. On top is the titration data showing the heat resulting from each injection of ligand into an aptamer solution. On bottom are the integrated heats corrected for the heat of dilution. Binding experiments were performed at 15°C in 20 mM Tris (pH 7.4) with the concentration of NaCl indicated.

7.3.4. Binding of short stem 1 constructs. The affinity of two different cocaine-binding aptamer constructs (OR7, OR8; Figure 7-1) with stem 1 lengths of 1 and 2 base pairs for amodiaquine and chloroquine were analyzed using ITC. Chloroquine was bound at both the high and low-affinity site by OR8 but no binding of chloroquine was observed by the OR7 aptamer (Figure 7-7; Table 7-4). In contrast, the tighter binding ligand, amodiaquine, is bound by OR7 at both the high and low-affinity sites (Figure 7-7; Table 7-4).

Table 7-4: Binding affinities and thermodynamic values for the interaction of amodiaquine and chloroquine with the short stem 1 aptamers OR7 and OR8.

	K_{d1} (μM)	ΔH_1 (kcal mol^{-1})	$-\text{T}\Delta S_1$ (kcal mol^{-1})	K_{d2} (μM)	ΔH_2 (kcal mol^{-1})	$-\text{T}\Delta S_2$ (kcal mol^{-1})
amodiaquine						
OR7	0.08 ± 0.04	-1.8 ± 0.2	-7.6 ± 0.5	20 ± 7	-5.6 ± 1.1	-0.6 ± 0.3
OR8				N/A		
chloroquine						
OR7				NB		
OR8	0.12 ± 0.09	-0.9 ± 0.1	-10 ± 0.8	18 ± 9	-3.8 ± 2.4	-2.5 ± 1.5

¹Data acquired at 15°C in 20 mM Tris (pH 7.4), 140 mM NaCl, 5 mM KCl, 3% DMSO. N/A denotes data not acquired. NB denotes no binding detected at these experimental conditions

These experiments were performed to expand on our previous studies where we destabilized the folded structure of the cocaine-binding aptamer by shortening stem 1 and using these destabilized aptamers to improve ligand selectivity for tight binding ligand⁷⁹. Previous study showed that OR8 (2 bp stem 1) could bind quinine, but not cocaine. The idea behind this is that the weaker binding ligands do not supply enough free energy (ΔG) from binding to both fold the aptamer and be bound

while tighter binding ligands supply enough free energy to both fold the aptamer and use the remaining ΔG from binding as an “effective” binding affinity.

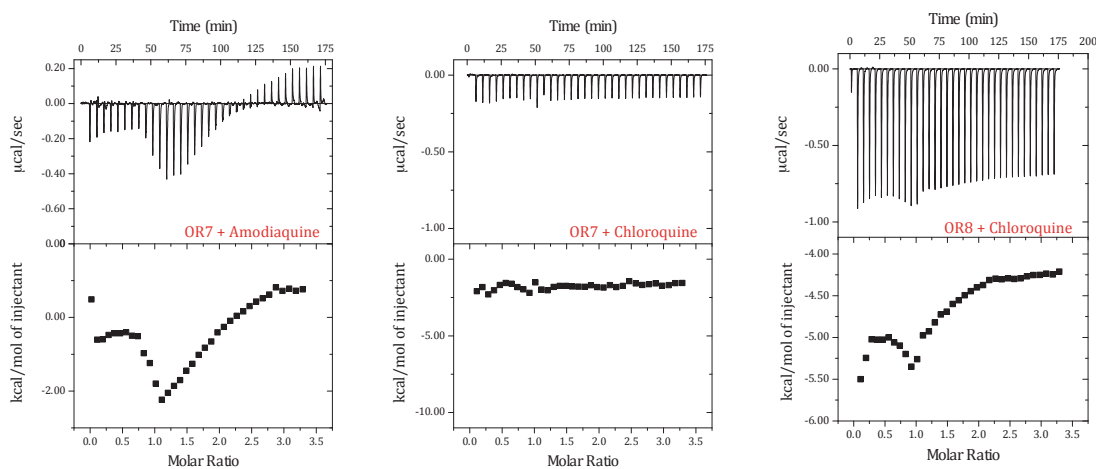


Figure 7-7: ITC data showing the interaction of two different stem 1 length aptamers with chloroquine and amodiaquine. On top is the raw titration data showing the heat resulting from each injection of ligand into aptamer solution. The bottom shows the integrated heat plot after correcting for the heat of dilution. Data were acquired in 20 mM Tris (pH 7.4), 140 mM NaCl, 5 mM KCl.

In this study the high affinity of amodiaquine is used to bind and fold the OR7, a cocaine-binding aptamer that contains only one base pair in stem 1 (Figure 7-1). The affinity of amodiaquine to OR7 is reduced compared to binding by MN4 with this reduction in affinity reflecting the contribution from the binding free energy to the folding of OR7. The next tightest binding ligand, chloroquine, was not bound by OR7 and binding by OR7 reflects a way distinguish between these two ligands. Similarly, chloroquine is bound by OR8 (Figure 7-1; 2 bp stem 1) as this aptamer needs less free energy from binding in order to fold compared with OR7.

7.4 Concluding remarks

In conclusion, the cocaine-binding aptamer tightly binds an even wider range of ligands than previously known, with amodiaquine the tightest binding ligand currently known. Binding of the three tightest ligands (amodiaquine, chloroquine and mefloquine) is both entropically and enthalpically favorable while the binding of cocaine, quinine and primaquine are enthalpically driven, with unfavorable entropy, at the conditions studied. The binding of these antimalarial compounds by the MN4 aptamer may have practical uses in drug delivery by using an aptamer-based DNA delivery mechanism. Also, it may be possible to use aptamer binding as a way of stabilizing or preserving a quinine-based antimalarial compound. Another use could be through the use of cocaine-binding aptamers with different lengths of stem 1. It should be possible, given the variation in affinity, to distinguish the binding of quinine (by MN19) from chloroquine/mefloquine (by MN19 and OR8) and amodiaquine (by MN19, OR7 and OR8) (Fig. 5).

Chapter 8 Antimalarial Compounds: Cocaine-binding aptamer specific or Generic DNA binders?

8.1 Introduction

Nucleic acids play an important role in biological activities such as gene storage, replication, transcription and translation as well as anticancer and antiviral processes^{17,185,186}. Nucleic acids are broadly categorized as having three major forms: A, B and Z duplex forms that differ from each other in helical sense, pitch, groove width, base orientation and sugar pucker. Moreover, nucleic acids can also be diverse in terms of three-dimensional structures, such as tree-way or four-way junctions or triplex or quadruplex – DNA. Several studies have been done studying small molecule interacting with threeway junctions¹⁸⁷⁻¹⁸⁹ and DNA duplex structures¹⁹⁰⁻¹⁹².

Junctions in nucleic acid structures occur when three or more helices meet at a junction point. Three-way junctions are comprised of three helical arms and a junction point with defined and stable Y-shaped three-dimensional structure¹⁹³⁻¹⁹⁵. These tertiary structures of nucleic acids occur in RNA, where they are involved in splicing, translation, gene regulation and expression, as well as DNA, where they are formed during DNA replication¹⁹⁶⁻¹⁹⁸. In addition to biological functions, three-way junctions are used in DNA nanotechnology including self-assembly of nanometer-scaled molecular fragments¹⁹⁹. Since threeway junctions are the smallest and

simplest type of junctions, they are often used as model system to study how multi-branched junction structures function (Figure 8-1a-c).

Another DNA oligomer that has been widely investigated is the Dickerson – Drew dodecamer (Figure 8-1d). It is a prototypic B-DNA molecule with the sequence $d[CGCGAATTCGCG]_2$ and is one of the earliest DNA structures whose crystal structure was solved^{200,201}. Similarly to generic threeway junction, the dodecamer is a model system as it has canonical B-form of DNA and has been studied extensively both experimentally and by molecular dynamics simulations²⁰²⁻²⁰⁴.

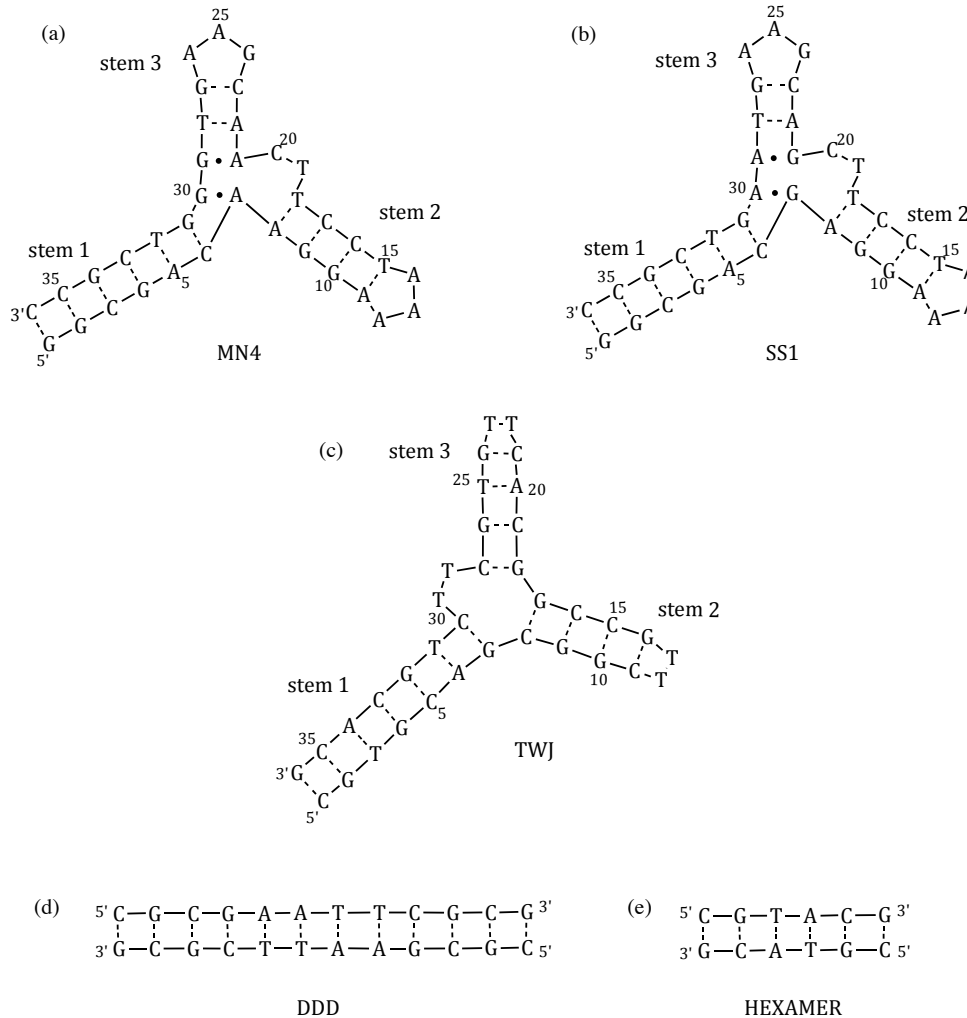


Figure 8-1: Secondary structures of (a) MN4, the cocaine-binding aptamer; (b) SS1 aptamer, a version of the cocaine-binding aptamer where two AG base pairs are switched to GA base pairs; (c) TWJ, a generic three-way junction; (d) DDD, a Dickerson – Drew dodecamer; and (e) hexamer. Dashes indicate Watson-Crick base pairs while dots indicate non Watson-Crick base pairs.

Antimalarial drugs such as chloroquine, amodiaquine and mefloquine (Figure 8-2) have been used to study drug action both *in vitro* and *in vivo*. Since its development in 1930s chloroquine (4-aminoquinoline) has been used as a therapeutic agent for treatment of malaria²⁰⁵. Safety, stability, low cost and ease of manufacture have made chloroquine a widely used antimalarial drug. However, chloroquine

resistance has been detected in the 1960s and demand for new effective drugs showed that mechanism of action is not understood though it is thought that they inhibit hematin polymerization²⁰⁶. Many quinine-analogues have been synthesized over the years with different chemical modifications such as position and nature of the substituents on the quinoline ring, for example amodiaquine and mefloquine^{207,208}. Mefloquine exists as enantiomers and both conformations have equal antimalarial activity unlike cinchona alkaloids, whose R enantiomer is more active than its S counterpart²⁰⁵. The first observation of chloroquine binding to DNA was made in mid 20th century, and several studies were published stating dissociation constant²⁰⁹. These values varied depending on experimental technique used. Both chloroquine and amodiaquine are found to intercalate into DNA through the classical model of intercalation introduced by Lerman^{205,210}. Davidson *et al.* showed that unlike chloroquine and amodiaquine, mefloquine does not strongly bind to DNA by intercalation²¹¹.

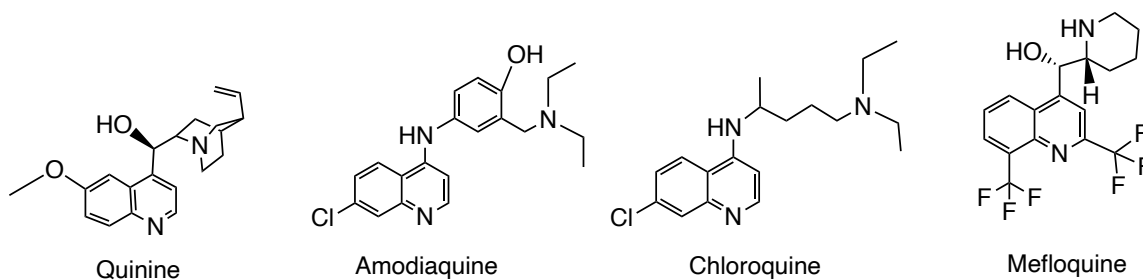


Figure 8-2: Structures of quinine-based antimalarial compounds used in this study.

Previous studies showed that quinine-based antimalarial compounds (Figure 8-2) bind to MN4, a long stem 1 version of the cocaine-binding aptamer at two sites under high NaCl conditions¹⁶⁸. This chapter explores if quinine-based antimalarial compounds prefer the cocaine-binding aptamer or if they bind to different DNA structures, such as different three-way junctions or DNA duplex and whether duplex length plays a role in binding (Figure 8-1).

8.2 Results

8.2.1. Binding of chloroquine and quinine. Both chloroquine and quinine bind only to MN4, a long stem 1 cocaine-binding aptamer construct, and do not bind to any other DNA structure used in this chapter (Figure 8-1). The K_d value for MN4 binding quinine in 140 mM NaCl is $0.20 \pm 0.05 \mu\text{M}$ with a ΔH of (-14 ± 1) kcal/mol and $-T\Delta S$ of (5 ± 1) kcal/mol at a temperature of 15°C ^{82,96,126}. Chloroquine binds to both high and low affinity site under the same buffer and temperature conditions. Binding affinity of high affinity site (K_{d1}) was determined to be $(0.037 \pm 0.002) \mu\text{M}$, the enthalpy (-3.5 ± 1.8) kcal/mol, and $-T\Delta S_1$ is (-6.3 ± 1.8) kcal mol⁻¹; while the binding affinity of the low affinity binding site (K_{d2}) is $(1.6 \pm 0.4) \mu\text{M}$, enthalpy (-7.4 ± 1.1) kcal mol⁻¹, and $-T\Delta S_2$ is (-0.2 ± 0.1) kcal mol⁻¹¹⁶⁸.

8.2.2. Binding of amodiaquine. ITC has been used to determine binding selectivity of amodiaquine for different DNA structures. Results in Table 8-1 show that this antimalarial compound binds to all oligonucleotides studied.

Table 8-1: Comparison of binding affinities and thermodynamic properties of amodiaquine by aptamers used in this study¹.

	K_{d1} (nM)	ΔH_1 (kcal mol ⁻¹)	$-T\Delta S_1$ (kcal mol ⁻¹)	K_{d2} (μ M)	ΔH_2 (kcal mol ⁻¹)	$-T\Delta S_2$ (kcal mol ⁻¹)
MN4 ²	7 ± 4	-2.8 ± 0.9	-7.9 ± 1.1	2.1 ± 0.5	-5 ± 2	-3 ± 2
SS1	26 ± 4	-1.5 ± 0.1	-8.5 ± 0.2	6.9 ± 0.5	-15 ± 1	8 ± 1
TWJ	51 ± 14	-1.8 ± 0.1	-7.8 ± 0.3	24 ± 4	-13 ± 2	7 ± 2
DDD	16 ± 6	-0.6 ± 0.1	-9.7 ± 0.4	6.9 ± 1.1	-9 ± 1	-2 ± 1
Hexamer	6 ± 3	-1.9 ± 0.2	-9 ± 1	2.7 ± 0.5	-17 ± 1	10 ± 1

¹Data collected at 15°C in 20 mM TRIS (pH 7.4), 140 mM NaCl, 5 mM KCl.

²Data taken from *Slavkovic et al. (2018)*¹⁶⁸

8.2.3. Binding of mefloquine. Unlike amodiaquine, mefloquine does not bind to all three-way junctions studied. It is selective for MN4, a long stem 1 cocaine-binding aptamer, but does not bind to the SS1 aptamer or the generic three-way junction, TWJ (Table 8-2). Mefloquine binds both DNA duplexes studied regardless of the length. However, duplex length impacts the binding affinity of both molecules, i.e. binding of mefloquine to hexamer is tighter than to dodecamer (Table 8-2).

Table 8-2: Comparison of binding affinities and thermodynamic properties of mefloquine by aptamers used in this study¹.

	K_{d1} (μ M)	ΔH_1 (kcal mol ⁻¹)	$-T\Delta S_1$ (kcal mol ⁻¹)	K_{d2} (μ M)	ΔH_2 (kcal mol ⁻¹)	$-T\Delta S_2$ (kcal mol ⁻¹)
MN4 ²	0.035 ± 0.005	-6.3 ± 1.8	-3.5 ± 1.8	15 ± 3	-15 ± 1	23 ± 1
SS1			NB			
TWJ			NB			
DDD	0.21 ± 0.08	1.3 ± 0.1	-10 ± 1	19 ± 5	-12 ± 5	6 ± 5
Hexamer	0.022 ± 0.013	0.6 ± 0.1	-11 ± 1	4 ± 1	-3 ± 1	-5 ± 1

¹Data collected at 15°C in 20 mM TRIS (pH 7.4), 140 mM NaCl, 5 mM KCl. NB denotes no binding.

²Data taken from *Slavkovic et al. (2018)*¹⁶⁸

8.3 Discussion

In this chapter, the selectivity of quinine, chloroquine, mefloquine and amodiaquine for the cocaine-binding aptamer over different three-way junctions and duplex structures of different length is explored (Figure 8-1). In order to determine how changes at the binding site affect binding of the ligands of interest, the SS1 aptamer was designed. This aptamer has the same sequence as MN4 except that the AG bases (A21/G29, A7/G30) are switched to become GA base pairs (G21/A29, G7/A30) (Figure 8-1). Binding of quinine, chloroquine and mefloquine is inhibited by this change (Figure 8-3), which is indicative of importance of the AG mismatch for binding. However, two molecules of amodiaquine bind to the SS1 aptamer, although the affinity at both sites is decreased three-fold compared to the MN4 construct. Binding is enthalpically and entropically driven at the high affinity site but has favorable enthalpy and unfavorable entropy for the low affinity site.

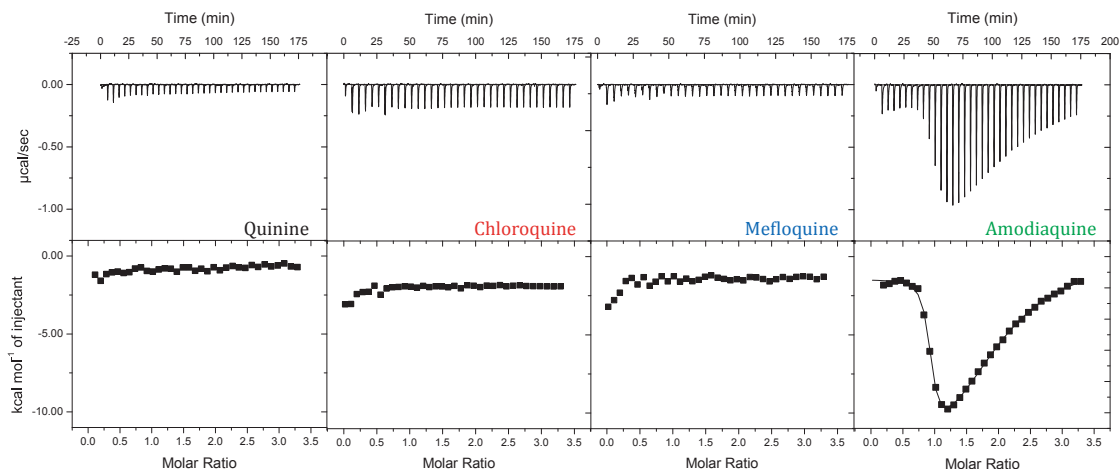


Figure 8-3: ITC thermograms showing binding of antimalarial compounds to a version of the cocaine-binding aptamer (SS1). On top is the raw titration data showing the heat resulting from each injection of ligand into aptamer solution. The bottom shows the integrated heat plot after correcting for the heat of dilution. Data for quinine and chloroquine were acquired in 20 mM Tris (pH 7.4), 140 mM NaCl, 5 mM KCl, while data for mefloquine and amodiaquine was acquired in the same buffer with addition of 3% (v/v) DMSO at 15°C.

To further study the selectivity of amodiaquine for the cocaine-binding aptamer, binding to generic three-way junction, TWJ was examined. Two molecules of amodiaquine bind to TWJ and binding is weaker at both sites compared to both MN4 and SS1 aptamers. Again, quinine, chloroquine and mefloquine do not bind to the TWJ DNA structure (Figure 8-4).

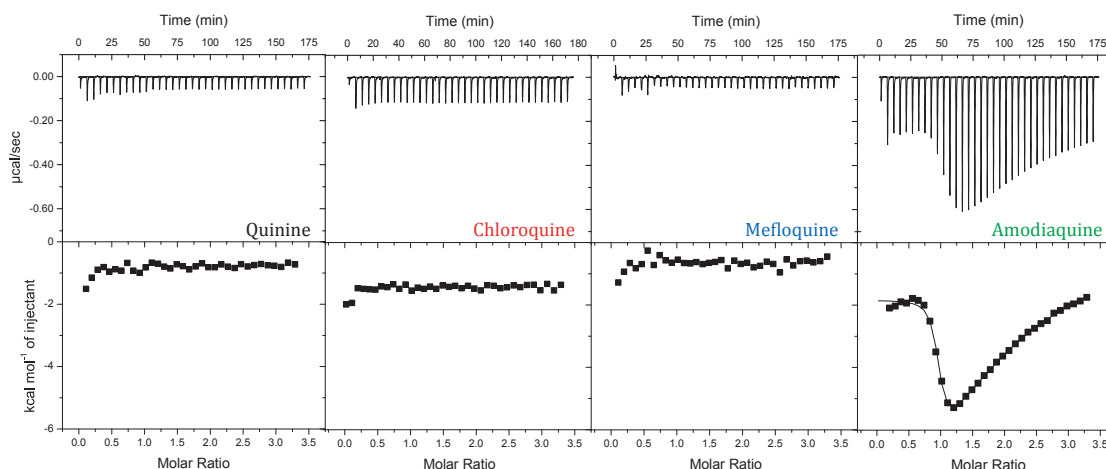


Figure 8-4: ITC thermograms showing binding of antimalarial compounds to the generic three-way junction (TWJ). On top is the raw titration data showing the heat resulting from each injection of ligand into aptamer solution. The bottom shows the integrated heat plot after correcting for the heat of dilution. Data for quinine and chloroquine were acquired in 20 mM Tris (pH 7.4), 140 mM NaCl, 5 mM KCl, while data for mefloquine and amodiaquine was acquired in the same buffer with addition of 3% (v/v) DMSO at 15°C.

ITC thermograms show that quinine and chloroquine do not bind duplex DNA structures regardless of the duplex length (Figures 8-5 and 8-6). However, two molecules of both amodiaquine and mefloquine bind to the duplex DNA regardless of the length. Shortening the length of the duplex from twelve to six base pairs increases the binding affinity of DNA for the ligand. A possible source of the difference in the affinity for ligand binding could be the different sequences of the two DNA duplexes.

Fluorescence studies¹ show blue shift upon titration of amodiaquine into hexamer solution, which is indicative of intercalation⁹³. Chloroquine is also a known intercalator, but its binding is not evident from the ITC thermogram. It could possibly bind, but with a much weaker affinity, which is not detectable at 20 μ M aptamer concentration and these buffer conditions.

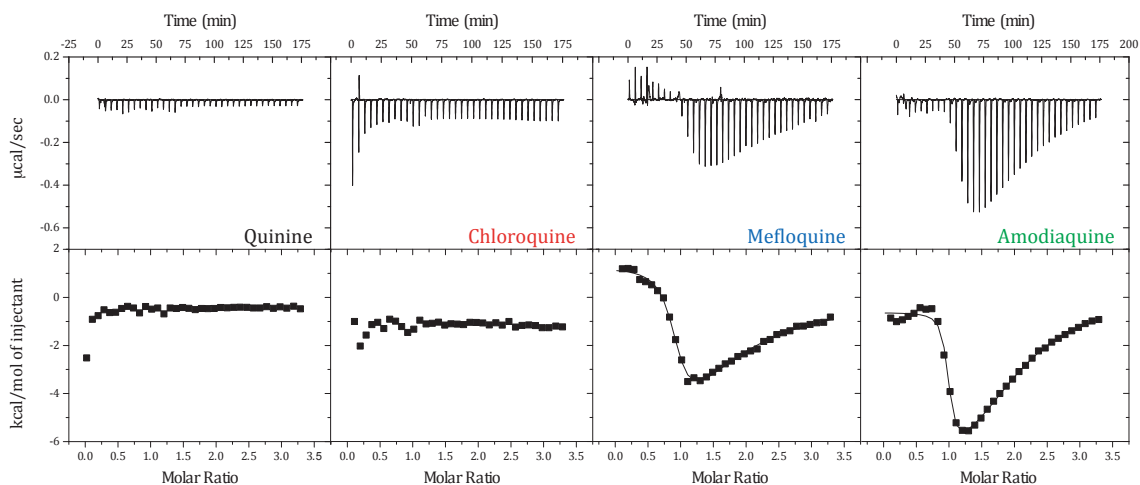


Figure 8-5: ITC thermograms showing binding of antimalarial compounds to Dickerson-Drew dodecamer (DDD). On top is the raw titration data showing the heat resulting from each injection of ligand into aptamer solution. The bottom shows the integrated heat plot after correcting for the heat of dilution. Data for quinine and chloroquine were acquired in 20 mM Tris (pH 7.4), 140 mM NaCl, 5 mM KCl, while data for mefloquine and amodiaquine was acquired in the same buffer with addition of 3% (v/v) DMSO at 15°C.

¹ Performed by Aron Shoara from Johnson lab, added here to further clarify results

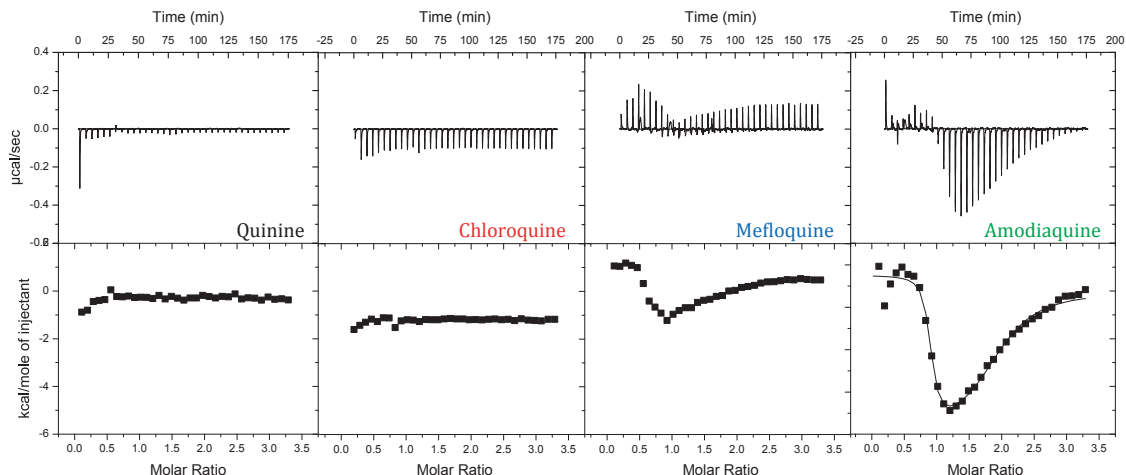


Figure 8-6: ITC thermograms showing binding of antimalarial compounds to the hexamer. On top is the raw titration data showing the heat resulting from each injection of ligand into aptamer solution. The bottom shows the integrated heat plot after correcting for the heat of dilution. Data for quinine and chloroquine were acquired in 20 mM Tris (pH 7.4), 140 mM NaCl, 5 mM KCl, while data for mefloquine and amodiaquine was acquired in the same buffer with addition of 3% (v/v) DMSO at 15°C.

8.4 Concluding remarks

Quinine and chloroquine are selective only for the structure of the cocaine-binding aptamer. On the other hand, of all the three-way junctions studied, mefloquine interacts with the cocaine-binding aptamer and removal of the tandem AG base pairs from the binding site hinders binding. Mefloquine also binds to duplex DNA regardless of length, while amodiaquine binds to all DNA structures studied. The selectivity of these antimalarial drugs for different DNA structures may have benefits in further studies to understand the binding mechanism and possibly selecting an aptamer to detect one antimalarial compound with a high specificity for that compound.

Chapter 9 Analysis of Artemisinin Binding to the Cocaine-binding Aptamer and other DNA structures

9.1 Introduction

Used in China for over 2000 years in the form of concoctions or teas, artemisinin was isolated in early 1970s from plant *Artemisia annua* and was found to be effective against chloroquine resistant *Plasmodium falciparum* strain^{212,213}. Since then, several derivatives of artemisinin have been synthesized, which together with artemisinin are used in antimalarial combinatorial therapy²¹⁴⁻²²⁰. Recently, it was found that artemisinin shows anticancer activity in both *in vitro* studies and *in vivo* models of colorectal cancer²²¹⁻²²³. It also shows activity against other parasites such as *Toxoplasma gondii*, *Schistosoma* and *Lishmania*²²⁴. Although, the mode of action of artemisinin is not fully known, studies show that the endoperoxide bridge plays an important role in anti-parasitic activity²²⁵⁻²²⁷.

Aptamers have generated great interest as biosensors as their selection process allows them to bind a wide variety of ligands often with high affinity and specificity. An aptamer that is an exception to this rule is the cocaine-binding aptamer as one of the unique features of this aptamer is its ligand-binding promiscuity. Despite being selected for cocaine, the cocaine-binding aptamer binds quinine, its analogues and quinine-based antimalarial compounds (amodiaquine, chloroquine and mefloquine) with much higher affinity than cocaine^{82,96,168}. The second unique feature of this aptamer is the salt-controlled two-site binding mechanism¹²⁶.

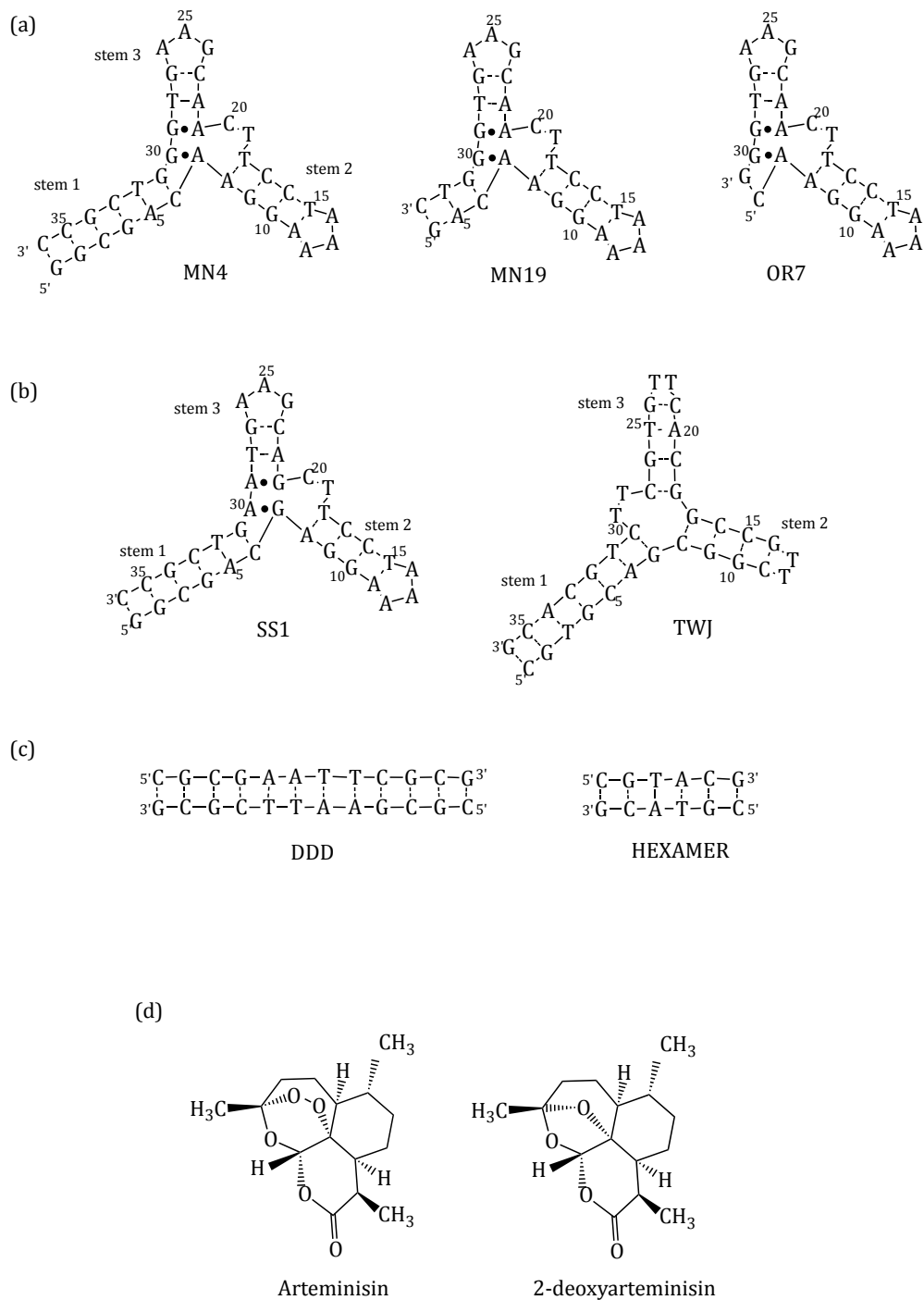


Figure 9-1: Secondary structures of (a) cocaine-binding aptamer constructs; (b) different three-way junctions; and (c) different DNA duplexes. Dashes indicate Watson-Crick base pairs while dots indicate non Watson-Crick base pairs. (d) Structures of ligands used in this study.

Previous studies showed that ligands containing bicyclic aromatic ring bind to the cocaine binding aptamer^{83,96,168}. Surprisingly, artemisinin (Figure 9-1) binds to the cocaine-binding aptamer tighter than quinine. In addition, the interaction of the artemisinin with different three-way junctions and DNA duplexes is also explored in this chapter.

9.2 Results

9.2.1. Effect of stem length on binding of artemisinin. ITC binding experiments show that two molecules of artemisinin bind to the cocaine-binding aptamer tighter than either quinine or cocaine. Two molecules of artemisinin are bound by the cocaine-binding aptamer regardless of the length of stem 1 as evident in a non-sigmoidal binding curve (Figure 9-2). Data is fit to two independent sites binding model and results are presented in Table 9-1.

Table 9-1: Comparison of binding affinities and thermodynamic properties of artemisinin by three-way junctions used in this study¹.

	K_{d1} (μM)	ΔH_1 (kcal mol^{-1})	$-T\Delta S_1$ (kcal mol^{-1})	K_{d2} (μM)	ΔH_2 (kcal mol^{-1})	$-T\Delta S_2$ (kcal mol^{-1})
MN4	0.03 ± 0.01	-4.4 ± 0.2	-5 ± 1	13 ± 4	-15 ± 1	9 ± 1
MN19	0.02 ± 0.01	-0.9 ± 0.1	-9 ± 1	5 ± 1	-11 ± 1	4 ± 1
OR7	0.03 ± 0.01	0.4 ± 0.1	-9 ± 1	5 ± 1	-22 ± 1	16 ± 1

¹Data collected at 15°C in 20 mM TRIS (pH 7.4), 140 mM NaCl, 5 mM KCl, 2.4% (v/v) DMSO.

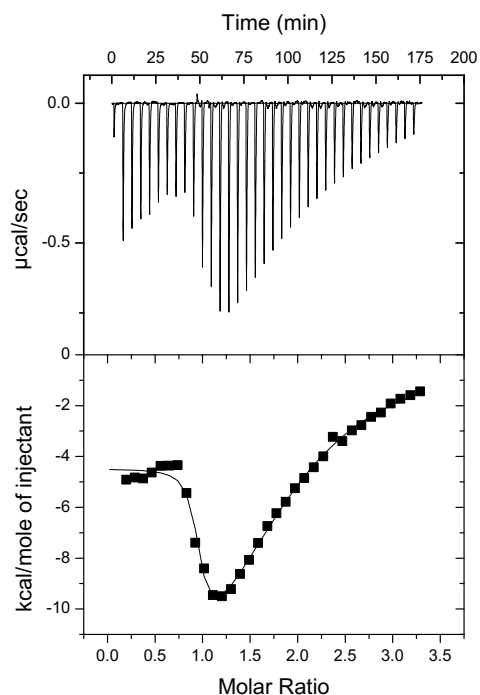


Figure 9-2: Thermogram showing the interaction of artemisinin with the cocaine-binding aptamer, MN4 in buffer containing 20 mM TRIS (pH 7.4), 140 mM NaCl, 5 mM KCl, 2.4% DMSO at 15°C.

9.2.2. Binding of artemisinin to three-way junctions. Isothermal titration calorimetry was also used to explore whether artemisinin is specific for the cocaine-binding aptamer or if it interacts with other three-way junctions. As examples of three-way junctions, a slightly modified version of the cocaine-binding aptamer, SS1 and generic three-way junction aptamer, TWJ were chosen (Figure 9-1). The SS1 cocaine aptamer has the same sequence as MN4 except that tandem AG base pairs are switched to become GA base pairs. This change resulted in an aptamer that does not bind to quinine as shown previously by ITC methods⁹³. Quinine does not bind to a generic TWJ aptamer as demonstrated in Chapter 8. However, artemisinin binds to all three-way junctions studied. Results presented in Table 9-2 indicate that

binding is the tightest for SS1 aptamer and weakest for TWJ, a generic three-way junction.

Table 9-2: Comparison of binding affinities and thermodynamic properties of artemisinin by three-way junctions used in this study¹.

	K_{d1} (μM)	ΔH_1 (kcal mol^{-1})	$-T\Delta S_1$ (kcal mol^{-1})	K_{d2} (μM)	ΔH_2 (kcal mol^{-1})	$-T\Delta S_2$ (kcal mol^{-1})
MN4	0.029 ± 0.014	-4.4 ± 0.2	-5 ± 1	13 ± 4	-15 ± 1	9 ± 1
SS1	0.004 ± 0.002	0.5 ± 0.1	-12 ± 1	2 ± 1	-7 ± 1	-0.8 ± 0.4
TWJ	0.064 ± 0.021	-0.1 ± 0.1	-9 ± 1	10 ± 3	-14 ± 6	7.4 ± 6

¹Data collected at 15°C in 20 mM TRIS (pH 7.4), 140 mM NaCl, 5 mM KCl, 2.4% (v/v) DMSO.

9.2.3. Binding of artemisinin to duplex DNA. The specificity of artemisinin for three-way junctions is further explored by studying its interaction with DNA duplexes, a self-complementary dodecamer and a self-complementary hexamer (Figure 9-1). Two molecules of artemisinin bind to both duplexes. ITC binding experiments show that artemisinin binds tighter to the hexamer than the dodecamer (Table 9-3).

Table 9-3: Comparison of binding affinities and thermodynamic properties of artemisinin by DNA duplexes¹.

	K_{d1} (μM)	ΔH_1 (kcal mol^{-1})	$-T\Delta S_1$ (kcal mol^{-1})	K_{d2} (μM)	ΔH_2 (kcal mol^{-1})	$-T\Delta S_2$ (kcal mol^{-1})
DDD	0.097 ± 0.028	-0.22 ± 0.03	-9 ± 1	31 ± 8	-12 ± 4	6 ± 4
Hexamer	0.007 ± 0.004	0.7 ± 0.1	-11 ± 1	3 ± 1	-6 ± 1	-2 ± 1

¹Data collected at 15°C in 20 mM TRIS (pH 7.4), 140 mM NaCl, 5 mM KCl, 2.4% (v/v) DMSO.

Competition binding results. In order to determine whether quinine and artemisinin share the same binding site, competition titration binding experiments were performed. The MN4 cocaine-binding aptamer was chosen as it is the only DNA structure in this study that binds quinine. In the first experiment, artemisinin was bound to MN4 in a 3:1 molar ratio, and quinine titrated in excess. Results (Table 9-4) show that quinine binds to the cocaine-binding aptamer with $K_{d,app}$ of $(1.1 \pm 0.1) \mu\text{M}$. In the second experiment, quinine was bound to MN4 in a 3:1 molar ratio, and artemisinin titrated in excess. In this case, a non-sigmoidal curve is observed indicating that two molecules of artemisinin bind to MN4 (Figure 9-3).

Table 9-4: Comparison of competitive binding of quinine and artemisinin by the MN4 aptamer.

	K_{d1} (μM)	ΔH_1 (kcal mol^{-1})	$-\text{T}\Delta S_1$ (kcal mol^{-1})	K_{d2} (μM)	ΔH_2 (kcal mol^{-1})	$-\text{T}\Delta S_2$ (kcal mol^{-1})
MN4 – Q + ART	0.09 ± 0.04	-1.4 ± 0.1	-7.9 ± 0.6	15 ± 9	9 ± 4	-15 ± 5
MN4 – ART + Q	1.06 ± 0.1	-4.8 ± 0.1	-5.7 ± 0.1	-	-	-

¹Data collected at 15°C in 20 mM TRIS (pH 7.4), 140 mM NaCl, 5 mM KCl, 2.9% (v/v) DMSO.

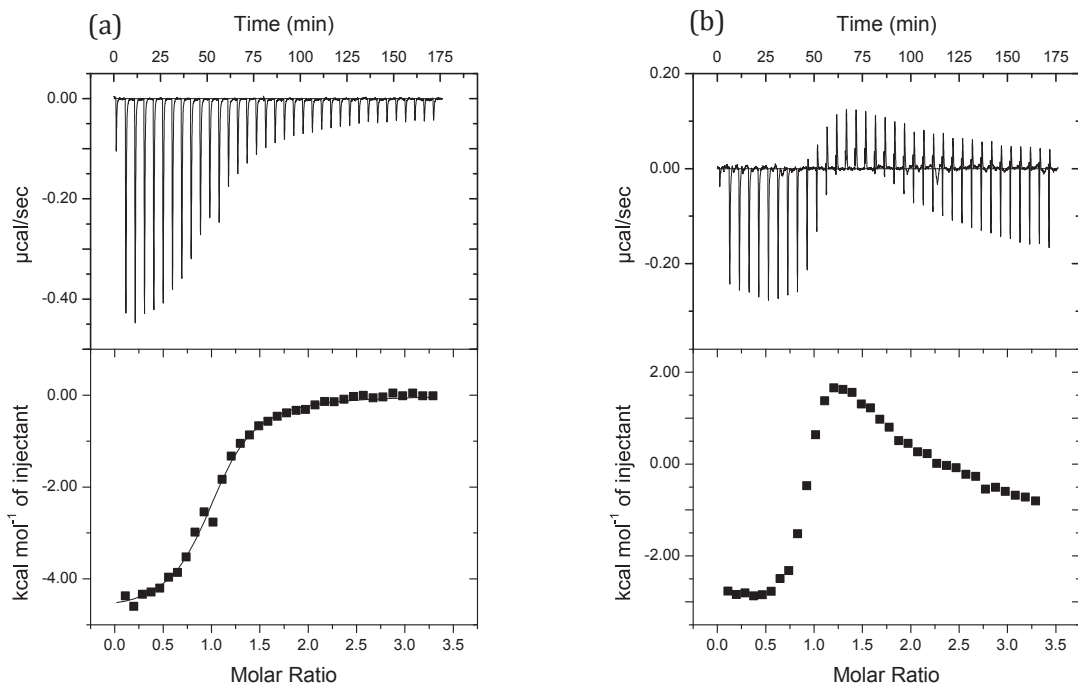


Figure 9-3: ITC thermograms showing competition titration. (a) MN4 bound to artemisinin and quinine was titrated. (b) MN4 bound to quinine and artemisinin was titrated. Data collected in buffer containing 20 mM TRIS (pH 7.4), 140 mM NaCl, 5 mM KCl, 2.4% DMSO at 15°C.

9.2.4. The cocaine-binding aptamer stem deletion. Three variants of the cocaine-binding aptamer have been constructed to study effect of stem deletion on artemisinin binding and possibly discern binding location of the two bound molecules (Figure 9-3).

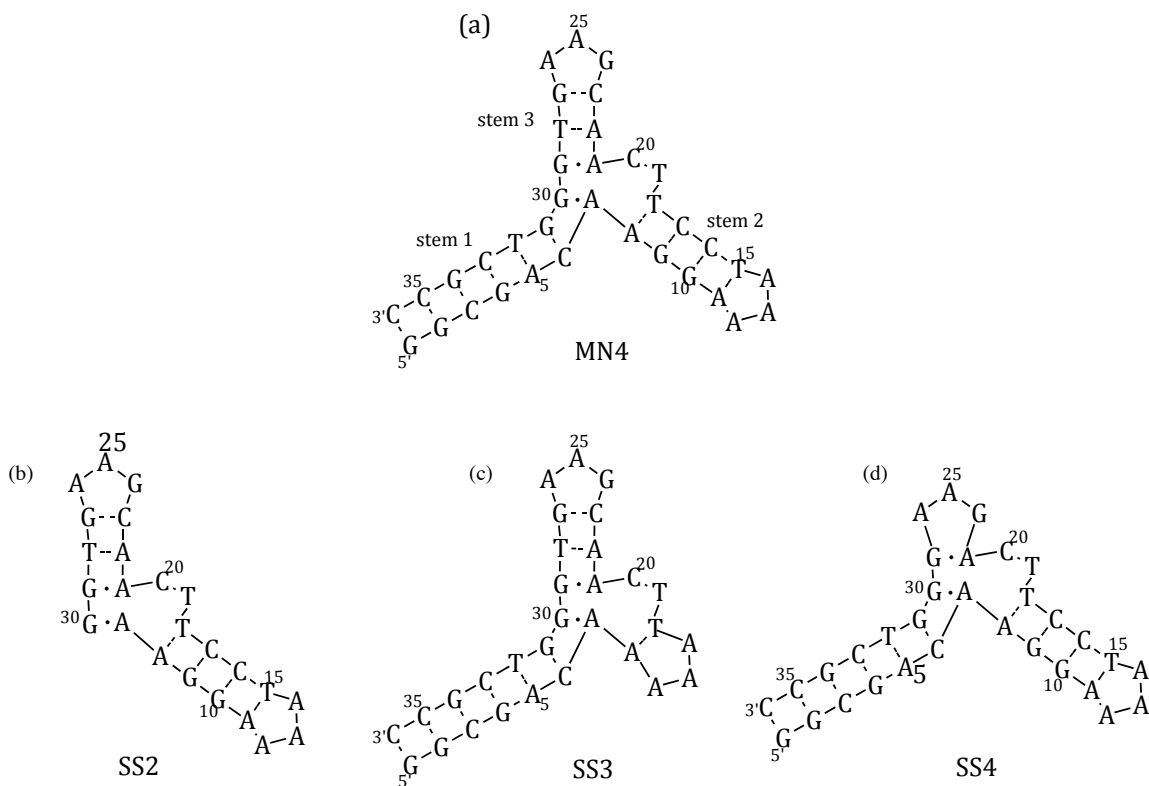


Figure 9-4: Secondary structures of (a) MN4 aptamer; (b) SS2 aptamer, the cocaine-binding aptamer with stem 1 deleted; (c) SS3 aptamer, the cocaine-binding aptamer with stem 2 deleted; and (d) SS4 aptamer, the cocaine-binding aptamer with stem 3 deleted.

Results presented in Table 9-5 show that deletion of stem 1 (SS2 aptamer) decreases the binding affinity of both molecules of artemisinin compared to the MN4 aptamer. Binding enthalpy also decreases, as more energy is needed to fold the aptamer. Removal of stem 2 (SS3 aptamer) has no effect on binding of either artemisinin molecule, as binding parameters are comparable to those of MN4 (Table 9-5). The SS4 aptamer has stem 3 removed, which in turn greatly reduces the binding affinity of the second molecule. These results suggest that stems 1 and 3 are necessary for tight binding of both molecules of artemisinin. Binding thermograms are shown in Figure 9-5.

Table 9-5: Comparison of binding affinities and thermodynamic properties of artemisinin by aptamers used in this study¹.

	K_{d1} (μM)	ΔH_1 (kcal mol^{-1})	$-\text{T}\Delta S_1$ (kcal mol^{-1})	K_{d2} (μM)	ΔH_2 (kcal mol^{-1})	$-\text{T}\Delta S_2$ (kcal mol^{-1})
MN4	0.03 ± 0.01	-4.4 ± 0.2	-5 ± 1	8 ± 1	-16 ± 2	9 ± 2
SS2	0.10 ± 0.04	-1.8 ± 0.1	-7 ± 1	15 ± 1	9 ± 5	-16 ± 5
SS3	0.02 ± 0.01	-3.2 ± 0.1	-7 ± 1	5 ± 2	-21 ± 4	15 ± 4
SS4	0.06 ± 0.03	-1.6 ± 0.1	-8 ± 2		vwb	

¹Data collected at 15°C in 20 mM TRIS (pH 7.4), 140 mM NaCl, 5 mM KCl, 2% DMSO. vwb denotes very weak binding.

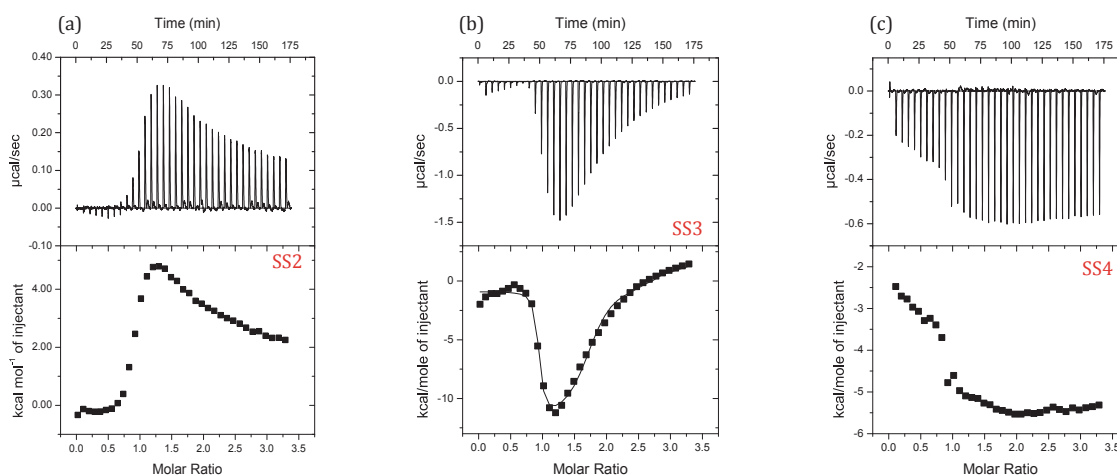


Figure 9-5: Thermograms showing binding of artemisinin to variants of the cocaine-binding aptamer where (a) stem 1 was deleted (SS2), (b) stem 2 was deleted (SS3), and (c) stem 3 was deleted (SS4). Data collected in buffer containing 20 mM TRIS (pH 7.4), 140 mM NaCl, 5 mM KCl, 2.4% (v/v) DMSO at 15°C.

9.2.5. Binding at 0 mM NaCl concentration. As seen in chapter 7, decreasing salt concentration in buffer increases the binding affinity of quinine, cocaine and primaquine and decreases affinity for amodiaquine, chloroquine and mefloquine^{126,168}. ITC was used to investigate how artemisinin interacts with the MN4 aptamer in buffer with low salt concentration. In this buffer, the affinity of artemisinin for the aptamer is decreased about 100-fold (Table 9-6) and only one

molecule of artemisinin is bound (Figure 9-6). Enthalpy becomes more favorable, while entropy becomes unfavorable (Table 9-6). This is in agreement with behavior of amodiaquine, chloroquine and mefloquine whose binding becomes weaker, enthalpy more favorable and entropy less favorable with decreasing salt concentration¹⁶⁸. However, this behaviour is opposite from the one seen for cocaine and quinine, where with decreasing salt concentration affinity for the ligand increases and second binding site is observable¹²⁶.

Table 9-6: Comparison of binding affinities and thermodynamic properties of artemisinin in different buffer conditions¹.

	K_{d1} (μM)	ΔH_1 (kcal mol^{-1})	$-T\Delta S_1$ (kcal mol^{-1})	K_{d2} (μM)	ΔH_2 (kcal mol^{-1})	$-T\Delta S_2$ (kcal mol^{-1})
140 mM NaCl	0.03 ± 0.01	-4.4 ± 0.2	-5 ± 1	13 ± 4	-15 ± 1	9 ± 1
0 mM NaCl	3.7 ± 0.3	-9.5 ± 0.3	2.3 ± 0.3	-	-	-

¹Data collected at 15°C in buffer that also contains 20 mM TRIS (pH 7.4), 5 mM KCl, 2.4% (v/v) DMSO.

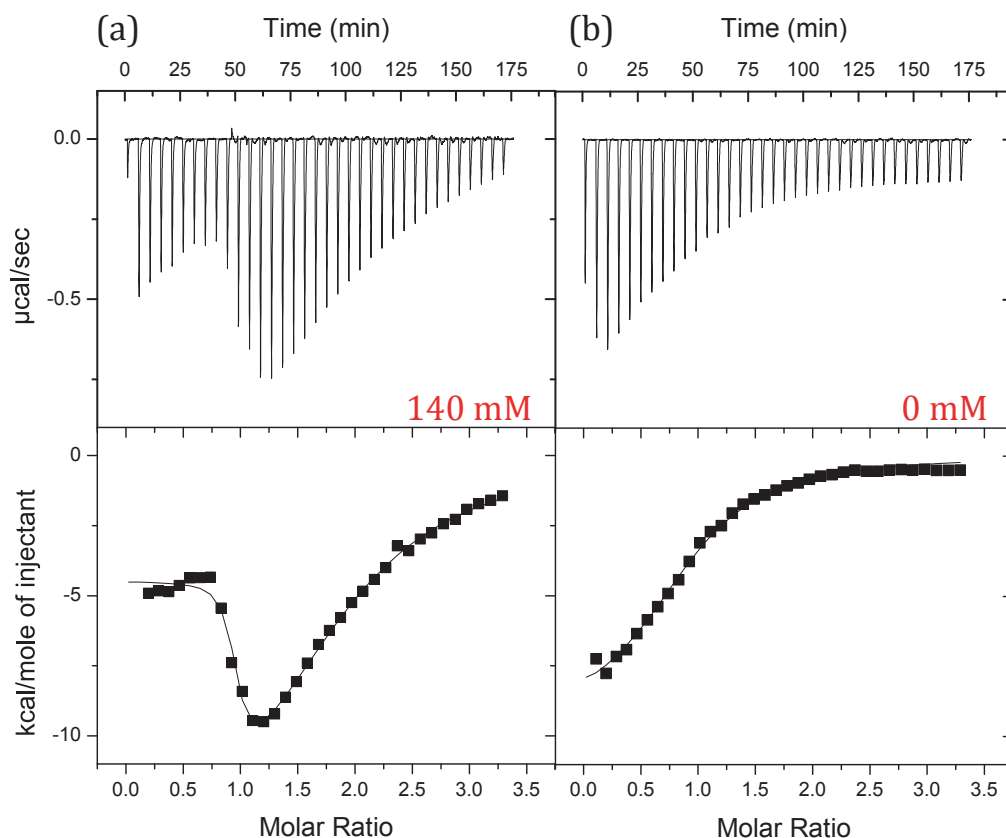


Figure 9-6: ITC thermograms showing interaction of artemisinin with MN4 aptamer in buffer containing 20 mM TRIS (pH 7.4), 5 mM KCl, 2% (v/v) DMSO and in (a) 140 mM NaCl, in (b) 0 mM NaCl at 15°C.

9.2.6. Effect of endoperoxide bridge. It has been shown that the removal of the endoperoxide bridge reduces the activity of artemisinin against malaria²²⁸. ITC thermogram shows only very weak affinity of the cocaine-binding aptamer for 2-deoxyartemisinin (Figure 9-1d), a ligand that contains one oxygen instead of two in the bridge (Figure 9-7b).

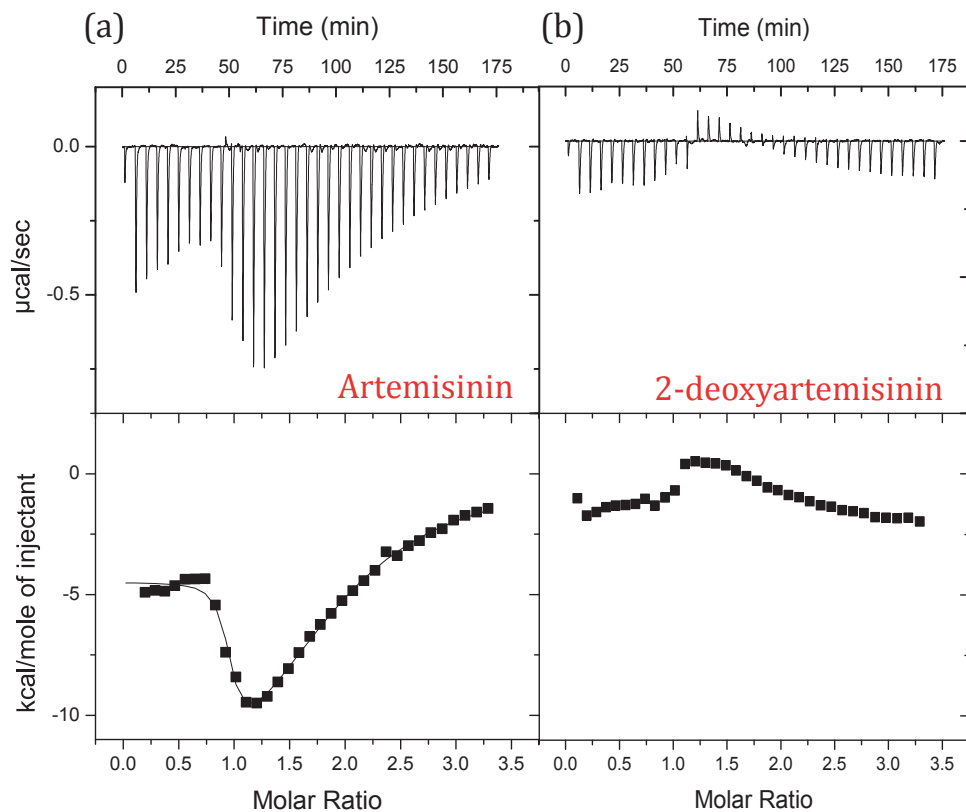


Figure 9-7: ITC thermogram showing (a) interaction of artemisinin with the MN4 aptamer; (b) interaction of 2-deoxyartemisinin with the MN4 aptamer. Data collected in buffer containing 20 mM TRIS (pH 7.4), 140 mM NaCl, 5 mM KCl, 2% DMSO at 15°C.

9.3 Discussion

Previous investigation showed that ligands possessing bicyclic aromatic rings bind to the cocaine-binding aptamer. Artemisinin, a sesquiterpene lactone containing a peroxide bridge, is an unusual ligand that binds to the cocaine-binding aptamer. Actually, two molecules of artemisinin bind to the cocaine-binding aptamer tighter than quinine in high salt buffer at both sites. When stem 1 of the cocaine-binding aptamer is shortened, quinine, cocaine and quinine-based antimalarial compounds

have decreased affinity for the aptamer^{77,79}. However, the length of stem 1 does not seem to significantly affect the binding affinity of artemisinin for the aptamer as results agree within the experimental error (Table 9-1). These results suggest that quinine and artemisinin may not share the same binding site. Enthalpy becomes less favourable with decreasing stem length, as more energy is required to fold the aptamer.

Interestingly, artemisinin binds to different three-way junctions as well as DNA duplexes. Binding is about 7-fold tighter for the SS1 aptamer where the AG base pairs are switched to become GA base pairs and about 2-fold weaker for a generic three-way junction compared to the MN4 aptamer. In case of the DNA duplex molecules, artemisinin binds tighter to hexamer than dodecamer. Binding in all cases is both enthalpically and entropically favourable for the high affinity site. This is unusual when compared to quinine and cocaine, where binding to the cocaine-binding aptamer is enthalpically favourable with an unfavourable entropy.

Affinity of artemisinin for the cocaine-binding aptamer in low salt buffer conditions was also explored. Other antimalarial compounds, such as chloroquine, mefloquine and amodiaquine showed decreased affinity at low salt concentrations¹⁶⁸. The affinity of artemisinin for the aptamer is reduced as the sodium concentration in buffer decreases. This is likely due to impact of ionic concentration on hydrophobic effect, i.e. increasing ionic concentration increases hydrophobic effect²²⁹. Since hydrophobic effect governs binding of artemisinin, decreasing the concentration of

sodium in buffer reduces binding. At 0 mM NaCl only one molecule of artemisinin is bound with an affinity about 100-fold weaker than at 140 mM NaCl. These findings are in agreement with studies which show that artemisinin interactions with parasite have favourable entropy, suggesting that binding is governed by hydrophobic effect²³⁰⁻²³².

To determine whether artemisinin shares the same binding site with quinine, a set of ITC-monitored competitive binding titrations were performed. From fitting data to a single-site binding model, a $K_{d,app}$ value of $(1.1 \pm 0.1) \mu\text{M}$ and enthalpy of $(-4.8 \pm 0.1) \text{ kcal mol}^{-1}$ were obtained. The presence of artemisinin in the complex decreases binding affinity of quinine to MN4 aptamer (K_d of $0.20 \pm 0.05 \mu\text{M}$ and enthalpy of $-14 \pm 1 \text{ kcal mol}^{-1}$). Next, artemisinin was titrated into quinine-bound MN4 and a non-sigmoidal binding curve was observed, suggesting that two molecules of artemisinin bind to the MN4-quinine complex (Figure 9-3). In this case, having quinine bound to the cocaine-binding aptamer changes the titration of artemisinin. The affinity of one artemisinin molecule for the aptamer remains unchanged, while the affinity of the second molecule decreases in the presence of quinine. These results are suggestive of partial competition and that the binding site of artemisinin and the binding site of quinine most likely overlap to some extent.

To further examine the binding location of artemisinin, three different variants of the cocaine-binding aptamer have been constructed. Each new construct had one of the stems deleted and binding parameters have been determined. Results indicate

that deletion of stem 2 (SS3 aptamer) has no impact on binding of artemisinin, as results are comparable to those of artemisinin binding to MN4 (Table 9-4). Deletion of stem 1 in SS2 aptamer decreases the binding affinity of both artemisinin molecules, while deletion of stem 3 in the SS4 aptamer has the greatest impact on the binding of the second molecule. Figure 9-5c does not show characteristic non-sigmoidal binding curve suggesting that only one molecule of artemisinin binds to the SS4 aptamer with detectable affinity. These results indicate that stems 1 and 3 play an important role in binding of artemisinin. Interestingly, MN4-bound quinine upon titration of artemisinin gives similar results as removal of stem 1 suggesting that one artemisinin molecule binds close to the quinine binding site. Previous results show that G31 is one of the bases most impacted upon quinine binding to MN4⁸². Artemisinin NMR results² show that G31 (stem 1, close to mismatch), T18 (part of bulge) and T28 (stem 3) are also affected by artemisinin binding. Artemisinin and quinine could partially compete for the binding site. Titration of quinine into the MN4-bound artemisinin complex also results in binding with decreased affinity for quinine. Most likely, both ligands bind to the cocaine-binding aptamer with either partial competition for one site or artemisinin hinders binding of quinine due to its size, hence decreased affinity for quinine.

,

Many studies have confirmed that artemisinin is not a DNA intercalator like quinine-based antimalarial compounds but interacts with parasite through its endoperoxide bridge^{217,225,230,232,233}. In order to test if artemisinin interacts with the cocaine-

² Performed by Zach Churcher from Johnson lab, added here to further clarify results. Data in this chapter has not been published yet.

binding aptamer in the same manner, affinity of the 2-deoxyartemisin for the aptamer was tested. This ligand is structurally very similar to artemisinin except that it has only one oxygen in the bridge instead of two (Figure 9-1d). With the removal of one oxygen from this peroxide link binding affinity is reduced indicating that artemisinin interacts through this peroxide bridge with the cocaine-binding aptamer.

9.4 Concluding remarks

Currently it is not known how artemisinin works as an antimalarial agent. It is not previously shown that it binds DNA, however in presence of ferrous ion endoperoxide bridge is cleaved generating reactive oxygen species²²⁶. Results presented here show that artemisinin binds to different DNA structures regardless of three-dimensional structure or length. Artemisinin is an unusual compound that binds two molecules to the cocaine-binding aptamer using endoperoxide link. Two molecules of this antimalarial compound also bind to other DNA structures with high affinity. Binding is mostly entropically driven with a favorable enthalpy. Artemisinin and quinine possibly do not share the same binding site. Binding of artemisinin to the cocaine binding aptamer could be useful in better understanding how this aptamer functions and what factors are important for binding. As the mechanism of action of artemisinin is not fully understood, its interaction with different DNA structures could possibly lead to a better understanding how it works as an antimalarial agent.

Concluding Remarks

10.1 Summary

The study of how aptamers function is still a relatively unexplored field of study. The work presented in this thesis has brought another step closer into understanding how aptamers function and how they bind to their ligands. The results in Chapter 3 illustrate that the cocaine-binding aptamer not only binds quinine but its analogues as well. Findings in this chapter show the importance of the quinoline ring for ligand detection. Other features of the ligand such as R-isomers binding tighter than S-isomers and a 6'-methoxy substituent on the quinoline ring increase binding affinity. Chapter 4 added information about a second binding site where the binding to this second, weaker site can be salt controlled, i.e. increasing NaCl concentration in buffer decreases the binding affinity of the second site for the ligand. In Chapter 5, this two-site binding was expanded to the ATP-binding aptamer and the appropriate binding model was determined. ATP and its analogues bind to the ATP-binding aptamer in a cooperative manner. However, if the two sites are separated by at least four base pairs, the mode of binding switches from cooperative to independent for adenosine. This is not true for ATP as the binding remains cooperative. In Chapter 6, the cocaine-binding aptamer is revisited and binding affinity to quinine is fine-tuned using a dangling nucleotide at either the 5' or 3' end. The last three chapters focused on the binding of quinine-based and non-quinine based antimalarial compounds to the cocaine-binding aptamer and different DNA structures. From the results, it can be

concluded that amodiaquine is the tightest known ligand that binds to the cocaine-binding aptamer and is a generic DNA binder. Surprisingly, artemisinin, which is a non-quinine based antimalarial compound binds not only to the cocaine binding aptamer but to all DNA structures studied. On the other hand, quinine and chloroquine are specific for the cocaine-binding aptamer. The research in this thesis was primarily based on isothermal titration calorimetry (ITC) techniques, although other techniques such as NMR, DSC and fluorescence were used to confirm ITC results.

10.2. Future work

One of the primary goals of this research is to better understand how the cocaine-aptamer functions and why does it bind ligands for which it was not selected. Thus far a great amount of insight into the cocaine-aptamer binding has been gained. Moving forward, more cocaine-binding aptamer-small molecule systems should be evaluated in order to determine what drives binding. It would be interesting to further study artemisinin binding to the cocaine-binding aptamer as it is a non-quinine based ligand that binds to the cocaine-binding aptamer. One of the goals would be to determine if artemisinin is reacting with DNA to form a covalent link and how important is the presence of ferrous ion for artemisinin binding to DNA.

A major goal would be to determine the three-dimensional structure of the aptamer both free and bound to the various ligands explored in this thesis. These findings

will give more insight into aptamer – ligand binding, such as binding location, number of binding site and nature of binding.

The cocaine-binding aptamer is often used in development of many different detection applications but not as a drug delivery “vehicle”. The ability of this aptamer to be split into overlapping strands and create multi-chain structure could be utilized to create aptamer-drug conjugate, which would deliver drug of interest to damaged cells. Of course, chemical modifications on the aptamer would have to be introduced in order to enhance the stability of the aptamer. These studies would broaden the use of the cocaine-binding aptamer not only in biosensor studies but possibly in therapeutic and diagnostic studies.

Appendix A

Isothermal titration calorimetry isotherms have been fitted to either one set of identical sites or two-set of independent sites or two sets of cooperative sites using a heat function Q , defined by following expression:

$$\Delta Q(i) = Q(i) + \frac{V_i}{V_c} \left(\frac{Q(i) + Q(i-1)}{2} \right) - Q(i-1) \quad (\text{A1})$$

which takes into consideration the sample displaced from the working volume of the cell by the injections²³⁴. Here V_i represents volume after i^{th} injections and V_c is the working volume of the sample cell. Since concentrations of each chemical speices are not known, binding equations are expressed in terms of total concentrations. The total concentration of ligand, X_t and aptamer concentration, M_t is given in Equations (A2) and (A3)²³⁵:

$$[X_t] = [X_0] \left(1 - \left(1 - \frac{V_i}{V_c} \right) \right) \quad (\text{A2})$$

$$[M_t] = [M_0] \left(1 - \frac{V_i}{V_c} \right)^i \quad (\text{A3})$$

where X_0 is the initial concentration of ligand in the syringe, M_0 is the initial aptamer concentration in the cell.

A1. Two-site independent binding model

This binding model defines n_1 site with dissociation constant K_1 and n_2 site with dissociation constant K_2 . Fractions of each site, f_1 and f_2 , that are populated by ligand can be expressed as:

$$f_1 = \frac{[X]}{K_{D1} + [X]} \quad (A4)$$

$$f_2 = \frac{[X]}{K_{D2} + [X]} \quad (A5)$$

Total concentration of ligand can be calculated using equation (11) where X is concentration of free ligand.

$$[X_t] = [X] + [M_t](n_1 f_1 + n_2 f_2) \quad (A6)$$

Solving equations (A5) and (A6) for f_1 and f_2 and then substituting into equation (A6) the third order polynomial is obtained

$$a + b[X] + c[X]^2 + d[X]^3 = 0 \quad (A7)$$

where

$$a = -K_{D1}K_{D2}[X_t]$$

$$b = (K_{D2}n_1 + K_{D1}n_2)M_t - (K_{D1} + K_{D2})[X_t] + K_{D1}K_{D2}$$

$$c = K_{D1} + K_{D2} + (n_1 + n_2)[M_t] - [X_t]$$

The concentration of free ligand $[X]$ for any combination of $[X_t]$ and $[P_t]$ and binding affinities corresponds to the positive real root of equation (A7), which can be

determined by using the bisection method²³⁶. The values of f_1 and f_2 can be determined by substituting $[X]$ into equations (A6) and (A7). Finally, the heat function for the independent site model is given by equation (A8)

$$Q = [M_t]V_c(n_1f_1\Delta H_1 + n_2f_2\Delta H_2) \quad (\text{A8})$$

A2. Two-site cooperative binding model

This model describes an aptamer with two cooperatively dependent sites. First ligand binds to the either site of the aptamer with dissociation constant K_{d1} and second ligand binds the second, unoccupied site of the singly bound aptamer with dissociation constant K_{d2} . Both dissociation constants can be calculated by equations (A9) and (A10), while fractions of each occupied site on the aptamer is given by the expressions (A11) and (A12)

$$K_{D1} = \frac{[M][X]}{[MX]} \quad (\text{A9})$$

$$K_{D2} = \frac{[MX][X]}{[MX_2]} \quad (\text{A10})$$

$$f_1 = \frac{2K_{D2}[X]}{K_{D1}K_{D2} + 2K_{D2}[X] + [X]^2} \quad (\text{A11})$$

$$f_2 = \frac{[X]^2}{K_{D1}K_{D2} + 2K_{D2}[X] + [X]^2} \quad (\text{A12})$$

Total aptamer concentration is given by equation (A13)

$$[X_t] = [X] + [M_t](f_1 + 2f_2) \quad (\text{A13})$$

Substituting equation (A11) and (A12) into equation (A13), a third-degree polynomial is obtained (A14)

$$a + b[X] + c[X]^2 + d[X]^3 = 0 \quad (\text{A14})$$

where

$$a = -K_{D1}K_{D2}[X_t]$$

$$b = K_{D1}K_{D2} + 2K_{D2}([M_t] - [X_t])$$

$$c = 2K_{D2} + 2[M_t] - [X_t]$$

The positive real root of equation (A14) gives the concentration of free ligand, $[X]$ which substituted into equations (A9) and (A10) provide values for f_1 and f_2 . The heat function for this model can then be expressed as

$$Q = [M_t]V_c(f_1\Delta H_1 + f_2(\Delta H_1 + \Delta H_2)) \quad (\text{A15})$$

Data is then fit by adjusting binding parameters to minimize the sum of residual squared differences (RSS) between experimental data points and those calculated using equation (1).

$$RSS = \sum_i (\Delta Q(i)_{calc} - \Delta Q(i)_{exp}) \quad (\text{A16})$$

Appendix B

B1. Hill coefficient determination

Cooperative binding can be further analyzed by examining binding isotherms in terms of the Wyman's Hill plot^{139,237,238}. Here, a method developed by Cattoni *et al.*²³⁸ is used to determine Hill coefficient, n_H .

From equations A2 and A3 total aptamer and total ligand concentration can be determined. Using equations A9 to A13, a third-degree polynomial is obtained (equation A14). The positive real root gives the free ligand concentration. Knowing the free ligand concentration, X and binding affinities for both binding sites K_1 and K_2 , the binding saturation parameter, n_{LB} can be determined (equation B1).

$$n_{LB} = \frac{K_1X + 2K_2X^2}{1 + K_1X + K_2X^2} \quad (B1)$$

Plotting $\ln(n_{LB}/(2-n_{LB}))$ vs $\ln(X)$ a binding isotherm can be generated (Figure B-1). This plot has two regions at low and high free ligand concentrations. It also has a transition region which can be fitted to the third order polynomial function:

$$y = a_3x^3 + a_2x^2 + a_1x + a_0 \quad (B2)$$

The Hill coefficient is calculated as the maximum (or minimum) value of the first derivative of equation B1.

$$\frac{dy}{dx} = 3a_3x^2 + 2a_2x + a_1 \quad (B3)$$

Equating the second derivative to zero, value of x can be calculated.

$$\frac{d^2y}{dx^2} = 6a_3x + 2a_2 = 0 \quad (\text{B4})$$

$$x = \frac{2a_2}{6a_3} \quad (\text{B5})$$

Replacing thus calculated value of x in equation B3, Hill coefficient can be estimated

$$n_H = a_1 - \frac{a_2^2}{3a_3}$$

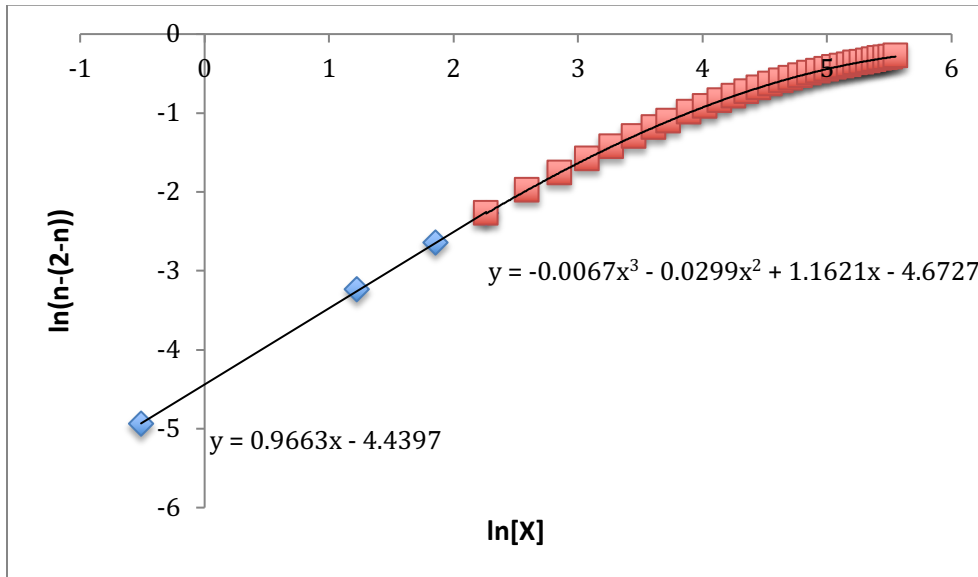


Figure B1: Hill plot for adenosine binding to ATP3 aptamer with two sites exhibiting positive cooperativity. Binding isotherms were generated as described on page 152. Blue dots represent lowest ligand concentration region with slope of 1. In this case, there is no high ligand concentration region as final ligand concentration is not high. Red dots represent the transition region fitted to the third order polynomial the fitting parameters $a_3 = -0.0067$, $a_2 = -0.0299$, $a_1 = 1.1621$, $a_0 = -4.6727$. The Hill coefficient for this example is $n_H = 1.2$.

Bibliography

1. Kaufmann, S. H. E. Immunology's foundation:the 100th anniversary of the nobel prize to Paul Ehrlich and Elie Metchnikof. *Nat. Immunol.* **9**, 705–712 (1908).
2. Winau, F., Westphal, O. & Winau, R. Paul Ehrlich - In search of the magic bullet. *Microbes Infect.* **6**, 786–789 (2004).
3. Cho, E. ., Lee, J. W. & Ellington, A. D. Applications of Aptamers as Sensors. *Annu. Rev. Anal. Chem.* **2**, 241–264 (2009).
4. Tuerk, C. & Gold, L. Systematic evolution of ligands by exponential enrichment:RNA ligands to bacteriophage T4 DNA polymerase. *Science* **249**, 505–510 (1990).
5. Ellington, A. D. & Szostak, J. W. In vitro selection of RNA molecules that bind specific ligands. *Nature* **346**, 818–822 (1990).
6. Ellington, A. D. & Szostak, J. W. Selection in vitro of single-stranded DNA molecules that fold into specific ligand-binding structures. *Nature* **355**, 850–852 (1992).
7. Robertson, D. L. & Joyce, G. F. Selection in vitro of an RNA enzyme that specifically cleaves single-stranded DNA. *Nature* **344**, 467–468 (1990).
8. Lin, C. H. & Patel, D. J. Structural basis of DNA folding and recognition in an AMP-DNA aptamer complex: distinct architectures but common recognition motifs for DNA and RNA aptamers complexed to AMP. *Chem. Biol.* **4**, 817–832 (1997).

9. Darmostuk, M., Rimpelova, S., Gbelcova, H. & Ruml, T. Current approaches in SELEX: An update to aptamer selection technology. *Biotechnol. Adv.* **33**, 1141–1161 (2014).
10. Hoppe-Seyler, F. *et al.* Peptide aptamers: New tools to study protein interactions. *J. Steroid Biochem. and Mol. Biol.* **78**, 105–111 (2001).
11. Ng, A. *et al.* Selection, characterization, and biosensing application of high affinity congener-specific microcystin-targeting aptamers. *Environ. Sci. Technol.* **46**, 10697–10703 (2012).
12. Cruz-Aguado, J. A. & Penner, G. Determination of Ochratoxin A with a DNA Aptamer. *J. Agric. Food Chem.* **56**, 10456–10461 (2008).
13. Mishra, G. K., Sharma, V. & Mishra, R. K. Electrochemical Aptasensors for Food and Environmental Safeguarding: A Review. *Biosensors* **8**, 28 (2018).
14. Ng, E. W. M. *et al.* Pegaptanib, a targeted anti-VEGF aptamer for ocular vascular disease. *Nat. Rev. Drug Discovery* **5**, 123–132 (2006).
15. Griffin, L. C., Tidmarsh, G. F., Bock, L. C., Toole, J. J. & Leung, L. L. K. In Vivo Anticoagulant Properties. *Blood* **81**, 3271–3276 (1993).
16. Sumedha D.J. Aptamers: An Emerging Class of Molecules That Rival Antibodies in Diagnostics. *Clin. Chem.* **45**, 1628–1650 (1999).
17. Shigdar, S. *et al.* Aptamers as theranostic agents: Modifications, serum stability and functionalisation. *Sensors* **13**, 13624–13637 (2013).
18. Lochrie, M. & Gold, L. Nucleic acid ligands which bind to hepatocyte growth factor/scatter factor (HGF/SF) or its receptor c-met and to integrins. US

Patent 6,344,321 B1 February 5, 2002.

19. Sampson, T. Aptamers and SELEX: The technology. *World Pat. Inf.* **25**, 123–129 (2003).
20. Vorobyeva, M. A., Davydova, A. S., Vorobjev, P. E., Pyshnyi, D. V. & Venyaminova, A. G. Key aspects of nucleic acid library design for in vitro selection. *Int. J. Mol. Sci.* **19**, (2018).
21. Song, K. M. *et al.* Gold nanoparticle-based colorimetric detection of kanamycin using a DNA aptamer. *Anal. Biochem.* **415**, 175–181 (2011).
22. Stoltenburg, R., Reinemann, C. & Strehlitz, B. FluMag-SELEX as an advantageous method for DNA aptamer selection. *Anal. Bioanal. Chem.* **383**, 83–91 (2005).
23. Meyer, S. *et al.* Development of an efficient targeted cell-SELEX procedure for DNA aptamer reagents. *PloS One* **8**, e71798–e71798 (2013).
24. Jenison, R. D., Gill, S. C., Pardi, A. & Polisky, B. High-resolution molecular discrimination by RNA. *Science* **263**, 1425 LP – 1429 (1994).
25. Coulter, L. R., Landree, M. A. & Cooper, T. A. Identification of a new class of exonic splicing enhancers by in vivo selection. *Mol. Cell. Biol.* **17**, 2143–2150 (2015).
26. Daniels, D. A., Chen, H., Hicke, B. J., Swiderek, K. M. & Gold, L. A tenascin-C aptamer identified by tumor cell SELEX: Systematic evolution of ligands by exponential enrichment. *Proc. Natl. Acad. Sci.* **100**, 15416–15421 (2003).
27. Kim, Y., Liu, C. & Tan, W. Aptamers generated by Cell SELEX for biomarker

- discovery. *Biomarkers Med.* **3**, 193–202 (2009).
28. Mendonsa, S. D. & Bowser, M. T. In Vitro Evolution of Functional DNA Using Capillary Electrophoresis. *J. Am. Chem. Soc.* **126**, 20–21 (2004).
 29. Mendonsa, S. D. S. D. & Bowser, M. T. M. T. In Vitro Selection of High-Affinity DNA Ligands for Human IgE Using Capillary Electrophoresis. *Anal. Chem.* **76**, 5387–5392 (2004).
 30. Dong, L. *et al.* Screening and Identifying a Novel ssDNA Aptamer against Alpha-fetoprotein Using CE-SELEX. *Sci. Rep.* **5**, 15552 (2015).
 31. Hamedani, N. S. & Müller, J. Capillary Electrophoresis for the Selection of DNA Aptamers Recognizing Activated Protein C BT - Nucleic Acid Aptamers: Selection, Characterization, and Application. in *Nucleic Acid Aptamers* (ed. Mayer, G.) 61–75 (Springer New York, 2016).
 32. Berezovski, M., Musheev, M., Drabovich, A. & Krylov, S. N. Non-SELEX selection of aptamers. *J. Am. Chem. Soc.* **128**, 1410–1411 (2006).
 33. Berezovski, M. V, Musheev, M. U., Drabovich, A. P., Jitkova, J. V & Krylov, S. N. Non-SELEX: selection of aptamers without intermediate amplification of candidate oligonucleotides. *Nat. Protoc.* **1**, 1359–1369 (2006).
 34. Rabal, O. *et al.* In silico aptamer docking studies: from a retrospective validation to a prospective case study-TIM3 aptamers binding. *Mol. Ther. - Nucleic Acids* **5**, 1–12 (2016).
 35. Jing, M. & Bowser, M. T. Isolation of DNA aptamers using micro free flow electrophoresis. *Lab Chip* **11**, 3703–3709 (2011).

36. Paniel, N. *et al.* Selection of DNA aptamers against penicillin G using Capture-SELEX for the development of an impedimetric sensor. *Talanta* **162**, 232–240 (2017).
37. Okhonin, V., Berezovski, M. & Krylov, S. N. Sweeping Capillary Electrophoresis: A Non-Stopped-Flow Method for Measuring Bimolecular Rate Constant of Complex Formation between Protein and DNA. *J. Am. Chem. Soc.* **126**, 7166–7167 (2004).
38. Klußmann, S., Nolte, A., Bald, R., Erdmann, V. A. & Fürste, J. P. Mirror-image RNA that binds D-Adenosine. *Nat. Biotechnol.* **14**, 1112–1115 (1996).
39. Nolte, A., Klußmann, S., Bald, R., Erdmann, V. A. & Fürste, J. P. Mirror-Design of L-oligonucleotide Ligands Binding to L-arginine. *Nat. Biotechnol.* **14**, 1116–1119 (1996).
40. Gold, L. *et al.* Aptamer-based multiplexed proteomic technology for biomarker discovery. *PLoS One* **5**, (2010).
41. Rohloff, J. C. *et al.* Nucleic acid ligands with protein-like side chains: Modified aptamers and their use as diagnostic and therapeutic agents. *Mol. Ther. - Nucleic Acids* **3**, e201 (2014).
42. Eid, C., Palko, J. W., Katilius, E. & Santiago, J. G. Rapid Slow Off-Rate Modified Aptamer (SOMAmer)-Based Detection of C-Reactive Protein Using Isotachophoresis and an Ionic Spacer. *Anal. Chem.* **87**, 6736–6743 (2015).
43. Volk, D. E. & Lokesh, G. L. R. Development of Phosphorothioate DNA and DNA Thioaptamers. *Biomedicines* **5**, 41 (2017).

44. Lokesh, G. L. *et al.* X-aptamer selection and validation. *Methods Mol. Biol.* **1632**, 151–174 (2017).
45. Riccitelli, N. J. & Lupták, A. Computational discovery of folded RNA domains in genomes and in vitro selected libraries. *Methods* **52**, 133–140 (2010).
46. Geiger, A., Burgstaller, P., Von der Eltz, H., Roeder, A. & Famulok, M. RNA aptamers that bind L-arginine with sub-micromolar dissociation constants and high enantioselectivity. *Nucleic Acids Res.* **24**, 1029–1036 (1996).
47. Sassanfer, M. & Szostak, J. W. An RNA motif that binds ATP. *Nature* **364**, 550–553. (1993).
48. Chen, L. *et al.* The isolation of an RNA aptamer targeting to p53 protein with single amino acid mutation. *Proc. Natl. Acad. Sci.* **112**, 10002–10007 (2015).
49. Mairal, T. *et al.* Aptamers: Molecular tools for analytical applications. *Anal. Bioanal. Chem.* **390**, 989–1007 (2008).
50. Nagatoishi, S., Isono, N., Tsumoto, K. & Sugimoto, N. Loop residues of thrombin-binding DNA aptamer impact G-quadruplex stability and thrombin binding. *Biochimie* **93**, 1231–1238 (2011).
51. Deng, B. *et al.* Aptamer binding assays for proteins: The thrombin example-A review. *Anal. Chim. Acta* **837**, 1–15 (2014).
52. Bunka, D. H. J. & Stockley, P. G. Aptamers come of age - at last, *Nat. Rev. Nat. Rev. Microbiol.* **4**, 588–596 (2006).
53. Bruno, J. G. & Kiel, J. L. In vitro selection of DNA aptamers to anthrax spores with electrochemiluminescence detection. *Biosens. Bioelectron.* **14**, 457–464

- (1999).
54. Wan, Y. *et al.* Surface-immobilized aptamers for cancer cell isolation and microscopic cytology. *Cancer Res.* **70**, 9371–9380 (2010).
 55. Bagalkot, V., Farokhzad, O. C., Langer, R. & Jon, S. An aptamer-doxorubicin physical conjugate as a novel targeted drug-delivery platform. *Angew. Chem., Int. Ed. Engl.* **45**, 8149–8152 (2006).
 56. Huang, Y. F. *et al.* Molecular assembly of an aptamer-drug conjugate for targeted drug delivery to tumor cells. *ChemBioChem* **10**, 862–868 (2009).
 57. Dam, D. H. M. *et al.* Direct observation of nanoparticle-cancer cell nucleus interactions. *ACS Nano* **6**, 3318–3326 (2012).
 58. Zhou, J. & Rossi, J. Aptamers as targeted therapeutics: current potential and challenges. *Nat. Rev. Drug Discovery* **16**, 181 (2016).
 59. SomaLogic, Inc. (2015) SSM017 Rev 3 DCN 14-194. SOMAmer® Technical note.
 60. Famulok, M. & Mayer, G. Aptamer modules as sensors and detectors. *Acc. Chem. Res.* **44**, 1349–1358 (2011).
 61. Zhou, W., Jimmy Huang, P. J., Ding, J. & Liu, J. Aptamer-based biosensors for biomedical diagnostics. *Analyst* **139**, 2627–2640 (2014).
 62. Zhou, W., Ding, J. & Liu, J. A highly specific sodium aptamer probed by 2-aminopurine for robust Na⁺ sensing. *Nucleic Acids Res.* **44**, 10377–10385 (2016).
 63. Ferapontova, E. E., Olsen, E. M. & Gothelf, K. V. An RNA aptamer-based

- electrochemical biosensor for detection of theophylline in serum. *J. Am. Chem. Soc.* **130**, 4256–4258 (2008).
64. Liu, J. & Lu, Y. Fast colorimetric sensing of adenosine and cocaine based on a general sensor design involving aptamers and nanoparticles. *Angew. Chem., Int. Ed. Engl.* **45**, 90–94 (2005).
65. Xiao, Y., Lai, R. Y. & Plaxco, K. W. Preparation of electrode-immobilized, redox-modified oligonucleotides for electrochemical DNA and aptamer-based sensing. *Nat. Protoc.* **2**, 2875 (2007).
66. Xiao, Y., Piorek, B. D., Plaxco, K. W. & Heeger, A. J. A reagentless signal-on architecture for electronic, aptamer-based sensors via target-induced strand displacement. *J. Am. Chem. Soc.* **127**, 17990–17991 (2005).
67. Mirkin, C. A., Letsinger, R. L., Mucic, R. C. & Storhoff, J. J. Macroscopic Materials. *Nature* **382**, 607–609 (1996).
68. Neves, M. A. D., Slavkovic, S., Reinstein, O., Shoara, A. A. & Johnson, P. E. A proof of concept application of aptachain: ligand-induced self-assembly of a DNA aptamer. *RCS Adv.* **9**, 1690–1695 (2019).
69. Pavlov, V., Xiao, Y., Shlyahovsky, B. & Willner, I. Aptamer-functionalized Au nanoparticles for the amplified optical detection of thrombin. *J. Am. Chem. Soc.* **126**, 11768–11769 (2004).
70. Mironov, A. S. *et al.* Sensing small molecules by nascent RNA: A mechanism to control transcription in bacteria. *Cell* **111**, 747–756 (2002).
71. Breaker, R. R., Winkler, W. & Nahvi, A. Thiamine derivatives bind messenger

- RNAs directly to regulate bacterial gene expression. *Nature* **419**, 952–956 (2002).
72. Serganov, A. & Nudler, E. A decade of riboswitches. *Cell* **152**, 17–24 (2013).
 73. Barrick, J. E. *et al.* New RNA motifs suggest an expanded scope for riboswitches in bacterial genetic control. *Proc. Natl. Acad. Sci.* **101**, 6421–6426 (2004).
 74. Kubodera, T. *et al.* Thiamine-regulated gene expression of *Aspergillus oryzae* thiA requires splicing of the intron containing a riboswitch-like domain in the 5'-UTR. *FEBS Lett.* **555**, 516–20 (2003).
 75. Stojanovic, M. N., Prada, P. De & Landry, D. W. Fluorescent sensors based on aptamer self-assembly. *J. Am. Chem. Soc.* **122**, 11547–11548 (2000).
 76. Stojanovic, M. N., Prada, P. de & Landry, D. W. Aptamer-based folding fluorescent sensor for cocaine. *J. Am. Chem. Soc.* **123**, 4928–4931 (2001).
 77. Neves, M. A. D., Reinstein, O. & Johnson, P. Defining a stem length-dependent binding mechanism for the cocaine-binding aptamer. A combined NMR and calorimetry study. *Biochemistry* **49**, 8478–8487 (2010).
 78. Neves, M. A. D., Reinstein, O., Saad, M. & Johnson, P. E. Defining the secondary structural requirements of a cocaine-binding aptamer by a thermodynamic and mutation study. *Biophys. Chem.* **153**, 9–16 (2010).
 79. Neves, M. A. D. *et al.* Optimizing stem length to improve ligand selectivity in a structure-switching cocaine-binding aptamer. *ACS Sens.* **2**, 1539–1545 (2017).
 80. Stojanović, M. N. *et al.* Cross-reactive arrays based on three-way junctions. *J.*

- Am. Chem. Soc.* **125**, 6085–6089 (2003).
81. Reinstein, O. *et al.* Engineering a structure switching mechanism into a steroid binding aptamer and hydrodynamic analysis of the ligand binding mechanism. *Biochemistry* **50**, 9368–9376 (2011).
 82. Reinstein, O. *et al.* Quinine binding by the cocaine-binding aptamer. thermodynamic and hydrodynamic analysis of high-affinity binding of an off-target ligand. *Biochemistry* **52**, 8652–8662 (2013).
 83. Pei, R. *et al.* High-resolution cross-reactive array for alkaloids. *Chem. Commun.* **22**, 3193–3195 (2009).
 84. Stojanovic, M. N. & Landry, D. W. Aptamer-based colorimetric probe for cocaine. *J. Am. Chem. Soc.* **124**, (2002).
 85. Sharma, A. K. & Heemstra, J. M. Small-molecule-dependent split aptamer ligation. *J. Am. Chem. Soc.* **133**, 12426–12429 (2011).
 86. Baker, B. R. *et al.* An electronic, aptamer-based small-molecule sensor for the rapid, label-free detection of cocaine in adulterated samples and biological fluids. *J. Am. Chem. Soc.* **128**, 3138–3139 (2006).
 87. Gulbakan, B. *et al.* Native electrospray ionization mass spectrometry reveals multiple facets of aptamer-ligand interactions: from mechanism to binding constants. *J. Am. Chem. Soc.* **140**, 7486–7497 (2018).
 88. Qiu, Y., Gu, C., Li, B. & Shi, H. Aptameric detection of quinine in reclaimed wastewater by using a personal glucose meter. *Anal. Methods* **10**, 2931–2938 (2018).

89. Long, S. B., Long, M. B., White, R. R. & Sullenger, B. A. Crystal structure of an RNA aptamer bound to thrombin. *RNA* **14**, 2504–2512 (2008).
90. Deng, Q., German, I., Buchanan, D. & Kennedy, R. T. Retention and separation of adenosine and analogues by affinity chromatography with an aptamer stationary phase. *Anal. Chem.* **73**, 5415–5421 (2001).
91. Wang, J. *et al.* Novel application of fluorescence coupled capillary electrophoresis to resolve the interaction between the G-quadruplex aptamer and thrombin. *J. Sep. Sci.* **40**, 3161–3167 (2017).
92. Liss, M., Petersen, B., Wolf, H. & Prohaska, E. An aptamer-based quartz crystal protein biosensor. *Anal. Chem.* **74**, 4488–4495 (2002).
93. Shoara, A. A., Slavkovic, S., Donaldson, L. W. & Johnson, P. E. Analysis of the interaction between the cocaine-binding aptamer and its ligands using fluorescence spectroscopy. *Can. J. Chem.* **95**, 1253–1260 (2017).
94. Dupont, D. M. *et al.* Protein-binding RNA aptamers affect molecular interactions distantly from their binding sites. *PLoS One* **10**, 1–22 (2015).
95. Slavkovic, S. & Johnson, P. E. Isothermal titration calorimetry studies of aptamer-small molecule interactions: practicalities and pitfalls. *Aptamers* **2**, 45–51 (2018).
96. Slavkovic, S., Altunisik, M., Reinstein, O. & Johnson, P. E. Structure-affinity relationship of the cocaine-binding aptamer with quinine derivatives. *Bioorg. Med. Chem.* **23**, 2593–2597 (2015).
97. Tellinghuisen, J. Optimizing experimental parameters in isothermal titration

- calorimetry. *J. Phys. Chem. B* **109**, 20027–20035 (2005).
98. Turnbull, W. B. & Daranas, A. H. On the value of c : can low affinity systems be studied by isothermal titration calorimetry? *J. Am. Chem. Soc.* **125**, 14859–14866 (2003).
 99. Tellinghuisen, J. Isothermal titration calorimetry at very low c . *Anal. Biochem.* **373**, 395–397 (2008).
 100. Tellinghuisen, J. Analysis of multitemperature isothermal titration calorimetry data at very low c : Global beats van't Hoff. *Anal. Biochem.* **513**, 43–46 (2016).
 101. Broecker, J., Vargas, C. & Keller, S. Revisiting the optimal c value for isothermal titration calorimetry. *Anal. Biochem.* **418**, 307–309 (2011).
 102. Mizoue, L. S. & Tellinghuisen, J. The role of backlash in the 'first injection anomaly' in isothermal titration calorimetry. *Anal. Biochem.* **326**, 125–127 (2004).
 103. Freiburger, L. A., Auclair, K. & Mittermaier, A. K. Elucidating Protein Binding Mechanisms by Variable- c ITC. *ChemBioChem* **10**, 2871–2873 (2009).
 104. Velazquez-Campoy, A. & Freire, E. Isothermal titration calorimetry to determine association constants for high-affinity ligands. *Nat. Protoc.* **1**, 186–191 (2006).
 105. Sigurskjold, B. W. Exact Analysis of Competition Ligand Binding by Displacement Isothermal Titration Calorimetry. *Anal. Biochem.* **277**, 260–266 (2000).

106. Fukada, H. & Takahashi, K. Enthalpy and Heat Capacity Changes for the Proton Dissociation of Various Buffer Components in 0.1 M Potassium Chloride. *Proteins: Struct., Funct., Bioinf.* **33**, 159–166 (1998).
107. Zhang, Z. & Liu, J. An engineered one-site aptamer with higher sensitivity for label-free detection of adenosine on graphene oxide. *Can. J. Chem.* **96**, 957-963 (2018).
108. Kawano, R. *et al.* Rapid detection of a cocaine-binding aptamer using biological nanopores on a chip. *J. Am. Chem. Soc.* **133**, 8474–8477 (2011).
109. Sharma, A. K. & Heemstra, J. M. Small Molecule Dependent Split Aptamer Ligation. *J. Am. Chem. Soc.* **133**, 12426–12429 (2011).
110. Sharma, A. K., Kent, A. D. & Heemstra, J. M. Enzyme-linked small-molecule detection using split aptamer ligation. *Anal. Chem.* **84**, 6104–6109 (2012).
111. Das, J. *et al.* An ultrasensitive universal detector based on neutralizer displacement. *Nat. Chem.* **4**, 642–648 (2012).
112. Zou, R. *et al.* Highly specific triple-fragment aptamer for optical detection of cocaine. *RSC Adv.* **2**, 4636–4638 (2012).
113. Kent, A. D., Spiropoulos, N. G. & Heemstra, J. M. General approach for engineering small-molecule-binding DNA split aptamers. *Anal. Chem.* **85**, 9916–9923 (2013).
114. Malile, B. & Chen, J. I. L. Morphology-based plasmonic nanoparticle sensors: controlling etching kinetics with target-responsive permeability gate. *J. Am. Chem. Soc.* **135**, 16042–16045 (2013).

115. Li, D. I., Song, S. & Fan, C. Target-responsive structural switching for nucleic acid-based sensors. *Acc. Chem. Res.* **43**, 631–641 (2010).
116. Plaxco, K. W. & Soh, H. T. Switch-based biosensors: A new approach towards real-time, in vivo molecular detection. *Trends Biotechnol.* **29**, 1–5 (2011).
117. Green, E. *et al.* A rational approach to minimal high-resolution cross-reactive arrays. *J. Am. Chem. Soc.* **128**, 15278–15282 (2006).
118. Sharp, K. I. M. Entropy – enthalpy compensation : fact or artifact? *Protein Sci.* **10**, 661–667 (2001).
119. Chodera, J. D. & Mobley, D. L. Entropy-enthalpy compensation: role and ramifications in biomolecular ligand recognition and design. *Annu. Rev. Biophys.* **42**, 121–42 (2013).
120. Olsson, T. S. G., Ladbury, J. E., Pitt, W. R. & Williams, M. A. Extent of enthalpy-entropy compensation in protein-ligand interactions. *Protein Sci.* **20**, 1607–1618 (2011).
121. Starikov, E. B. & Nordén, B. Enthalpy-entropy compensation: A phantom or something useful? *J. Phys. Chem. B* **111**, 14431–14435 (2007).
122. Smith, J. E. *et al.* Colorimetric detection with aptamer-gold nanoparticle conjugates coupled to an android-based color analysis application for use in the field. *Talanta* **121**, 247–255 (2014).
123. Bao, J., Krylova, S. M., Reinstein, O., Johnson, P. E. & Krylov, S. N. Label-free solution-based kinetic study of aptamer-small molecule interactions by kinetic capillary electrophoresis with UV detection revealing how kinetics

- control equilibrium. *Anal. Chem.* **83**, 8387–8390 (2011).
124. Spiropulos, N. G. & Heemstra, J. M. Templating effect in DNA proximity ligation enables use of non-bioorthogonal chemistry in biological fluids. *Artificial DNA: PNA and XNA* **3**, 1–7 (2012).
125. Chaires, J. B. Calorimetry and thermodynamics in drug design. *Annu. Rev. Biophys.* **37**, 135–151 (2008).
126. Neves, M. A. D., Slavkovic, S., Churcher, Z. R. & Johnson, P. E. Salt-mediated two-site ligand binding by the cocaine-binding aptamer. *Nucleic Acids Res.* **45**, 1041–1048 (2016).
127. Breaker, R. R. Engineered allosteric ribozymes as biosensor components. *Curr. Opin. Biotechnol.* **13**, 31–39 (2002).
128. Vinkenborg, J. L., Karnowski, N. & Famulok, M. Aptamers for allosteric regulation. *Nat. Chem. Biol.* **7**, 519 (2011).
129. Sachan, A., Ilgu, M., Kempema, A., Kraus, G. A. & Nilsen-Hamilton, M. Specificity and ligand affinities of the cocaine aptamer: impact of structural features and physiological NaCl. *Anal. Chem.* **88**, 7715–7723 (2016).
130. Yu, H., Canoura, J., Guntupalli, B., Lou, X. & Xiao, Y. A cooperative-binding split aptamer assay for rapid, specific and ultra-sensitive fluorescence detection of cocaine in saliva. *Chem. Sci.* **8**, 131–141 (2016).
131. Freeman, R., Sharon, E., Teller, C. & Willner, I. Control of biocatalytic transformations by programmed DNA assemblies. *Chem. Eur. J.* **16**, 3690–3698 (2010).

132. Shlyahovsky, B. *et al.* Spotlighting of cocaine by an autonomous aptamer-based machine. *J. Am. Chem. Soc.* **129**, 3814–3815 (2007).
133. Harkness, R. W., Slavkovic, S., Johnson, P. E. & Mittermaier, A. K. Rapid characterization of folding and binding interactions with thermolabile ligands by DSC. *Chem. Commun.* **52**, 13471–13474 (2016).
134. Trausch, J. J., Ceres, P., Reyes, F. E. & Batey, R. T. The structure of a tetrahydrofolate-sensing riboswitch reveals two ligand binding sites in a single aptamer. *Structure* **19**, 1413–1423 (2011).
135. Huizenga, D. E. & Szostak, J. W. A DNA aptamer that binds adenosine and ATP. *Biochemistry* **34**, 656–665 (1995).
136. Cowan, J. A., Ohyama, T., Wang, D. & Natarajan, K. Recognition of a cognate RNA aptamer by neomycin B: quantitative evaluation of hydrogen bonding and electrostatic interactions. *Nucleic Acids Res.* **28**, 2935–42 (2000).
137. Jose, A. M., Soukup, G. A. & Breaker, R. R. Cooperative binding of effectors by an allosteric ribozyme. *Nucleic Acids Res.* **29**, 1631–7 (2001).
138. Freiburger, L., Auclair, K. & Mittermaier, A. Global ITC fitting methods in studies of protein allostery. *Methods* **76**, 149–161 (2015).
139. Freire, E., Schön, A. & Velazquez-Campoy, A. Isothermal titration calorimetry: general formalism using binding polynomials. *Methods Enzymol.* **455**, 127–155 (2009).
140. Porchetta, A., Vallée-Bélisle, A., Plaxco, K. W. & Ricci, F. Using distal-site mutations and allosteric inhibition to tune, extend, and narrow the useful

- dynamic range of aptamer-based sensors. *J. Am. Chem. Soc.* **134**, 20601–20604 (2012).
141. Douglas, S. M., Bachelet, I. & Church, G. M. A Logic-Gated Nanorobot for Targeted Transport of Molecular Payloads. *Science* **335**, 831 LP – 834 (2012).
 142. Nutiu, R. & Li, Y. In vitro selection of structure-switching signaling aptamers. *Angew. Chem., Int. Ed. Engl.* **44**, 1061–1065 (2005).
 143. Xia, T., Yuan, J. & Fang, X. Conformational dynamics of an ATP-binding DNA aptamer: a single-molecule study. *J. Phys. Chem. B* **117**, 14994–15003 (2013).
 144. Armstrong, R. E. & Strouse, G. F. Rationally manipulating aptamer binding affinities in a stem-loop molecular beacon. *Bioconjugate Chem.* **25**, 1769–1776 (2014).
 145. Nakamura, I., Shi, A. C., Nutiu, R., Yu, J. M. Y. & Li, Y. Kinetics of signaling-DNA-aptamer-ATP binding. *Phys. Rev. E: Stat., Nonlinear, Soft Matter Phys.* **79**, 1–9 (2009).
 146. Wang, J., Jiang, Y., Zhou, C. & Fang, X. Aptamer-based ATP assay using a luminescent light switching complex. *Anal. Chem.* **77**, 3542–3546 (2005).
 147. Urata, H., Nomura, K., Wada, S. & Akagi, M. Fluorescent-labeled single-strand ATP aptamer DNA: chemo- and enantio-selectivity in sensing adenosine. *Biochem. Biophys. Res. Commun.* **360**, 459–463 (2007).
 148. Hao, L. H. & Zhao, Q. A fluorescein labeled aptamer switch for thrombin with fluorescence decrease response. *Anal. Methods* **7**, 3888–3892 (2015).
 149. Pérez-Ruiz, T., Martínez-Lozano, C., Tomás, V. & Martín, J. Determination of

- ATP via the photochemical generation of hydrogen peroxide using flow injection luminol chemiluminescence detection. *Anal. Bioanal. Chem.* **377**, 189–194 (2003).
150. Sun, N. *et al.* A signal-on fluorescence biosensor for detection of adenosine triphosphate based on click chemistry. *Anal. Methods* **6**, 3370–3374 (2014).
 151. Ladbury, J. E. & Chowdhry, B. Z. Sensing the heat: the application of isothermal calorimetry to thermodynamic studies of biomolecular interactions. *Chem. Biol.* **3**, 791–801 (1996).
 152. Feig, A. L. Applications of Isothermal Titration Calorimetry in RNA Biochemistry and Biophysics. *Biopolymers* **87**, 293–301 (2007).
 153. Zhang, Y. L. & Zhang, Z. Y. Low-affinity binding determined by titration calorimetry using a high-affinity coupling ligand: A thermodynamic study of ligand binding to protein tyrosine phosphatase 1B. *Anal. Biochem.* **261**, 139–148 (1998).
 154. Houtman, J. C. D. *et al.* Studying multisite binary and ternary protein interactions by global analysis of isothermal titration calorimetry data in SEDPHAT: application to adaptor protein complexes in cell signaling. *Protein Sci.* **16**, 30–42 (2007).
 155. Brautigam, C. A. Fitting two- and three-site binding models to isothermal titration calorimetric data. *Methods* **76**, 124–136 (2015).
 156. Wiseman, T., Williston, S., Brandts, J. F. & Lin, L. N. Rapid Measurement of Binding Constants and Heats of Binding Using a New Titration Calorimeter.

- Anal. Biochem.* **179**, 131–137 (1989).
157. Tellinghuisen, J. Optimizing isothermal titration calorimetry protocols for the study of 1:1 binding: keeping it simple. *Biochim. Biophys. Acta, Gen. Subj.* **1860**, 861–867 (2016).
158. Krepl, M., Otyepka, M., Banáš, P. & Šponer, J. Effect of guanine to inosine substitution on stability of canonical DNA and RNA duplexes: molecular dynamics thermodynamics integration study. *J. Phys. Chem. B* **117**, 1872–1879 (2013).
159. Jiang, F., Kumar, R. A., Jones, R. A. & Patel, D. J. Structural basis of RNA folding and recognition in an AMP–RNA aptamer complex. *Nature* **382**, 183–186 (1996).
160. Nonin-Lecomte, S., Lin, C. H. & Patel, D. J. Additional hydrogen bonds and base-pair kinetics in the symmetrical AMP-DNA aptamer complex. *Biophys. J.* **81**, 3422–31 (2001).
161. SantaLucia, J. & Hicks, D. The thermodynamics of DNA structural motifs. *Annu. Rev. Biophys. Biomol. Struct.* **33**, 415–440 (2004).
162. Nutiu, R. & Li, Y. Structure-switching signaling aptamers: transducing molecular recognition into fluorescence signaling. *Chem. Eur. J.* **10**, 1868–1876 (2004).
163. Feagin, T. A., Maganzini, N. & Soh, H. T. Strategies for creating structure-switching aptamers. *ACS Sens.* **3**, 1611–1615 (2018).
164. Catherine, A. T., Shishido, S. N., Robbins-Welty, G. A. & Diegelman-Parente, A.

- Rational design of a structure-switching DNA aptamer for potassium ions. *FEBS Open Bio* **4**, 788–795 (2014).
165. Kalra, P., Dhiman, A., Cho, W. C., Bruno, J. G. & Sharma, T. K. Simple methods and rational design for enhancing aptamer sensitivity and specificity. *Front. Mol. Biosci.* **5**, 1–16 (2018).
 166. Ricci, F., Vallée-Bélisle, A., Simon, A. J., Porchetta, A. & Plaxco, K. W. Using nature's 'tricks' to rationally tune the binding properties of biomolecular receptors. *Acc. Chem. Res.* **49**, 1884–1892 (2016).
 167. Neves, M. A. D., Blaszykowski, C., Bokhari, S. & Thompson, M. Ultra-high frequency piezoelectric aptasensor for the label-free detection of cocaine. *Biosens. Bioelectron.* **72**, 383–392 (2015).
 168. Slavkovic, S., Churcher, Z. R. & Johnson, P. E. Nanomolar binding affinity of quinine-based antimalarial compounds by the cocaine-binding aptamer. *Bioorg. Med. Chem.* **26**, 5427–5434 (2018).
 169. Kara, M. & Zacharias, M. Stabilization of duplex DNA and RNA by dangling ends studied by free energy simulations. *Biopolymers* **101**, 418–427 (2014).
 170. Isaksson, J. & Chattopadhyaya, J. A uniform mechanism correlating dangling-end stabilization and stacking. *Biochemistry* **44**, 5390–5401 (2005).
 171. Rosemeyer, H. & Seela, F. Modified purine nucleosides as dangling ends of DNA duplexes: the effect of the nucleobase polarizability on stacking interactions. *J. Chem. Soc., Perkin Trans. 2* 746–750 (2002).
 172. Bommarito, S., Peyret, N. & SantaLucia, J. Thermodynamic parameters for

- DNA sequences with dangling ends. *Nucleic Acids Res.* **28**, 1929–1934 (2000).
173. Burkard, M. E., Kierzek, R. & Turner, D. H. Thermodynamics of unpaired terminal nucleotides on short RNA helices correlates with stacking at helix termini in larger RNAs. *J. Mol. Biol.* **290**, 967–982 (1999).
174. Röthlisberger, P. & Hollenstein, M. Aptamer chemistry. *Adv. Drug Delivery Rev.* **134**, 3–21 (2018).
175. Nimjee, S. M., White, R. R., Becker, R. C. & Sullenger, B. A. Aptamers as Therapeutics. *Annu. Rev. Pharmacol. Toxicol.* **57**, (2017).
176. Nguyen, V. T., Kwon, Y. S. & Gu, M. B. Aptamer-based environmental biosensors for small molecule contaminants. *Curr. Opin. Biotechnol.* **45**, 15–23 (2017).
177. Ding, F., Gao, Y. & He, X. Recent progresses in biomedical applications of aptamer-functionalized systems. *Bioorg. Med. Chem. Lett.* **27**, 4256–4269 (2017).
178. Du, Y. & Dong, S. Nucleic acid biosensors: recent advances and perspectives. *Anal. Chem.* **89**, 189–215 (2017).
179. Grytz, C. M., Marko, A., Cekan, P., Sigurdsson, S. T. & Prisner, T. F. Flexibility and conformation of the cocaine aptamer studied by PELDOR. *Phys. Chem. Chem. Phys.* **18**, 2993–3002 (2016).
180. Churcher, Z. R., Neves, M. A. D., Hunter, H. N. & Johnson, P. E. Comparison of the free and ligand-bound imino hydrogen exchange rates for the cocaine-binding aptamer. *J. Biomol. NMR* **68**, 33–39 (2017).

181. Neves, M. A. D., Blaszykowski, C. & Thompson, M. Utilizing a Key Aptamer Structure-Switching Mechanism for the Ultrahigh Frequency Detection of Cocaine. *Anal. Chem.* **88**, 3098–3106 (2016).
182. Bozokalfa, G. *et al.* Polypeptide Functional Surface for the Aptamer Immobilization: Electrochemical Cocaine Biosensing. *Anal. Chem.* **88**, 4161–4167 (2016).
183. Combrinck, J. M. *et al.* Insights into the role of heme in the mechanism of action of antimalarials. *ACS Chem. Biol.* **8**, 133–137 (2013).
184. World Health Organization. *World Malaria Report 2010*. <https://www.who.int/malaria/publications/world-malaria-report-2018/en/> (2010).
185. Cox, M. & Nelson, D. *Lehninger Principles of Biochemistry*. (WH Freeman, 2000).
186. Gurova, K. New hopes from old drugs: revisiting DNA-binding small. *Future Oncol.* **5**, 1–28 (2010).
187. Vuong, S. *et al.* Identifying three-way DNA junction-specific small-molecules. *Biochimie* **94**, 442–450 (2012).
188. Novotna, J. *et al.* Cationic azacryptands as selective three-way DNA junction binding agents. *Org. Biomol. Chem.* **13**, 215–222 (2015).
189. Amor, S. *et al.* Identification of three-way DNA junction ligands through screening of chemical libraries and validation by complementary in vitro assays. *J. Med. Chem.* **62**, 4456–4466 (2019).

190. Persil, Ö., T. Santai, C., S. Jain, S. & V. Hud, N. Assembly of an antiparallel homoadenine DNA duplex by small-molecule binding. *J. Am. Chem. Soc.* **126**, 8644–8645 (2004).
191. Carter, E. K., Laughlin-Toth, S., Dodd, T., Wilson, W. D. & Ivanov, I. Small molecule binders recognize DNA microstructural variations via an induced fit mechanism. *Phys. Chem. Chem. Phys.* **21**, 1841–1851 (2019).
192. Bhaduri, S., Ranjan, N. & Arya, D. P. An overview of recent advances in duplex DNA recognition by small molecules. *Beilstein J. Org. Chem.* **14**, 1051–1086 (2018).
193. Seeman, N. C. Nucleic acid junctions and lattices. *J. Theor. Biol.* **99**, 237–247 (1982).
194. Duckett, D. R. & Lilley, D. M. The three-way DNA junction is a Y-shaped molecule in which there is no helix-helix stacking. *EMBO J.* **9**, 1659–1664 (1990).
195. Guo, Q., Lu, M., Churchill, M. E. A., Tullius, T. D. & Kallenbach, N. R. Asymmetric structure of a three-arm DNA junction. *Biochemistry* **29**, 10927–10934 (1990).
196. Guthrie, C. & Patterson, B. Spliceosomal snRNAs. *Annu. Rev. Genet.* **22**, 387–419 (1988).
197. Wimberly, B. T. *et al.* Structure of the 30S ribosomal subunit. *Nature* **407**, 327–339 (2000).
198. Singleton, M. R., Scaife, S. & Wigley, D. B. Structural analysis of DNA replication

- fork reversal by RecG. *Cell* **107**, 79–89 (2001).
199. Muhuri, S., Mimura, K., Miyoshi, D. & Sugimoto, N. Stabilization of three-way junctions of DNA under molecular crowding conditions. *J. Am. Chem. Soc.* **131**, 9268–9280 (2009).
200. Wing, R. *et al.* Crystal structure analysis of a complete turn of B-DNA. *Nature* **287**, 755–758 (1980).
201. Drew, H. R. *et al.* Structure of a B-DNA dodecamer: conformation and dynamics. *Proc. Natl. Acad. Sci.* **78**, 2179–2183 (1981).
202. Tereshko, V., Minasov, G. & Egli, M. The Dickerson-Drew B-DNA dodecamer revisited at atomic resolution. *J. Am. Chem. Soc.* **121**, 470–471 (1999).
203. Orozco, M., Morozov, A. V., Jir, S. & Lankas, F. Structure, stiffness and substates of the Dickerson-Drew dodecamer. *J. Chem. Theory Comput.* **9**, 707–721 (2013).
204. Dans, P. D. *et al.* Long-timescale dynamics of the Drew – Dickerson dodecamer. *Nucleic Acids Res.* **44**, 4052–4066 (2016).
205. Slater, A. F. G. Chloroquine: mechanism of drug action and resistance in *Plasmodium falciparum*. in *Pharmac. Ther.* (ed. Köhler, P.) vol. 57 203–235 (Pergamon Press Ltd, 1993).
206. Howells, R. E. Chemotherapy and Drug Resistance in Malaria. *Parasitology* **97**, 503–503 (1988).
207. Thompson, P. & Werbel, L. 4-Aminoquinolines. in *Antimalarial Agents* (eds. Thompson, P. E. & Werbel, L. M.) vol. 12 150–196 (Elsevier, 1972).

208. Thompson, P. & Werbel, L. Quinolinemethanols and Related Compounds. in *Antimalarial Agents* (eds. Thompson, P. E. & Werbel, L. M.) vol. 12 79–99 (Elsevier, 1972).
209. Kwakye-Berko, F. & Meshnick, S. R. Binding of chloroquine to DNA. *Mol. Biochem. Parasitol.* **35**, 51–55 (1989).
210. Lerman, L. S. Structural considerations in the interaction of DNA and acridines. *J. Mol. Biol.* **3**, 18–30 (1961).
211. Davidson, M. W., Griggs, B. G., Boykin, D. W. & Wilson, W. D. Molecular structural effects involved in the interaction of quinolinemethanolamines with DNA. Implications for antimalarial action. *J. Med. Chem.* **20**, 1117–22 (1977).
212. Li, Y. & Wu, Y.-L. An over four millennium story behind qinghaosu (artemisinin) - a fantastic antimalarial drug from a traditional chinese herb. *Curr. Med. Chem.* **10**, 2197–2230 (2003).
213. Guoqiao, L., Li, Y., Li, Z. & Meiyi, Z. Chapter 1 - Discovery of qinghaosu (artemisinin)—history of research and development of artemisinin-based antimalarials. in *Artemisinin-Based and Other Antimalarials* (eds. Guoqiao, L., Ying, L., Zelin, L. & Meiyi, Z.) 1–67 (Academic Press, 2018).
214. White, N. Antimalarial drug resistance and combination chemotherapy. *Philos. Trans. R Soc. Lond. B Biol. Sci.* **354**, 739–749 (1999).
215. Nosten, F. & White, N. J. Artemisinin-based combination treatment of falciparum malaria. *Am. J. Trop. Med. Hyg.* **77**, 181–192 (2007).

216. Whitty, C. J. M., Chandler, C., Ansah, E., Leslie, T. & Staedke, S. G. Deployment of ACT antimalarials for treatment of malaria: Challenges and opportunities. *Malar. J.* **7**, 1–7 (2008).
217. Kamchonwongpaisan, S. & Meshnick, S. R. The mode of action of the antimalarial artemisinin and its derivatives. *Gen. Pharmacol.* **27**, 587–592 (1996).
218. Avery, M. A. *et al.* Structure-activity relationships of the antimalarial agent artemisinin. 4. Effect of substitution at C-3. *J. Med. Chem.* **39**, 2900–2906 (1996).
219. Paitayatat, S., Tarnchompoo, B., Thebtaranonth, Y. & Yuthavong, Y. Correlation of antimalarial activity of artemisinin derivatives with binding affinity with ferroprotoporphyrin IX. *J. Med. Chem.* **40**, 633–638 (1997).
220. Gopalakrishnan, A. M. & Kumar, N. Antimalarial action of artesunate involves DNA damage mediated by reactive oxygen species. *Antimicrob. Agents Chemother.* **59**, 317–325 (2015).
221. Wong, Y. K. *et al.* Artemisinin as an anticancer drug: Recent advances in target profiling and mechanisms of action. *Med. Res. Rev.* **37**, 1492–1517 (2017).
222. Zhang, Y. *et al.* Antitumor Research on Artemisinin and Its Bioactive Derivatives. *Nat. Prod. Bioprospect.* **8**, 303–319 (2018).
223. Konstat-Korzenny, E., Ascencio-Aragón, J., Niezen-Lugo, S. & Vázquez-López, R. Artemisinin and Its Synthetic Derivatives as a Possible Therapy for Cancer. *Med. Sci.* **6**, 19 (2018).

224. Krishna, S., Bustamante, L., Haynes, R. K. & Staines, H. M. Artemisinins: their growing importance in medicine. *Trends Pharmacol. Sci.* **29**, 520–527 (2008).
225. Meshnick, S. R. The mode of action of antimalarial endoperoxides. *Trans. R. Soc. Trop. Med. Hyg.* **88**, 31–32 (1994).
226. Haynes, R. K. *et al.* The Fe²⁺-mediated decomposition, PfATP6 binding, and antimalarial activities of artemisone and other artemisinins: the unlikelihood of C-centered radicals as bioactive intermediates. *ChemMedChem* **2**, 1480–1497 (2007).
227. O'Neill, P. M., Barton, V. E. & Ward, S. A. The molecular mechanism of action of artemisinin - The debate continues. *Molecules* **15**, 1705–1721 (2010).
228. Balint, G. A. Artemisinin and its derivatives: an important new class of antimalarial agents. *Pharmacol. Ther.* **90**, 261–265 (2001).
229. Zangi, R., Hagen, M. & Berne, B. J. Effect of ions on the hydrophobic interaction between two plates. *J. Am. Chem. Soc.* **129**, 4678–4686 (2007).
230. Naik, P. K. *et al.* The binding modes and binding affinities of artemisinin derivatives with Plasmodium falciparum Ca²⁺-ATPase (PfATP6). *J. Mol. Model.* **17**, 333–357 (2011).
231. Veerappan, A., Eichhorn, T., Zeino, M., Efferth, T. & Schneider, D. Differential interactions of the broad spectrum drugs artemisinin, dihydroartemisinin and artesunate with serum albumin. *Phytomedicine* **20**, 969–974 (2013).
232. Sun, C. & Zhou, B. The molecular and cellular action properties of artemisinins: what has yeast told us? *Microb. Cell* **3**, 196–205 (2016).

233. Meshnick, S. R. Artemisinin: mechanisms of action, resistance and toxicity. *Int. J. Parasitol.* **32**, 1655–1660 (2002).
234. Microcal. ITC Data Analysis in Origin®. *Reading* 121 (2004).
235. Velazquez-Campoy, A., Ohtaka, H., Nezami, A., Muzammil, S. & Freire, E. Isothermal Titration Calorimetry. *Curr. Protoc. Cell Biol.* **23**, 17.8.1-17.8.24 (2004).
236. Microcal. ITC Data Analysis in Origin ®. (2004).
237. Wyman, J. Linked Functions and Reciprocal Effects in Hemoglobin: A Second Look. *Adv. Protein Chem.* **19**, 223–286 (1964).
238. Cattoni, D. I., Chara, O., Kaufman, S. B. & Flecha, F. L. G. Cooperativity in binding processes: New insights from phenomenological modeling. *PLoS One* **10**, 1–14 (2015).